2022

The role of Shoc2 in embryonic development

Rebecca G. Norcross
University of Kentucky, rgnorcross@gmail.com
Author ORCID Identifier:
https://orcid.org/0000-0003-3163-739X
Digital Object Identifier: https://doi.org/10.13023/etd.2022.333

STUDENT AGREEMENT:

I represent that my thesis or dissertation and abstract are my original work. Proper attribution has been given to all outside sources. I understand that I am solely responsible for obtaining any needed copyright permissions. I have obtained needed written permission statement(s) from the owner(s) of each third-party copyrighted matter to be included in my work, allowing electronic distribution (if such use is not permitted by the fair use doctrine) which will be submitted to UKnowledge as Additional File.

I hereby grant to The University of Kentucky and its agents the irrevocable, non-exclusive, and royalty-free license to archive and make accessible my work in whole or in part in all forms of media, now or hereafter known. I agree that the document mentioned above may be made available immediately for worldwide access unless an embargo applies.

I retain all other ownership rights to the copyright of my work. I also retain the right to use in future works (such as articles or books) all or part of my work. I understand that I am free to register the copyright to my work.

REVIEW, APPROVAL AND ACCEPTANCE

The document mentioned above has been reviewed and accepted by the student's advisor, on behalf of the advisory committee, and by the Director of Graduate Studies (DGS), on behalf of the program; we verify that this is the final, approved version of the student's thesis including all changes required by the advisory committee. The undersigned agree to abide by the statements above.

Rebecca G. Norcross, Student

Dr. Emilia Galperin, Major Professor

Dr. Trevor Creamer, Director of Graduate Studies

THE ROLE OF SHOC2 IN EMBRYONIC DEVELOPMENT

DISSERTATION

A dissertation submitted in partial fulfillment of the
requirements for the degree of Doctor of Philosophy in the
College of Medicine
at the University of Kentucky

By

Rebecca G. Norcross

Lexington, Kentucky

Director: Dr. Emilia Galperin, Professor of Molecular and Cellular Biochemistry

Lexington, Kentucky

2022

0000-0003-3163-739X

ABSTRACT OF DISSERTATION

THE ROLE OF SHOC2 IN EMBRYONIC DEVELOPMENT

The canonical ERK1/2 signaling cascade regulates cellular functions critical in vertebrate embryonic development such as proliferation, apoptosis, differentiation, and migration. Thus, its signals are controlled by a variety of mechanisms. Scaffold proteins are considered central to the mechanisms regulating the transmission of the ERK1/2 signals. Yet, their functions in development nor the molecular mechanisms by which they exert their control are not well understood.

This study focuses on the essential regulator of ERK1/2 signals during development – the scaffold protein Shoc2. Loss of Shoc2 leads to early embryonic lethality in mice and zebrafish. Germline mutations in the *shoc2* gene result in the developmental disorder 'Noonan syndrome like with loose anagen hair' (NSLH) with a spectrum of developmental abnormalities, including craniofacial dysmorphism, cardiac defects, growth delays, and neurologic issues. The loss of Shoc2 and the *shoc2* NSLH-causing mutations affect the tissues of neural crest origin.

This dissertation addressed the role of Shoc2 in the development of neural crest cell-derived tissues. Studies here established that the loss of Shoc2 significantly alters the expression of transcription factors regulating the specification, migration, and differentiation of neural crest cells. Comparative transcriptome analysis of neural crest-derived cells from *shoc2* CRISPR/Cas9 mutant larvae shows that Shoc2-mediated signals regulate gene programs at several levels. This study demonstrates that the loss of Shoc2 affected the expression of extracellular matrix (ECM) proteins and ECM regulators. Together, these results demonstrate that Shoc2 is an essential regulator of neural crest development and indicates that disbalance in the turnover of the ECM may lead to the abnormalities found in NSLH patients.

The work presented here also identifies the requirement of Shoc2-mediated signals for the development of lymphatic vasculature. Using a novel Shoc2 model (*shoc2* c.1546 G>A) we determined that critical lymphatic vessels such as the thoracic duct and its derivative (the parachordal line) are absent in Shoc2 *null* larvae. These data suggest that the expression of Shoc2 is essential for lymphangiogenesis.

In summary, studies presented in this dissertation make significant advances in delineating the role of Shoc2 during the development of several diverse tissues. These findings will facilitate future work to explain the etiology of NSLH.

KEYWORDS: Neural crest, zebrafish, development, Shoc2, ERK1/2

Rebecca G. Norcross

07/21/2022

Date

THE ROLE OF SHOC2 IN EMBRYONIC DEVELOPMENT

By
Rebecca G. Norcross

Emilia Galperin, Ph.D.
Director of Dissertation

Trevor Creamer, Ph.D.
Director of Graduate Studies

07/21/2022
Date

Dedicated to the parents of RASopathy patients

.

ACKNOWLEDGMENTS

I would like to first acknowledge the sustained training and support from my professor Dr. Emilia Galperin. Dr. Galperin gave me her full attention, thorough instruction, and coaching throughout my PhD journey. Her openness and accessibility to discuss projects, ideas, and concerns is a credit to her lab and its culture. She is generous with her time in training me and challenged me beyond my perceived limits to make me a better scientist. Emily's instruction has helped me develop into a capable independent researcher qualified for a successful career. I would also like to thank my committee members Drs. Dutch, Gao, Morris, Kilgore, and Bae. I am immensely fortunate to have had their support and I greatly appreciate the time and insights they each invested in my work. Drs. Artinger, Weinstein, and Jung deserve special gratitude for their expert collaborations which enabled me to complete portions of my research. I acknowledge the Galperin lab members: Patricia, Lina, Kanal, HyeIn, Olivia, Jeffrey, Erin, Sophie and Daileen. They supported me throughout the highs and lows of data collection, aided with experiments, presentations, and provided friendships. I appreciate the department's faculty, staff, and admin. members for fostering a supportive and collaborative environment and I extend special thanks to our DIR. of Grad. Studies, Dr. Creamer.

Finally, I acknowledge my family and friends – especially my parents, Paul and Nita, and my sisters, Emily and Jessica. Your endless supportive love is irreplaceable. Thank you for always being there for me no matter life's challenges. Evan, thank you for your many southern-bound drives to KY and for being a contributory light at the end of

the tunnel during the latter third of my PhD. I have a unique gratitude to HyeIn and David. Without either of them I would not be defending. In some regards this PhD belongs to them as much as to me. HyeIn, you get ∞ thanks. I could not ask for a better friend nor lab trainer. Dr. David, you made the bad days good during my 1st and 2nd years. Thank you. This has been a team effort degree with much gratitude due to my many additional cheerleaders (alphabetically): Abigail L., Adam L., Brittany V., Center Point Church as a whole, Jenny H., Kristen S., Lauren P., Lisa W., Mallory F., Mark M., Dr. Millar, Pam L., Shadan H., Smita J., Terri M., and The Moore Family. There are absolutely more individuals not included here but who also deserve my thanks. Thank you.

TABLE OF CONTENTS

LIST OF TABLES

LIST OF FIGURES

CHAPTER 1. INTRODUCTION

1.1 The Extracellular Signal-Regulated Kinase (ERK1/2) Signaling Cascade

The canonical extracellular signal-regulated kinase 1/2 (ERK1/2) signaling cascade regulates a range of cellular responses including cell cycle, growth, proliferation, apoptosis, differentiation, and motility. The biological effects of the ERK1/2 pathway have been extensively studied and are reviewed in [1-3]. Abnormal activity of the ERK1/2 pathway is detected in various pathogenic conditions, including cancer, neurodegenerative diseases, diabetes and congenital abnormalities [4-6]. Aberrant ERK1/2 signaling is associated with increased neuronal death in Alzheimer's and Parkinson's diseases [7, 8]. Genetic manipulation to induce low or high basal levels of ERK1/2 activity in mice are respectively associated with resistance to, or a higher susceptibility for the development of insulin resistance (characteristic of type 2 diabetes) [9, 10]. Finally, activating mutations in the ERK1/2 pathway are the underlying causes driving approximately half of all cancers [11]. Thus, proper regulation of the ERK1/2 pathway is critical for disease prevention.

Briefly, the core components of the ERK1/2 cascade include small GTPases such as Ras- (K, H, and M) [12, 13]. GTPases cycle between GTP-bound active and GDP-bound inactive forms under the control of specific regulatory proteins that control this catalytic cycle: the guanine nucleotide exchange factors (GEFs) and the GTPase-activating proteins (GAPs) [14]. Active GTP-bound RAS recruits serine/threonine RAF kinases to the plasma membrane (PM) where they are activated in a complex fashion [15]. Once active, all RAF family members (A-RAF, B-RAF, c-RAF (RAF-1)) are capable of activating another serine/threonine kinase, mitogen-activated protein kinase 1/2

(MEK1/2), which in turn is able to activate ERK1/2 via sequential phosphorylation (**Figure 1.1**).

Phosphorylated ERK1/2 kinases are the primary effectors responsible for the aforementioned critical downstream cellular events and are reported to phosphorylate nearly 500 substrates [1, 16]. Activation of ERK1/2 by MEK1/2 triggers their dimerization and translocation to the nucleus where ERKs target a range of transcription factors [15]. Additionally, multiple studies have reported that active ERK1/2 also targets a number of cytosolic substrates including phospholipase A2 (PLA2), cAMP phosphodiesterase (PDE4), ribosomal S6 protein kinases (RSKs), death associated protein kinase (DAPK), Bcl-2 family proteins (Bik) and many others [2, 17]. To maintain the duration, amplitude, location, and specificity of the ERK1/2 signal fidelity and to produce the correct biological response, cells utilize multiple mechanisms including positive and negative feedback loops, post-translational modifications, crosstalk with other signaling pathways, and the assembly of dynamic signaling complexes. These are all often facilitated by signaling scaffold proteins [18, 19].

Multiple mechanisms control the fidelity of the ERK1/2 signal [20, 21]. Feedback mechanisms and loops targeting specific components of the ERK1/2 pathway and modulating spatiotemporal signaling dynamics play an essential role in controlling the wide range of biological responses [22-26]. Signaling scaffold proteins are considered to be central in regulating multi-enzyme signaling complexes and are essential for controlling signaling branching. In addition, to bringing signaling components together, scaffolds can have some catalytic function, influence signaling by allosteric mechanisms, are feedback-

regulated, localize signaling activity to distinct regions of the cell, or increase pathway fidelity.

1.2 ERK1/2 pathway specificity by scaffold protein Shoc2

1.2.1 Scaffold proteins of the ERK1/2 pathway

While kinases and phosphatases of the ERK1/2 pathway are well-studied, relatively little is understood of the mechanisms by which signaling scaffolds the control assembly and dynamics of multi-enzyme complexes within the ERK1/2 pathway. Scaffold proteins within the ERK1/2 pathway include the well-studied scaffolds - kinase suppressor of Ras (KSR1), MP1, Paxillin, β-arrestins and IQGAP 1 [27-34] These proteins are often noncatalytic, multi-valent, enzyme-binding, molecular platforms that optimize intracellular signaling by enabling the formation of intricate and diverse protein complexes [35]. They can tether multiple proteins of the ERK1/2 cascade in close proximity to facilitate protein-protein interactions, target protein complexes to specific microenvironments, and aid in positive/negative feedback mechanisms. For example, under epidermal growth factor receptor activation, KSR1 translocates to the plasma membrane and positively regulates the ERK1/2 pathway by facilitating the phosphorylation of MEK by RAF [36-38]. Thus, scaffolds' cellular distributions place them at a junction to optimize signal organization and transmittance (**Figure 1.2)**.

1.2.2 Scaffold protein Shoc2

The scaffold protein Shoc2 is a critical mediator of ERK1/2 signals. Shoc2 (Sur-8/Soc2, *suppressor of clear*) was first identified in *C. elegans* as a conserved gene that codes for a cytosolic protein composed of nearly all leucine-rich repeats (LRR) and was detected in all tested tissues [39]. Shoc2 orthologues have two major domains: a short, unstructured N-terminus (spanning 56 to 145 total amino acids in different taxa) followed by a stretch of LRRs [40, 41]. Consistent with other proteins containing LRR repeats, Shoc2 forms a solenoid structure and assembles complex protein machinery [41]. Its curvature enables the N-terminus and LRR domains to simultaneously hold multiple partners although most interact within the LRR region. A table of Shoc2 interacting proteins is provided in **Table 1.1** and will be further discussed here.

Although Shoc2 lacks apparent enzymatic activity, it recruits catalytic proteins to fine-tune transmitted signals through the scaffolding complex. Li et al., identified that not only does Shoc2 binds with multiple Ras isoforms, but that inhibited binding of Shoc2 and Ras suppressed the activity of a constitutively active Ras [42]. Furthermore, Shoc2 was determined to facilitate the interaction between Ras and Raf forming a ternary complex through an indirect interaction with Raf. Consequently, the overexpression of *shoc2* increased the Ras-MAPK pathway activity.

Further studies have identified that Shoc2 forms a holoenzyme with the catalytic subunit of the protein phosphatase 1 (PP1c) [43]. Specific to the Shoc2 interaction with the M-Ras isoform, the Shoc2-PP1c holoenzyme is targeted to the PM where it stimulates Raf-1 kinase activity by dephosphorylating the S259 inhibitory site of Raf-1 [43]. The M-Ras/Shoc2/PP1c complex then activates Raf-1 recruited by other Ras proteins or Ras

family GTPases. At the PM, the M-Ras-Shoc2 subunit competes for PP1c binding against Scribbled Homolog (SCRIB), a known regulator of the ERK1/2 pathway [44]. Similarly, Erbin, a member of the LAP protein family (contains LRR and PDZ domains) also acts as a negative regulator of the ERK1/2 pathway [45-48] by disrupting the Shoc2 facilitated interaction between RAS and RAF proteins. Regulatory mechanisms, such as the competitive binding of SCRIB and PP1c for Shoc2, are critical for the ERK1/2 pathway.

In addition to tethering proteins that amplify ERK1/2 signals, Shoc2 also interacts with proteins that fine-tune ERK1/2 signals transmitted *via* the Shoc2 module. These proteins, deubiquitinase (DUB) USP7, the HECT-domain E3 ligase HUWE1, VCP/p97, and PSMC5, form enzymatic machinery that allow for a highly coordinated feedback mechanism [24, 49-51]. Furthermore, the amplitude of Shoc2-mediated ERK1/2 signals is modified by induced post-translational modifications [24]. Growth factor activation of the ERK1/2 pathway triggers HUWE1-mediated ubiquitination of Shoc2 and is a prerequisite for the subsequent ubiquitination of the Shoc2-bound RAF-1 kinase. Data from the Galperin lab suggest that these ubiquitin modifications serve as negative feedback that reduces the amplitude of RAF-ERK1/2 signals. In the Shoc2 complex, USP7 controls the catalytic activity of HUWE1 to modify Shoc2 and Raf-1. Shoc2 partners and the well-known ‘remodelers’, AAA + ATPases PSMC5 and VCP/p97, also coordinate the levels of the HUWE1-modulated ubiquitination of Shoc2/RAF. Interestingly, PSMC5, which does not modulate the stability of Shoc2 or its known partners, is essential for the targeting of Shoc2 to late endosomes.

Once translocated to the surface of late endosomes, yet another player, VCP, interacts [50]. VCP is an unfoldase and AAA+ ATPase that acts by controlling the level of total ubiquitination by HUWE1 to modulate the assembly of the Shoc2 complex's molecules. Loss of VCP leads to increased Shoc2 and RAF-1 ubiquitination and reduced ERK phosphorylation. Taken together, multiple dynamic molecular mechanisms regulate the highly conserved and intricate signaling by the ERK1/2 pathway.

1.3 ERK1/2 signals in embryogenesis and congenital disorders (RASopathies)

1.3.1 ERK1/2 signaling during embryogenesis

ERK1/2 signaling is one of several critical regulatory pathways responsible for integrating multiple *de novo* structures such as the skeleton, vasculature, spinal cord and muscles into a functional organism [52-56]. It is universally significant in all cell populations including neural crest (NC), a unique, multipotent cell type critical for embryogenesis and development [57-59]. (An overview of NC development is in **Introduction 1.5**). During embryogenesis, perturbations in ERK1/2 signaling can cause the loss of embryo viability or a wide range of severe congenital abnormalities[60, 61]. These developmental impairments including craniofacial defects (micrognathia, hypoplastic maxilla, cleft palate), osteoblast differentiation defects, total loss of/deficient peripheral nervous system cell populations (Schwann cells and dorsal root ganglia), reduced cell proliferation, increased apoptosis, muscle weakness, and cardiovascular phenotypes (double outlet right ventricle, ventricular septal defects, persistent truncus arteriosus, and hypoplastic pulmonary arteries) [62]. Deregulated signaling may arise from

reduced spatial organization, the loss of temporal sequence, or aberrant signal amplitude (hyper/hypo activation).

1.3.2 "RASopathy" defined

The term "RASopathy" defines a collection of congenital developmental syndromes in which the ERK1/2 pathway is misregulated due to pathogenic variations in gene(s) within or regulating ERK1/2 signaling **(Figure 1.3)** [6, 63]. To date, a formal report of RASopathy patient mortality is incomplete, yet patient morbidity is severe. The common pathogenic mechanism (dysregulated ERK1/2 signaling) causes hallmark phenotypes that often include distinct facial features, cardiac defects, growth delays, neurologic deficits, gastrointestinal difficulties, delayed development, and a propensity to neoplasia/cancers in some RASopathy syndromes[64]. Infant and children's RASopathy anatomical deficits and symptoms are not static; an early diagnosis is critical to mitigate patient sign and symptom severity [65]. Therefore, the mechanistic role of each RASopathy-associated gene is required to delineate RASopathy etiology for patient diagnoses and treatment.

1.3.3 Noonan syndrome-like with loose anagen hair (NSLH)

Missense mutations in the *shoc2* gene result in the RASopathy termed Noonan syndrome like with loose anagen hair (NSLH). It was first suggested to be a distinct syndrome in 2003 when three patients displayed phenotypes similar to two known syndromes (Noonan and cardio-facio-cutaneious syndromes), yet presented the markedly distinct phenotypes: easily pluckable, sparse, anagen hair and darkly pigmented skin [66]. However, the specific NSLH inducing mutation was not first reported until 2009 [67]. In

that study, an *in silico* analysis identified *shoc2* as a potential candidate for a gene associated with NS. Further analysis of *shoc2* exonic sequences identified a cohort of patients harboring the *shoc2* c. 4A>G mutation. A review of the clinical features of the *shoc2* mutation-positive individuals revealed a consistent phenotype for NSLH. A summary of phenotypes currently reported for patients with the Shoc2 S2G substitution is presented in **Table 1.2** [67-96]. Although the most common NSLH-associated Shoc2 mutation is c.4A>G, several additional *shoc2* substitutions have been reported **(Table 1.3)** [67, 97, 98]. However, unlike the other Shoc2 variants with substitutions within the LRR curvature, the S2G substitution leads to an N-myristoylation and aberrantly targets Shoc2 to the PM [67, 99].

1.4 *Danio rerio* as an animal model for developmental studies

The zebrafish (*Danio rerio*) vertebrate animal model is an excellent model for studies of embryonic development. The zebrafish molecular pathways are highly conserved and 70% of the 26,206 protein-coding zebrafish genes have human counterparts [100]. Zebrafish embryos are particularly well suited for studies of tissue development and morphogenesis due to their rapid development, *ex vivo* embryogenesis, and optical clarity. This permits approaches to follow them over time through *in vivo* microscopy thus creating data in the context of a living vertebrate organism [101]. Zebrafish also allow for relatively easy to perform genetic manipulations such as ENU treatment, morpholino, and CRISPR/Cas9-gene editing transgenesis [101, 102]. Furthermore, a growing collection of generated mutants, knockout, and transgenic lines provides valuable resources for investigators. Of note, human and zebrafish Shoc2 amino acid sequences are 88% identical

[103]. Therefore, to investigate the role Shoc2 plays in embryonic development, we utilize the zebrafish vertebrate model.

1.5 Introduction to zebrafish neural crest

Neural crest cells (NCCs) are a transient, multipotent cell population that are critical for vertebrate embryonic development [104]. Neural crest (NC), often called the 'fourth germ layer' is a seemingly homogenous "pseudo" germ layer with the remarkable ability to migrate great distances throughout the development of an embryo [105]. NCCs are ultimately responsible for giving rise to multiple tissues including craniofacial cartilage, bone, pigment cells, and the majority of the neurons and glia of the peripheral nervous system. Minor perturbations in signals regulating NC development can result in severely deficient NCC-derived tissues.

The Galperin lab previously generated and characterized a zebrafish Shoc2 *null* model and determined that Shoc2 is NCC autonomously expressed [103]. Furthermore, the loss of Shoc2 resulted in abnormal development of NC-derived craniofacial cartilage and bone structures and melanocytes. These studies unravel the previously unrecognized role of Shoc2 in the formation of NC-derived tissues. Therefore, to understand the pathology of NSLH it is necessary to decipher the mechanism by which the Shoc2 scaffold regulates NCCs' developmental processes.

Within this chapter, briefly discussed is each progressive stage of NC development and its governing gene regulatory network (GRN). In short, the NC fold is initially induced at the neural plate border (NPB) and cells are subsequently specified as bonafide NCCs during neurulation [106]. Following an epithelial-to-mesenchymal transition (EMT),

NCCs delaminate from the dorsal neural tube and migrate to far-reaching locations throughout the forming embryo **(Figure 1.4)** [104]. Following delamination and migration, the NCCs undergo terminal differentiation. This complex series spanning the initial NPB establishment, cell relocalization, to the final differentiation is carefully conducted by a GRN composed of transcription factors that cross-regulate each other (**Figure 1.5**) [107]. The GRN temporally and spatially directs the development of the NC through each critical step and provides the NCCs with their characteristic properties such as robust migratory abilities and maintained multipotency until their final differentiation [107, 108].

1.5.1 Formation of the NPB

The neural plate border (NPB) is a transient territory containing all ectodermal precursor cells adjacent to the neural plate [109, 110]. Its formation during gastrulation is a critical, progressive step during embryogenesis. Initially, four distinct multipotent progenitors (future central nervous system neuroepithelial cells, NCCs, placodal progenitors, and epidermal cells) dwell intermingled at the undefined border [106]. These populations require distinct segregation while their identity and multipotency is maintained to sustain the populations' full lineage capacity. The spatial boundaries outlining the NPB region from future neural progenitors and epidermal regions are defined by a carefully orchestrated mediolateral gradient of BMP and WNT activity [111, 112]. BMP and Wnt antagonists are secreted in the medial region of the early embryo while BMP and Wnt signals are in the lateral aspect of the embryo. A molecular gradient is generated spanning the entire embryo. Of note, low BMP concentration induces neural specification while an intermediate BMP concentration supports the formation of the NPB. Thus, the NPB will be established in a region with balanced activating and inhibitory signals. Then, the BMP

and Wnt pathways cooperatively induce the expression of a set of transcription factors. These are known as NPB specifiers and are critical for the establishment of defined NPB boundaries. A number of NPB specifier genes have been the focus of the investigation presented in **chapter 4** including SRY-box transcription factor 2 (*sox2*), Paired Box 7 (*pax7*), PR domain zinc finger protein 1 (*prdm1a*) (**Figure 1.5**).

Sox2 is one of the earliest expressed neural progenitor transcription factors. It promotes spinal cord fate and is predominantly expressed in the neural ectoderm medial to the future NPB. The expression of *Pax7* however is restricted to the NPB thereby critical for establishing the territory borders [113]. P*rdm1a* is expressed at the NPB and activates Forkhead box D3 (*foxd3*) – a transcription factor essential for the sequential NCC specification and differentiation NC development processes (discussed in **1.5.2** and **1.5.5**). Finally, inhibitory transcription factor interactions between neural plate and NPB transcription factors further sharpens the spatial border between the two areas.

After its formation, the NPB is located between the neural (gives rise to the neural tube) and non-neuronal (epidermal) ectoderm (**Figure 1.4)**. All future multipotent NCCs will arise from the emergent NBP. Furthermore, the establishment of the NBP is closely associated to neural induction and both are presumed to be controlled by the same signaling pathways, positive and inhibitory regulatory interactions.

1.5.2 NC specification

Transcription factors expressed in the NPB and signaling gradients activate and/or maintain the expression of NC specifier genes (**Figure 1.5**). The NC specifier gene module is expressed by pre-migratory NCCs to drive the active phase of specification. This initiates

at the end of gastrulation and the start of somite specification (approximately 10.5 hpf). Some of the best-characterized transcription factors are *foxd3, SRY-Box transcription factor 9 and 10 (sox9 and sox10),* and *snai2 family transcriptional repressor 2 (snai2)* and are discussed briefly below. These specification transcription factors are utilized for the maintenance of the NCCs' undifferentiated state, full plasticity potential, and stability of the NC. Abnormal expression of these transcription factors will hinder NC development and NC-derived tissues [108].

For example, *foxd3* is one of the earliest NC specifiers in zebrafish. It is required for the expression of additional NCC specifiers and is essential for NCC formation [114, 115] It is activated by the NPB specifier *prdm1a* directly binding to its enhancer. Knockdown of *prdm1a* using MO and *prdm1a* knockout mutant (*narrowminded* and *u-boot*) embryos all exhibited a reduced number of NCCs and deficient *foxd3* expression. This resulted in abnormal craniofacial cartilage development and the loss of sympathetic and enteric neurons [116, 117].

Sox10 is another critical transcription factor broadly involved in multiple stages of NCC-related development processes. *Sox10* expression is activated by *prdm1a* and *sox9* (a transcription factor expressed in pre-migratory NCC) and is required for NC specification [118, 119] The loss of *sox10* during NC specification results in abnormal NC derivatives pigment cells, craniofacial cartilage, and cranial and dorsal root ganglia[120, 121].

Zebrafish have two orthologues of *sox9* (*a* and *b*) which are expressed in the specifying NCCs [122, 123]. Together, they act within NCC progenitors for the specification of cranial NCCs destined to be the pharyngeal arches. The loss of *sox9* results

in deficient NCC specification and abnormal craniofacial structures. Later in development (3 dpf), *sox9a* drives the expression of the ECM coding genes *col2a1, acana,* and *acanb*.

Finally, the expression of s*nai2* is critical for NCC specification and prepares cells for their epithelial mesenchymal transition (EMT). In humans, both over and under expression of *snai2* is associated with aberrant NC development. Thus, the specific role of *snai2* during NC specification is critical for the development of NC-derived tissues [124-126].

Once NCCs are specified, they will express *crestin*, a pan-NCC specific marker [127]. *Crestin* is a family member of retroelements and is expressed in all bonafide NCCs. It is a general marker to identify NCC patterning and distribution within an embryo. While *crestin* expressing NCCs remain undifferentiated at this stage, the specification process drives the fate of NCCs into their initial sub-lineage prior to their long-distance migration.

Taken together, specification is a critical process to prepare NCCs for their final destination and terminal lineage differentiation. Misregulation of the hierarchical developmental processes propagates irregular gene expression and ultimately anatomical abnormalities. Thus, the fidelity of each subsequent NC development process is critical for proper embryogenesis.

1.5.3 The epithelial to mesenchymal transition

Migration of NCCs to their final destination is a complex process that requires changes in NCCs' morphology, adhesive properties, and polarity [128, 129]. At this stage, specified NCCs transition into actively migrating mesenchymal cells and pass through an

epithelial-to-mesenchymal transition (EMT) [130, 131]. A discrete hpf for the EMT is not clear because specified NCC cells undergo a progressive transition. The notion that EMT is not a 'binary switch' from adhesive epithelial to dispersed mesenchymal cells, but, rather is a gradual process during which cells pass through a spectrum of morphologies (neither entirely epithelial nor mesenchymal) is supported by literature [132]. This morphological transition is regulated by many effector genes including several transcription factors that are also involved in NCC specification (e.g. *foxd3, pax3/7, snai1/2,* and *twist*) [130]. In zebrafish, the transcription factors *snai2a/b* and *twist1a/b* are expressed in NCCs at the time of EMT and are often used as markers of NCCs undergoing EMT.

The protein effectors Epithelial cadherin (E-cadherin, *cdh1*) and Neural cadherin (N-cadherin, *cdh2*) also facilitate the NCCs' EMT [133, 134]. These cadherins' expression is dynamic according to the cellular directives. E-cadherin (*cdh1*) provides cells with adhesion and tissue integrity by binding with catenin proteins while N-cadherin (*cdh2*) expression is expressed in motile cells. Thus, *cdh1* is typically expressed in premigratory cells while *cdh2* is prominent in migratory cells. Interestingly, *snai2* drives this cadherin conversion by binding directly to the *cdh1* promotor to downregulate the expression of E-cadherin [135] (**Figure 1.6**).

1.5.4 NC migration

Migratory NCCs travel collectively along pre-determined pathways before reaching their end destination and differentiating into various derivatives including osteoblasts, chondrocytes, melanocytes and Schwann cells (**Figure 1.7**). NCCs are divided into three groups, cranial, vagal, and trunk NCCs (**Figure 1.8**) and will populate their respective

destinations. Their migration is driven by cell-to-cell interactions combined with microenvironment attractive and repulsive cues. Transcription factors regulating NCC migration include *sox10, distal-less homeobox2a* (*dlx2a*) *foxd3, sox9* and *snai2*. Arguably, *sox10* is a key regulator of NCC migration and is expressed in both cranial and trunk migrating NCCs.

Zebrafish cranial and trunk NCCs begin their migration at approximately 13 and 15 hours post fertilization (hpf) respectively. Cranial NCCs have two subpopulations that either migrate anteriorly from the midbrain to help form the neurocranium or, they migrate ventrally into the pharyngeal arches and visceroranium in streams of cells [136]. *Dlx2a* marks migrating NCC that contribute to the pharyngeal arches [137] while *sox10* and *sox9a* are crucial regulators of the cranial NC GRN [138].

Trunk NCCs migrate on two separate pathways and are clearly labeled with *crestin, sox10, foxd3,* and *snai2*. Initially they migrate laterally along the medial line, anterior to posterior, between the neural tube and the nascent somites. Subsequently, they expand ventrally between the somites and the dorsally located ectoderm. The migratory mesenchymal streams of NCCs ultimately colonize multiple parts of the embryo. They then undergo a reverse EMT transition in compartmentalized territories that are distinctly regulated for the appropriate fated lineage. Finally, NCC will unite creating complex structures that will ultimately become neurons, glia, cartilage, bone, and contribute to organs.

The distinct origin (midbrain/hindbrain and/or anterior portion of the somite region) of zebrafish vagal NCCs that contribute to cardiac cells is unclear. However, post-otic

vagal NCCs arise entirely from somites numbers 1-7 and give rise to the enteric nervous system (ENS). Around 32 hpf, the ENS precursor NCCs begin migrating anteroposteriorly in two parallel streams reaching the most posterior destination by 66 hpf prior to differentiation.

1.5.5 NC differentiation

Terminal differentiation of NC sub-lineages is the final phase for the developing NCCs. Based upon cascades of networking signals that began during their specification, NCC are induced to form specified tissues according to their signaling environment. A curtailed summary of the GRN regulating NCC chondrocyte, melanocyte, and glia differentiation is outlined below.

The transcription factor *sox9* is required for chondrocyte differentiation. It is a direct regulator of protein coding genes *col2α1* (Collagen Type II, alpha 1 chain) and the cartilage differentiation marker *acan* (also known as *agc1*, Aggrecan) [139]. The loss of *sox9* disrupts cartilage formation by reduced Collagen Type II and Aggrecan expression [122, 140].

The differentiation of NCC into melanocytes primarily relies on the transcription factors *sox10* and *melanocyte inducing transcription factor* (*mitf*), a marker of melanocytes, by a feed-forward mechanism. *Sox10* drives melanocyte differentiation directly by activating *mitf* [141]. *Mitf* in turn activates enzymes that are responsible for melanin synthesis to produce pigmentation.

Finally, NCC differentiate into glia (non-neuronal nervous system support cells), specifically, Schwann cells (supportive and/or myelin producing glia of the peripheral nervous system) [142, 143]. This lineage differentiation is under the influence of *sox10* and *krox20* (also known as e*arly growth response 2*, *egr2*). Aberrant expression of these genes can ablate Myelin expression and lead to neuronal dysfunction.

In summary, the development of the NC is tightly regulated by a governing GRN. Each sequential process of NC development, NPB formation, NC specification, NCC EMT and migration, and final terminal differentiation is crucial during embryo development for normal tissue morphogenesis. Developmental abnormalities can be attributed to specific stages or gene perturbations through a comprehensive understanding of the molecular mechanisms driving NC development.

1.6 The lymphatic system and fluid homeostatsis

The lymphatic system is a whole-body, physiological system composed of nodes, vessels, ducts, organs, and tissues. It is responsible for three major physiological functions. First, it plays an integral role for the immune system *via* immune cell production and foreign body surveillance. Second, it facilitates the absorption of large molecules such as fatty acids and hormones into the peripheral blood circulatory system. Finally, and most relevant within this study, the lymphatic system functions to return extravasated fluid from tissues' interstitial space to the peripheral blood circulation [144]. This process thereby maintains an organisms' fluid homeostasis.

To this end, lymphatic vessels and capillaries form an interwoven vasculature network through tissues and are integrated among blood circulatory vessels. There, they

take up excess interstitial fluid and facilitate its transport into a vein (**Figure 1.9**). Aberrant lymphatic system physiology from damaged, blocked, developmentally impaired, or absent lymphatic vessels can cause severe fluid accumulation interstitially, subcutaneously, or in body extremities communally termed lymphedemas [145]. Primary lymphedemas, relevant to this study, are caused by inherited genetic mutations in genes that are essential for the development of lymph vessels.

For example, lymphedema formation has been reported in multiple congenital RASopathy syndromes, including NSLH [79, 146, 147] (**Figure 1.10**). Furthermore, RASopathy induced edemas can occur *in utero* resulting in fetal hydrops (a condition from the accumulation of interstitial fluid within fetal compartments) [79]. Despite the severity, treatment is only symptomatic. Vital information about the aberrant regulation and formation of RASopathy patient lymphatic system is missing for improved treatment.

Novel zebrafish models (discussed later in chapter 5) have recently expanded the fields' knowledge about lymphatic vessel development. The nascent formation of functional lymphatic vessels requires sequential developmental steps. Typically, the lymphatic vasculature network is formed primarily from a limited number of lymphatic endothelial cell (LEC) progenitors that differentiate from pre-established blood endothelial cells (BECs). In zebrafish, LECs then sprout from the cardinal vein and steadily delaminate from to form primitive lymphatic vessels prior to their additional migration and specification (**Figure 1.11**) [148].

1.7 Scope of the dissertation study

The studies presented in this dissertation are focused on deciphering the molecular mechanisms of the scaffold protein Shoc2 in NCC during embryonic development. Additionally, preliminary data demonstrates the novel, critical requirement of Shoc2 for lymphatic vessel development. **Chapter 2** supports data reproducibility by presenting the detailed methodology utilized in this study. **Chapter 3** summarizes a set of data that examines the physiological role of Shoc2-transmitted ERK1/2 signals in neural crest cells during embryonic development. I found that Shoc2 is essential for Neural Crest Cell specification, migration, and terminal differentiation. Furthermore, Shoc2 regulates NCC ECM components' expression and processing. **Chapter 4** presents a characterization of a novel Shoc2 *null* zebrafish line. **Chapter 5** summarizes preliminary data suggestive that Shoc2 is required for lymphangiogenesis and disruption of Shoc2-mediated ERK1/2 signaling results in embryo edemas. Finally, **Chapter 6** discusses the physiological function of Shoc2 in NCCs during development, the role of Shoc2 for lymphangiogenesis and will explore possible future directions for both of these studies.

1.8 Tables and Figures, Ch. 1

Shoc2 interacting partners	Binding domain of Shoc2
Rat sarcoma virus (RAS)	N-terminus
Valosin containing protein (VCP)	LLR 12-14
Ubiquitin carboxyl-terminal hydrolase 7 (USP7)	LLR 13
HECT-domain E3 ligase (HUWE1)	LLR 12-14
Proteasome 26S subunit, ATPase 5 (PSMC5)	LLR 20-21
Scribbled homolog (SCRIB)	C-terminus
Catalytic subunit of protein phosphatase 1c (PP1c)	LLR domain
Erbb2 Interacting protein (ERBIN)	LLR domain

Table 1.1 Shoc2 binding partners and Shoc2 binding domains

The scaffold protein Shoc2 has multiple interacting partners. Both the unstructured N-terminus and the LLR region can facilitate protein interactions. The significant binding region for these proteins has been narrowed to specific termini or LLRs within Shoc2.

	Patients (%)	Reported characteristic
>75%	99%	Short stature
	80%	Macrocephaly
	80%	Low set/posteriorly rotated ears
	76%	Hypertelorism
	76%	Thin/loose anagen hair
>50%	73%	Cognitive delays/retardation
	63%	Ptosis
	57%	Prominent forehead
	53%	Webbed/short neck
	51%	Pectus anomaly
≥30%	44%	Delayed development
	43%	Atrial or ventricular septal defect
	41%	Pigmentation spots/dark skin
	33%	General ocular deficits
	32%	Ichthyosis
	30%	Pulmonic valve stenosis
	30%	Feeding difficulties

Table 1.2 Shoc2 S2G varient induced phenotypes

The most frequently reported clinical phenotypes from 79 patients carrying the pathogenic *shoc2* c. 4>G variant (p.Ser2Gly). An additional 50 phenotypes (not listed; 67 total) were recorded in the examined clinical articles demonstrating the wide range of physiological effects from aberrant Shoc2-mediated ERK1/2 signaling.

DNA mutation	Amino acid substitution	Reference
c. 4A>G	p. Ser2Gly	[67]
c.807_808delinsTT	p.Gln269_His270delinsHisTyr	[97]
c.806A>G	p. Gln269Arg	[98]
c.1231A>G	p. Thr411Ala	
c.806A>G	p. Gln269Arg	
c.157G>A	p. Gly53Arg	
c. 519_520delinsAT	p.Met173_Leu174 delinsIlePhe	
c. 519A>G	p. Met173Ile	[149]
c. 713G>A	p. Cys238Tyr *	[49]
c. 267G>C	p. Glu89Asp *	
c. 1417T>A	p. Leu473Ile *	

Table 1.3 Shoc2 mutations reported in patients

Clinical reports of *shoc2* mutations and the corresponding amino acid substitution improves patient diagnosis. The DECIPHER database is an online database of rare genomic variants with associated phenotypes. Amino acids substitutions reported on DECIPHER are marked with an asterisk have been validated *in vitro* and *in vivo* [49]. Substitutions at residues p. 269 and 173 were previously recorded by different gene mutations and are marked with color.

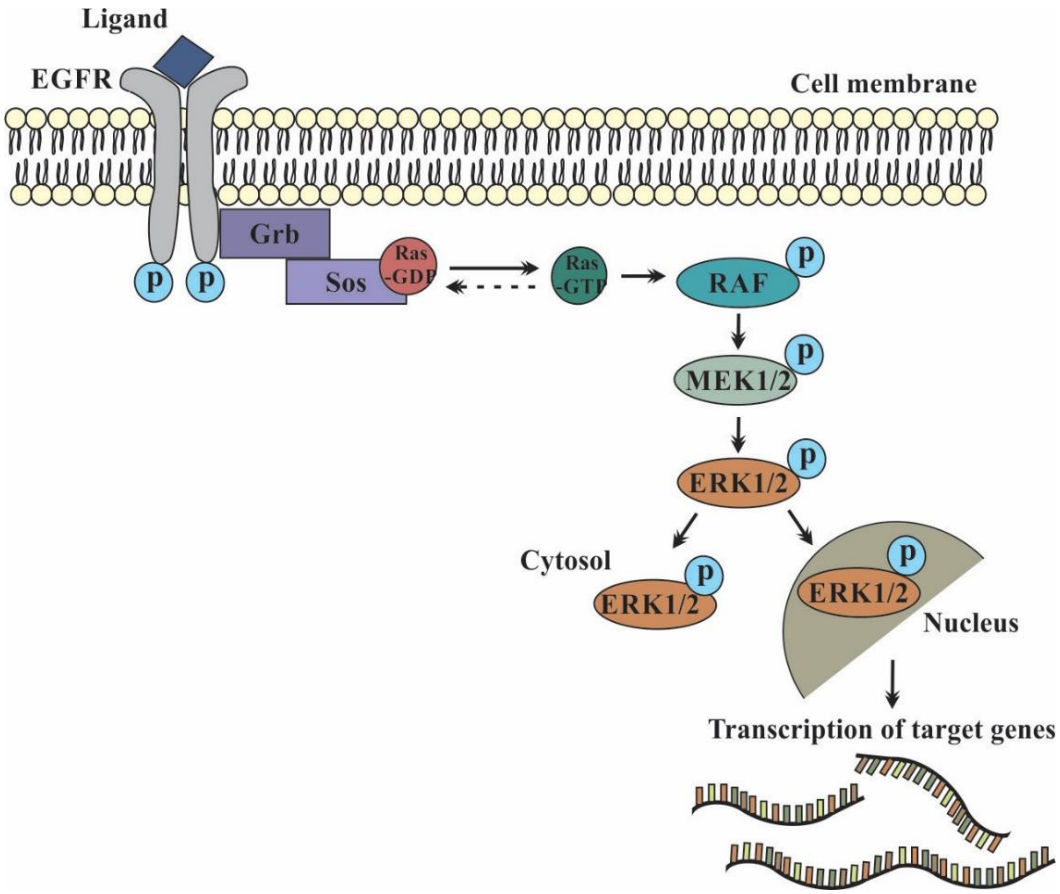

Figure 1.1 The ERK1/2 signaling pathway

The RAF-MEK-ERK pathway is a linear triad that ensues cellular signaling propagation by a phosphorylation cascade. The pathway is initiated when extracellular ligands (growth factors and cytokines) bind to the extracellular receptors at the cell membrane. The ligand (EGF shown above) bound EGF receptor dimerizes, undergoes autophosphorylation, then recruits the adaptor protein, Grb2, which is bound to Sos, a guanine nucleotide exchange factor. GDP-RAS is then activated while at the cell membrane. The now active GTP-bound RAS further conveys the signal by recruiting and binding protein kinases Raf (cRAF-1, B-RAF, and A-RAF) which also becomes phosphorylated. Subsequently, MEK1/2 is phosphorylated by RAF which then phosphorylates ERK1/2. Finally, for a cellular effect, downstream cytosolic and nuclear targets are activated by pERK1/2.

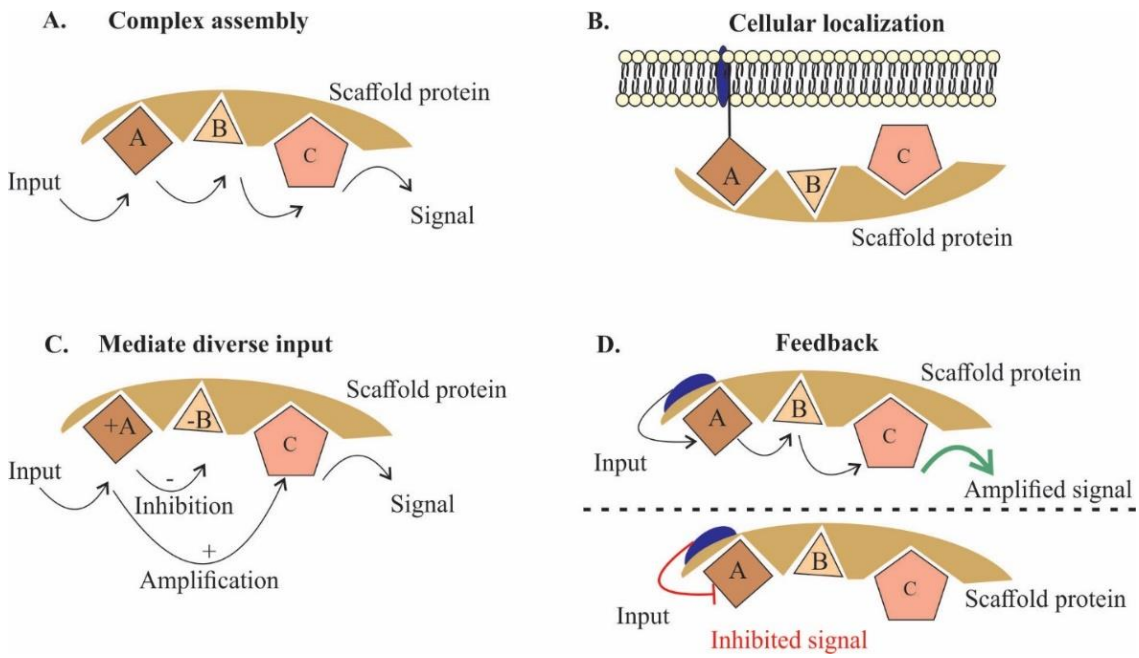

Figure 1.2 Properties of scaffold proteins

Scaffold proteins can simultaneously interact with multiple proteins to promote efficient signal transduction (**A**), facilitate the signaling complex to a specific cellular site such as the cell membrane **(B)**, integrate both positive and negative signaling input **(C)**, and regulate the pathway by providing and mediating feedback **(D)**.

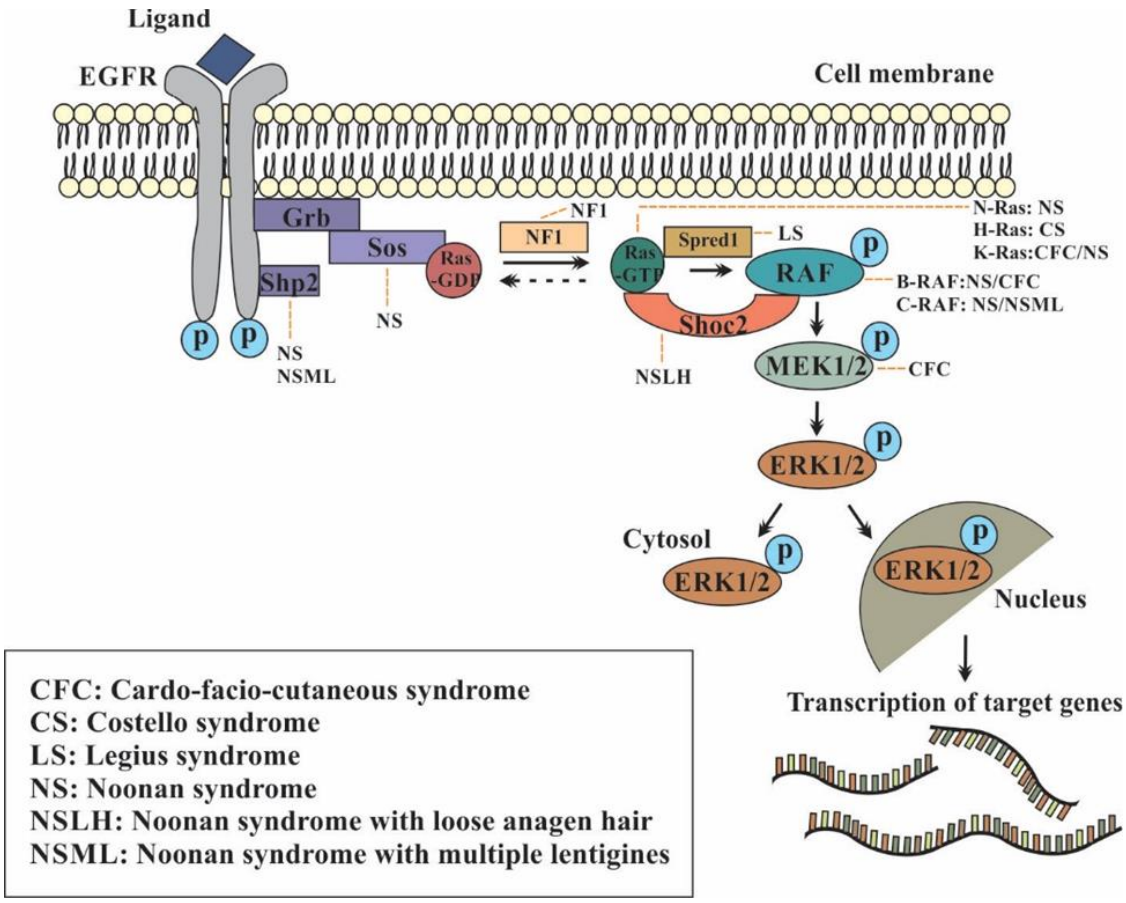

Figure 1.3 The RAS/ERK1/2 pathway and associated RASopathy syndromes

Together, RASopathies are a classification of individual, congenital medical syndromes that arise from pathogenic germline variants in genes that encode components of the RAS/MAPK pathway. Here, the hyphenated lines indicate a causative component for each individual syndrome. This gene-RASopathy compilation is not comprehensive of the possible pathogenic variant genes nor the resultant syndromes.

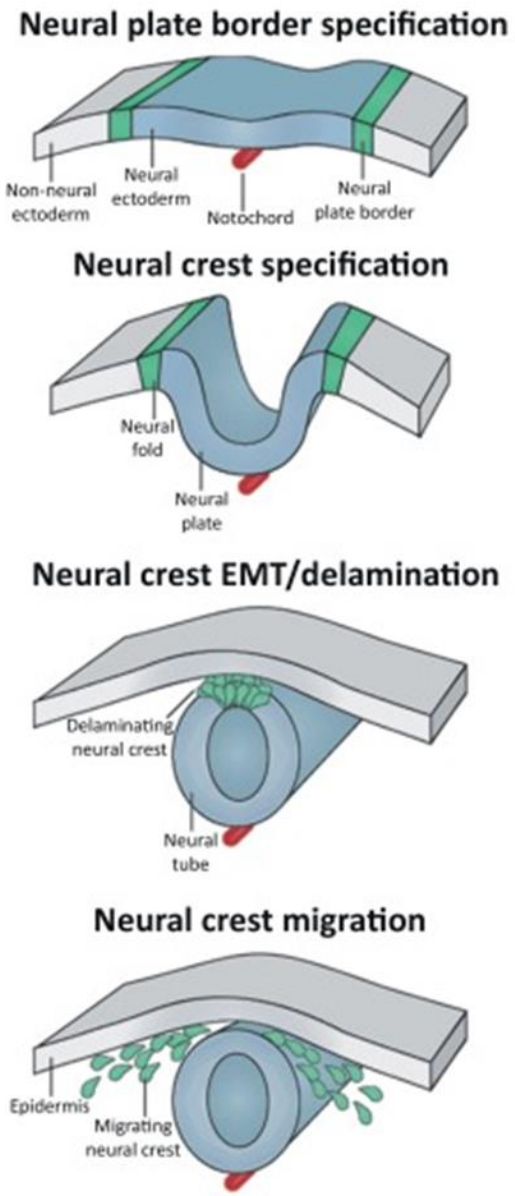

Figure 1.4 Neural crest formation and development

Modified from [108]. Boundaries between the neural ectoderm and the NPB are clearly established during embryogenesis gastrulation. The neural plate folds inward to become the neural tube while tightly regulated signaling invokes a myriad of transcription factor activation that specifies cells into established NCCs. After the neural tube closes, premigratory NCCs undergo an EMT prior to delaminating from the dorsal side of the neural tube and initiating their extensive migration to various end destinations.

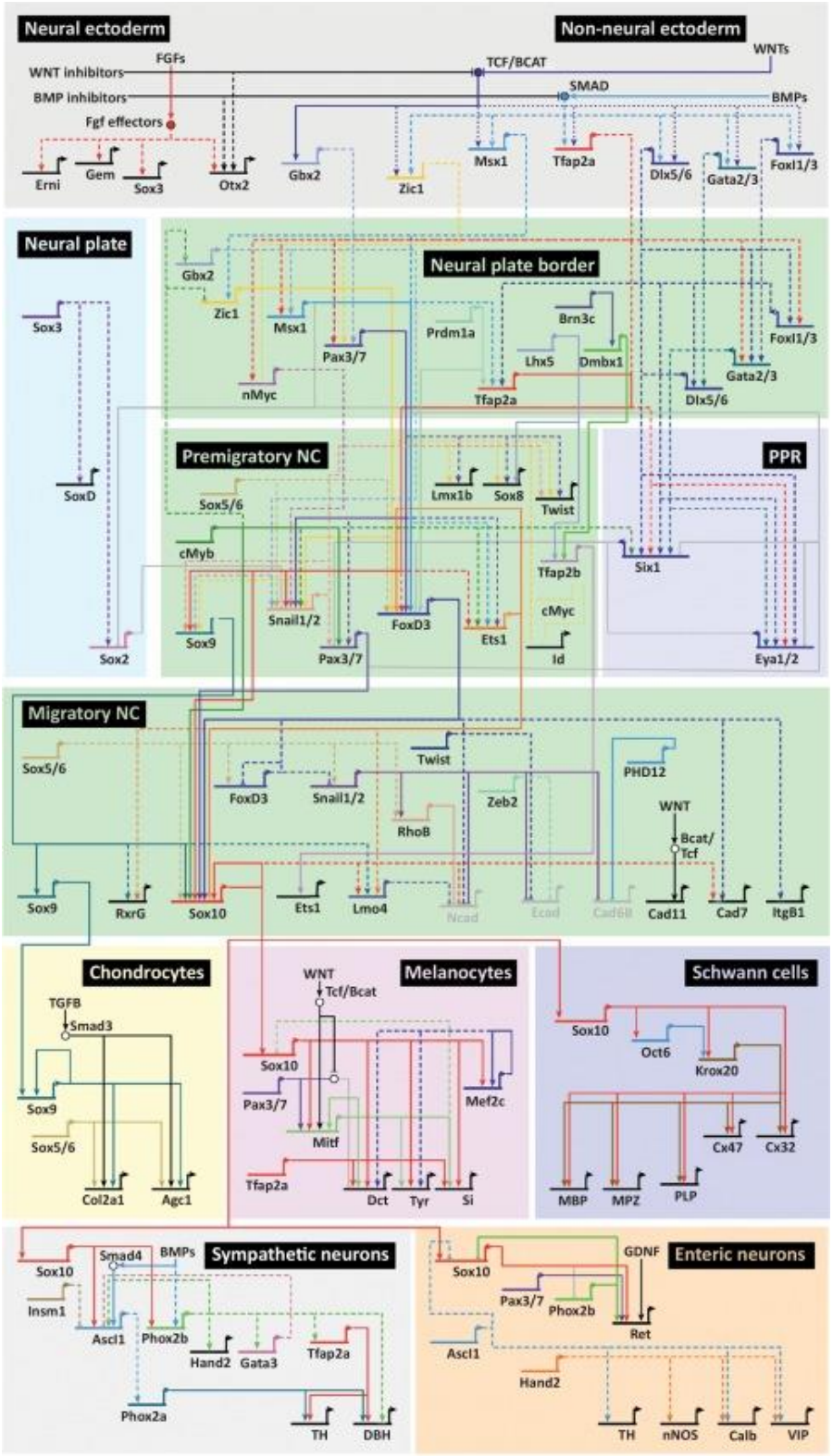

Figure 1.5 Gene regulatory network controls NC development

Modified from [108]**.** A complex GRN elicits the NPB formation, and NC specification, delamination, migration, and terminal differentiation. The underlying circuitry provides insight into development mechanisms, cell programming, and developmental diseases. Improved technology is advancing the insight of NC development at each process. PPR: Pre-placodal region.

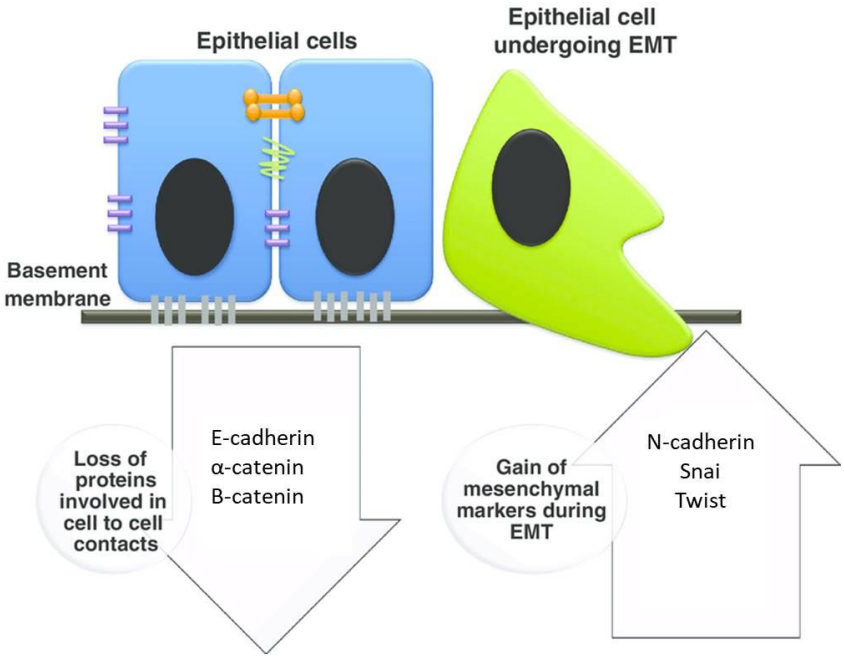

Figure 1.6 EMT molecular changes

Modified from [135]. E-cadherin and catenins are lost during EMT while N-cadherin, *snai* and *twist* are upregulated. The adheren junctions are lost enabling NCC migration.

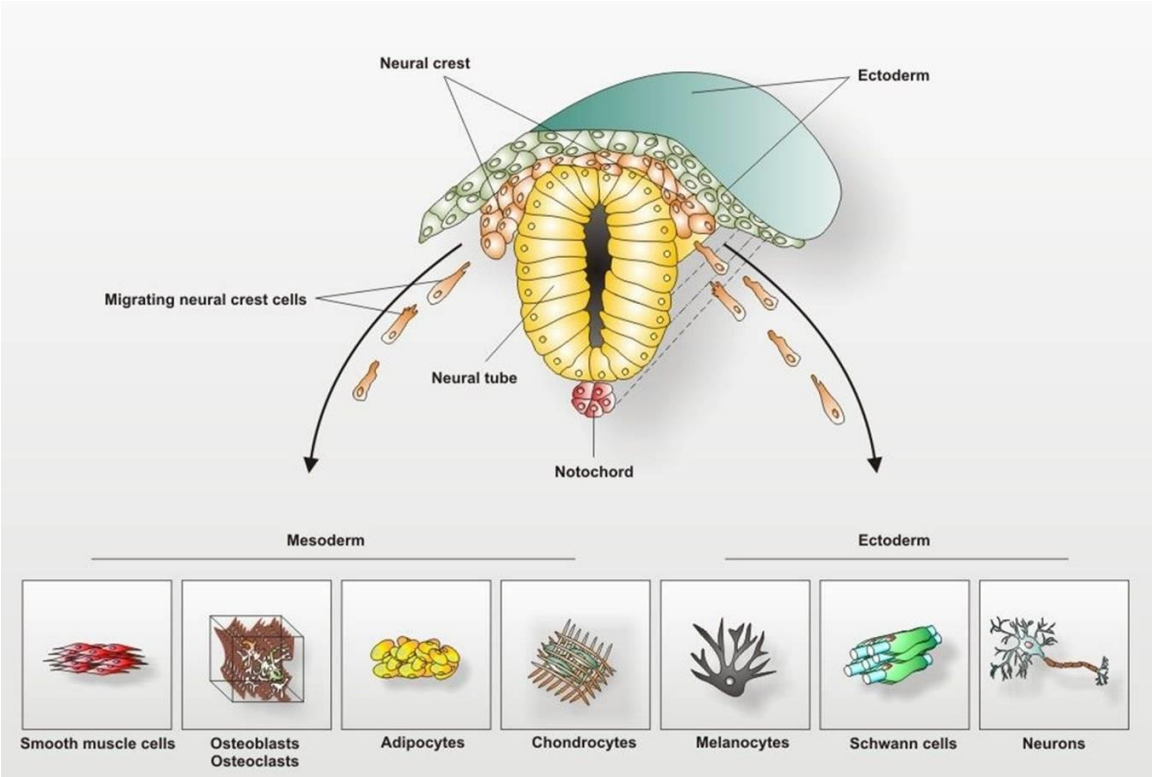

Figure 1.7 NCC migration and terminal lineages

Modified from [150]. Specified NCC are located between the ectoderm and the dorsal aspect of the neural tube. Subsequent to their EMT, NCC will delaminate and migrate throughout the embryo and terminally differentiate into multiple distinct lineages including osteoblasts, chondrocytes, melanocytes and neurons.

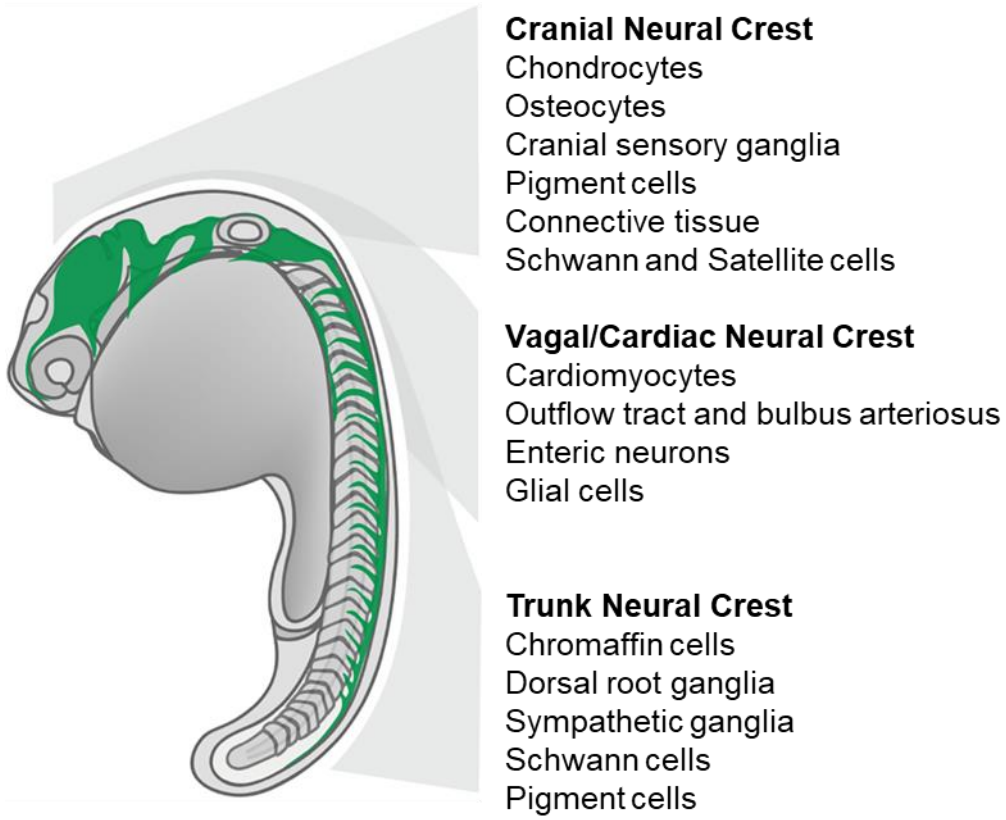

Figure 1.8 NCC regionalization and derivatives

Modified from [109]. The lineage fates of the zebrafish anteroposterior level NCCs are indicated in the schematic.

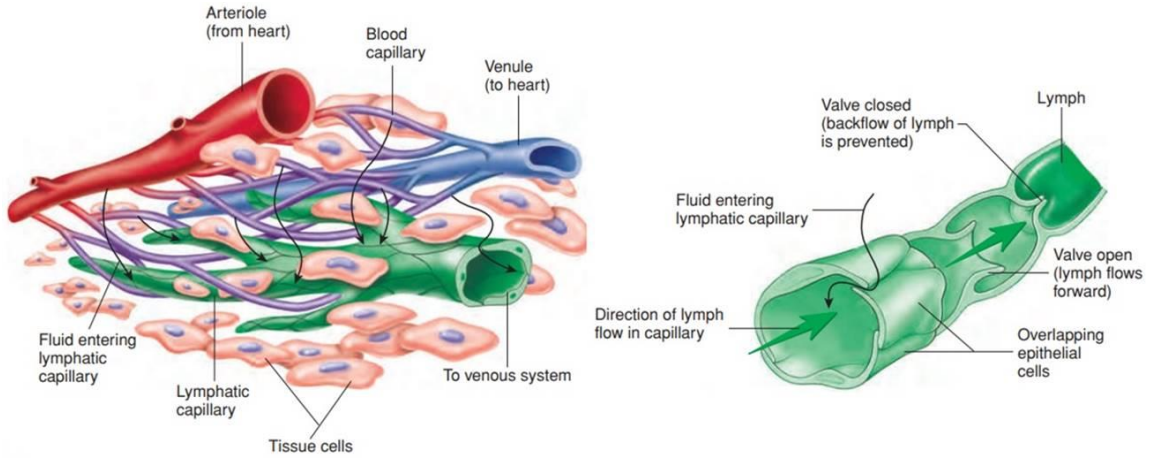

Figure 1.9 Lymph vessel network and structure

Modified from [151]. Lymph vessels form a vasculature network that is integrated through tissues and intermingled among peripheral blood vasculature. Lymphatic capillaries take up interstitial fluid exuded from arterial capillaries. Their overlapping epithelial cell wall prevents the loss of the accumulated lymph and facilitates a unidirectional flow. Ultimately, lymph is returned to the blood circulatory system via venous vessels after its transport through lymphatic vasculature.

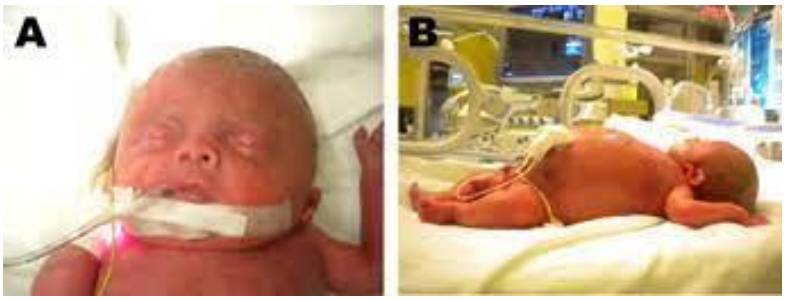

Figure 1.10 *Shoc2* mutation c.4A>G causes hydrops fetalis in preterm newborn

Craniofacial features of the newborn. Skin edema, hypertelorism, slight downslanting palpebral fissures, posteriorly angulated lowset ears, with thick helix, and up-lifted lobes. B: Diffuse thick cutaneous edema, distension of the abdomen with severe ascites. Image taken from [79].

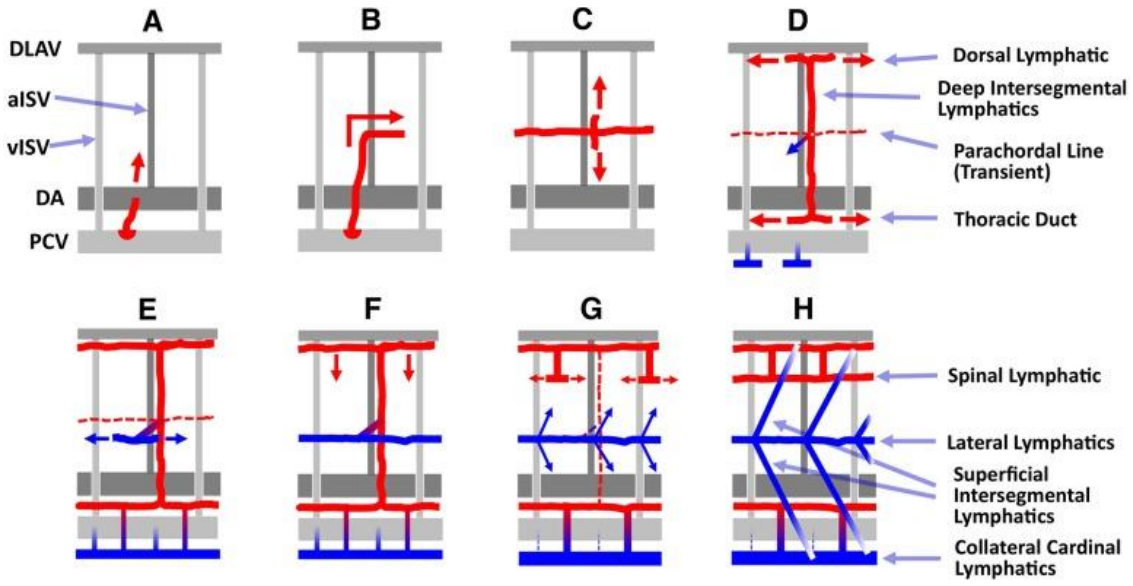

Figure 1.11 Trunk lymphatic network establishment

Modified from [152]. The early lymphatic vascular network is established during from 1-5 dpf (**A-D)** while the later network is formed from 6-14 dpf (**E-H**). A stereotyped and pattered formation of the lymphatic vasculature network is critical to its proper development. The lymphatic vasculature network initiates its formation as sprouts from the cardinal vein at 1.5 hpf. These immature sprouts contribute to the formation of the transient parachordal line by 3 dpf. Sprouts from the parachordal line expand dorsally and ventrally following the intersegmental arteries between days 3-5. These lymphatic sprouts anastomose forming the most major lymphatic vessel, the thoracic duct located just inferior to the dorsal aorta. Major arteries: dark gray. Major veins: light gray. Lymphatics: red. Lateral lympathcis and CCLs: blue. CCL: collateral cardinal lymphatics. SL: spinal lymphatics. DA: dorsal aorta. PCV: postior cardinal vein. DLAV: dorsal longitudinal anastomotic vessel. aISV: arterial intersegmental vessels. vISV: venous intersegmental vessels.

CHAPTER 2. MATERIAL AND METHODS

Zebrafish strains and maintenance

All zebrafish (Danio rerio) strains were bred, raised, and maintained in accordance with established animal care protocols for zebrafish husbandry. Embryos were staged as previously described [153]. All animal procedures were carried out in accordance with guidelines established by the University of Kentucky Institutional Animal Care and Use Committee. Briefly, zebrafish embryos were raised at 28.5°C and kept in 14/10h light/dark cycle. When necessary, 1-Phenyl-2- 673 thiourea (0.002%) was added to the embryo media to prevent pigment development. Shoc2Δ22 zebrafish were maintained as heterozygotes and incrossed to generate homozygous mutant embryos. The Shoc2Δ22 heterozygous mutant line was crossed with available reporter lines Tg(sox10:RFP). The mutant shoc2 zebrafish line Shoc2 E2Δ22+/- (ZDB-GENE-050208-523) was reported previously [103] The double-transgenic zebrafish reporter line Tg(mrc1a:egfp)y^{251}; Tg(kdrl:mcherry)y^{171} was previously published [152] F2 fish carrying the *shoc2* sa24400 allele was generated *via* mutagenesis with N-ethyl-N-nitrosourea and acquired from The Sanger Institute Zebrafish Mutation Project [154]. Sa24400 fish were subsequently outcrossed with AB WT fish a minimum of four times prior to experimental data collection.

Morpholino and mRNA injection

All MOs were obtained from Gene Tools, LLC (Philomath, OR) and injected into 1-2 cell stage zebrafish embryos. The following MOs were used in this study: standard control MO: 5'- CCTCTTACCTCAGTTACAATTTATA-3'; shoc2 MO1: 5'-

TACTGCTCATGGCGAAAGCCCCGCA-3'. Embryos were injected with 5.2 ng each of MOs.

Genotyping

Genomic DNA was extracted from individual embryos or adult tail clips. Briefly, 20 µl of the ThermoPol Buffer (New England Biolabs, # B9004S) was added to the samples and boiled for 5 min. Samples were digested with 50µg (5µL) Proteinase K (Millipore Sigma, #p22308) for 12 hours at 55 °C. Proteinase K was then inactivated by boiling for 10 min. PCR was carried out in a 25 µl reaction solution containing: 1 µl of 10 mM dNTP, 1 µl of 10 mM forward and reverse 691 primer, 2.5 µl of 1x ThermoPol buffer and 0.5 units of Taq Polymerase (New England Biolabs, #M0267). The shoc2Δ22 heterozygous mutant allele was detected using the primers forward 5'-CCATCAAGGAGCTGACCCAG-3' and reverse 5'- AGTCAGGTAGGCTGGTCAGA -3'. The *shoc2* sa24200 mutant allele was detected using the primers forward 5'-TCCCTTTTGGCATTTTCTCTCG-3' and reverse 5' -GAGTTTGTTCAGCCAGCATCC-3'. The PCR products underwent a 2 hour HphI restriction enzyme (New England BioLabs, MA) digest at 37°C. Samples' allele homozygosity or heterozygosity was determined by samples' DNA digestion or lack thereof at the restriction enzyme and *shoc2* (1546G>A) mutation site of interest (G<u>G</u>TGAN_8). The PCR product was visualized on 4% high resolution agarose gel (GoldBio, MO) run in 0.5 TAE buffer (Bio-Rad, CA).

Skeletal stain

For Alcian blue staining, zebrafish larvae were fixed in 4% paraformaldehyde for 2 h at room temperature and stained according to Kimmel et al., [153]. Calcified structures were examined by acid-free Alizarin Red S staining. Larvae were fixed in 4% PFA for 2 h and stained in a 0.05% Alizarin Red S solution for 30 min in the dark on low agitation. Larvae were then rinsed in a 50% glycerol, 0.1% KOH solution to remove excessive staining and kept at 4◦C in the same solution for imaging.

In situ hybridization

Linearized plasmid DNA was cleaned using DNA Clean & concentrator-5 (Zymo Research #D4014). In situ hybridization was completed according to a standard protocol [155] using DIG RNA labeling kit T7/SP6 (Millipore Sigma #11175025910). RNA probes were cleaned using SigmaSpin Sequencing Reaction Clean-UP (Millipore Sigma #S5059-70EA). Briefly, embryos were permeabilized with Proteinase K and hybridized in probes diluted to 3 ng/µl overnight at 65-68°C. The probe was removed and embryos were washed and blocked for a minimum of 1 hour prior to incubation in antidigoxigenin-AP, Fab fragments 1:2,000 (Roche, #11093274910). Signal was detected using NBT:BCIP (1.38:1.0 ratio) (Roche, NBT #11383213001 & BCIP #11383221001). Background staining was removed using brief five-minute washes with methanol. Embryos were cleared through a glycerol series and imaged on the system listed below. Typical spatial gene expression by the control morphants' was verified from published literature. Zebrafish spatial gene expression via WISH is readily assessable through The Zebrafish Information Network (zfin.org) Regions of *sned1* were amplified from cDNA using the

primers forward 5'- CATTACTCCCAGGTCAGATGTAC-3' and reverse 5'-TCAGGCTTAATGCGGTGTCT -3'. This amplified region was cloned into the pJET1.2/blunt Cloning Vector (ThermoFisher, #K1232) to generate both sense and anti-sense probes. Additional antisense DIG conjugated probes were synthesized from plasmids kindly gifted from: collagen2a1 (Dr. Tatjana Piotrowski, The Graduate School of the Stowers Institute for Medical Research, Kansas City, MO), acana & acanb (Dr. Adele Faucherre, Institut de Génomique Fonctionnelle, Montpellier, France), *sox10* (Dr. Rebecca Cunningham, Washington University in St. Louis, St. Louis, MO), and *crestin*, *dlx2a*, *foxd3*, *krox20*, *mbp*, *pax7*, *prdm1a*, *snai2*, *sox2*, *sox9a*, *runx2a*, and *runx2b* (Dr. Kristin Artinger, University of Colorado Anschutz Medical Campus, Aurora, Colorado).

TUNEL

Apoptotic cells in whole body embryos were detected using Millipore Sigma ApopTag Red In Situ Apoptosis Detection Kit S7165. TUNEL was performed as described in [156]. Briefly, embryos were fixed in 4% PFA/PBS, washed through a PBS/methanol gradient ending in 100% methanol and incubated at -20°C for at least one hour. Embryos were then sent through a PBSTw (0.1% tween-20 in PBS) gradient wash ending in 5 x five-minute washes in PBSTw. Embryos, 24 and 48 hpf were permeabilized for 4 or 27 minutes respectively in 20µg/100µL proteinase K (GoldBioP-480-1) prior to being re-fixed in 4% PFA/PBS. Whole embryos were incubated in 50uL equilibrium buffer for 15 minutes at 37°C before the 4 °C overnight incubation in the reaction mix (20uL equilibrium buffer, 12uL reaction buffer, 6uL TDT, 10% Tween-20). Five washes with PBST were completed before adding the stop/wash buffer for 5 minutes. Embryos were then blocked for 1 hour.

Finally, anti-DIG solution in blocking buffer was added to embryos and incubated for 30 minutes in the dark. Anti DIG was removed and embryos were washed PBST and incubated for 1 hour at 37°C in the Fluorescein in the dark. Images were captured as described below.

Phospho-Histone H3 Immunolabeling

Briefly, embryos were fixed in 4% PFA/PBS for 1 hour at room temperature. Embryos were washed in water for 5 minutes and then incubated one hour at room temperature in a blocking solution (2% goat serum, 1% BSA, 1% DMSO, 0.1% Triton-X-100, 1X PBS). Embryos were then incubated overnight at 4°C in primary antibody diluted in a blocking solution (Anti phospho-Histone H3 (Ser10) Antibody, Mitosis Marker, Millipore Sigma, 06-570). Embryos were thoroughly rinsed in PBS-Triton-X (0.1%). Next, embryos were incubated in the dark overnight in an Alexa488 conjugated secondary antibody diluted in blocking solution (1:750). Finally, embryos were rinsed with 0.1% Trition-X-100 and imaged.

Imaging methods and analysis

Images of whole-mount in situ hybridization and whole body Alcian blue staining were captured with a Leica DFC450 digital camera. Alcian blue ceratohyal images were acquired with a Zeiss Imager AzioCam MRm. Fluorescent images from methods TUNEL and pH3 immunolabeling were captured with a Leica M165FC microscope. Confocal fluorescence imaging was completed with a Nikon Yokogawa CSU-W1 spinning disk confocal microscope. Images were analyzed using Adobe Photoshop (Adobe) and NIS-Elements (Nikon) software.

Embryo deyolking

Embryo yolks were removed in deyolking buffer (55mM NaCl, 1.8mM KCl, 1.25mM $NaHCO_3$) on ice or at 4°C in a 1500µL microcentrifuge tube by the following protocol: dechorionated embryos were washed in cold 1x PBS and centrifuged for 1 min at 300g. The PBS was removed and embryos were resuspended in 300uL of cold deyolking buffer while intermittently vortexed for a total time of 5 min with alternating rest on ice. Embryos were centrifuged at 300g and the supernatant decanted. The pellet was washed with deyolking buffer and spun down three times at 300g.

Western blot analysis

Cell lysate protein expression was evaluated through western blot analysis completed as in [24, 103]. Proteins were extracted from de-chorionated and de-yolked embryos/larvae and resolved by SDS-PAGE. In short, water was removed from approximately 25 embryos in a microcentrifuge tube. One solid glass bead and 50 µL RIPA buffer containing protease inhibitors were added to the embryos. Gentle manual agitation physically lysed the embryos. Samples were centrifuged at 4 °C for 10 minutes at 14,000 RPM. Total protein lysate was removed from pellet and bead. 25µg of total lysate per sample was run on a 10% acrylamide gel. Western blot analysis was performed as described previously [49]. Quantification was performed using the densitometry analysis mode of Image Lab software (Bio-Rad, CA). Antibodies against the following proteins were used: MMP13 polyclonal antibody: Proteintech. #18165-1-AP. Collagen Type II. Developmental Studies Hybridoma Bank. #II-II6B3. Anti- actinin Antibody (H-2). Santa

Cruz. #17829. Anti-Sur-8 Antibody (E-4). Santa Cruz. #514886. Anti-β-Actin Antibody (C4). Santa Cruz #47778. Anti -p-ERK (E-4). Santa Cruz #sc-7383.

RNA-seq analysis

Zebrafish transgenic larvae were homogenized and fluorescence-activated cell sorted. Briefly, 6 dpf embryos were dissociated in trypsin using a 20G needle and incubated for 2 minutes at 37°C. This was repeated four times. Dissociated cells were strained through a 50µm strainer into 2mM EDTA/5%goat serum/PBS and centrifuged for 10 minutes at 3,500rpm. The cell pellet was resuspended in 1mM EDTA/10% goat serum/PBS. Cells were sorted for RFP+ identity at the University of Kentucky Flow Cytometry and Immune Monitoring Core at the Markey Cancer Center. After sorting, cells were centrifuged at 3,000rmp for 10 minutes. Supernatant was discarded and the RFP+ cells were frozen (-80°C) in PureZol (Bio-Rad. #732- 6890). Triplicates of RNA from RFP+ cells were purified as described above.

For library preparation, mRNA was first extracted from total RNA using oligo (dT) magnetic beads and sheared into short fragments of about 200 bases. The cDNA library was sequenced using Illumina NextSeq 500 sequencer. Quality control (QC) of the raw sequence data was performed using FastQC (version 0.11.7). The concatenated sequences were directly aligned to the Danio rerio GRCz11 reference genome assembly (GRCz11.fa) using STAR (version 2.6), generating alignment files in bam format. The alignment rate for each sample is above 90%. Fragments per kilobase per million mapped (FPKM) reads were determined for all RefSeq genes using CuffDiff 2 (FDR $\leq$ 0.05). For the Cuffdiff2 analysis, Cuffnorm was used to produce FPKM (Fragments Per Kilobase Million)

normalized counts. The counts were then filtered to include only genes with minimum expression of one FPKM in three or more samples and an average expression of at least one FPKM. The RNA-seq data is publicly available as GEO series GSE198231. The data is MIAME compliant [157].

Gene ontology (GO) and pathway and network analysis

Differentially expressed genes determined by RNA-seq analysis were used for functional enrichment including the Category Compare that predicts molecular and cellular functions using the Ingenuity Knowledge base as the background. Gene ontology terms within the data set were provided by Protein Analysis Through Evolutionary Relationships [158].

Drug treatments

To evaluate embryos' immune response in the absence of Shoc2, embryos were dechorionated at 48hpf and incubated at 28°C in E3 media containing one of the following anti-inflammatory glucocorticoids: dexamethasone (100uM), betamethasone 17-valerate (1uM), prednisolone (25uM) or DMSO equivalent concentration for at least 6 days. Medium was changed daily.

Albumin-Evans blue dye extravasation method

To detect potential blood vessel permeability defects, live 4, 5, and 6 dpf embryos were anesthetized (0.006% tricaine) and injected with an Evans Blue Dye and FITC-dextran injection mix into their pericardial region common cardinal vein as previously

described in [159, 160]. One minor modification was made to the established Evans blue dye injection protocol; the volume of FITC was reduced by half in the final injection mixture to reduce nonspecific autofluorescence. Embryos were incubated 4-6 hours in E3 media at 28°C prior to imaging vasculature.

Cell culture and infection of lymphatic endothelial cells

Human primary lymphatic endothelial cells (Cell Biologics #H-6092) were cultured in VascuLife VEGF Endothelial medium (complete kit) (#LL-0003) on 0.1% gelatin-coated tissue flasks. To silence or overexpress protein expression, cells were infected with *shoc2* targeting or nontargeting or lentivirus shRNA as in [161].

Iridophores cell counts

Incident light images of four-day old embryos' iridophores were captured with a Leica M165FC microscope. All iridophores in a 1350um long region in the tail (spanning approximately 11 somites) were quantified as in [162].

Statistical analysis

Results are expressed as means $\pm$ SEM. All statistical analyses were carried out using GraphPad Prism 9.3.0 software package. $P<0.05$ was considered statistically significant. Statistical significance was denoted as follows: not significant (ns) $p > 0.05$, $*p<0.05$, $**p<0.01$, and $***p<0.001$.

Real-time quantitative polymerase chain reaction (RT-qPCR)

Total RNA was isolated from cells or a pool of 25 embryos (or dissected embryo tissue) using PureZOL RNA Isolation Reagent (Bio-Rad, #732-6890) and Aurum Total RNA Isolation Kit (Bio-Rad, #732-6820). Aliquots containing equal amounts of RNA were subjected to RT-PCR analysis (Bio-Rad, iScript™ Reverse Transcription Supermix for RT-qPCR, # 1708840). qPCR was performed using Bio-Rad iTaq™ Universal SYBR® Green Supermix (#1725120) and a Bio-Rad CFX detection system (Bio-Rad, CA). Relative amounts of RNAs were calculated using the comparative CT method. Sequence-specific primer sets are presented in **Table 2.1**. The values for the samples were normalized against those for the reference gene, and the results are presented as the Log2fold change in the amount of mRNA recovered from WT and mutant embryo. The data represent the means ± SEM from three independent experiments.

Tables and figures, Ch 2

	Gene	Fwd	Rev	NT	Source
Zebrafish	*acana*	5'-GTCCGGTATCCCATCGTGTC-3'	5'-TGCATGGAAAACTTGACCCCT-3'	150	NCBI Primer Blast
	acanb	5'-GAGTTGAATGCATAAGGGGCATAG-3'	5'-GCACTCTGTGCTATTTTGTCTGT-3'	416	NCBI Primer Blast
	cdh1	5'-CCAAGATCCACCATCTCCAA-3'	5'-CCCTTGTCACCAGCAATGAT-3'	345	Babb et al., 2001
	cdh2	5'-TGTGAATCGCGTGAAAAGAG-3'	5'-AGCGTGTTGCTCTTGTCCTT-3'	120	Tuttel et al., 2014
	col2a1	5'-GTGTGTGATTCGGGGACTGT-3'	5'-TTTGCACCAAGTGACCCGAT-3'	144	Traber. 2020
	gapdh	5'-TGCTGGTATTGCTCTCAAC-3'	5'-GAGAATGGTCGCGTATCAA-3'	161	Wen et al., 2015
	hapln1	5'-AACGACTATGGCACATACCGG-3'	5'-AAGGTTGTACCGCCCCAAA-3'	147	Govindan & Lovine 2014.
	isg15	5'-TGGCACATCACTTGATTTCGG-3'	5'-AGCTGCATCGTCACCGAG-3'	127	NCBI Primer Blast
	matn1	5'-ATTGTGACAGACGGCAGACC-3'	5'-TCCGACACAACCGCACAAAAG-3'	227	NCBI Primer Blast
	mmp13a	5'-ATGGTGCAAGGCTATCCCAAGAGT -3'	5'-GCCTGTTGTTGGAGCCAAACTCAA-3'	289	Nesan et al., 2012
	mmp13b	5'-CTCCTGGAATCGGCATTGGT-3'	5'-CAGCCTCCAGTAAAACCTGTC-3'	362	NCBI Primer Blast
	osx	5'-GCATCCTTACGGCTCATGGT-3'	5'-GGCAATCGCAAGAAGACCTCC-3'	419	NCBI Primer Blast
	runx2a	5'-GACGGTGGTGACGGTAATGG-3'	5'-TGCGGTGGGTTCGTGAATA-3'	174	Chen et al., 2017
	runx2b	5'-GACGTCTTCCAGGTTCGACA-3'	5'-GAACCGGGAGGTTGGGATTG-3'	393	NCBI Primer Blast
	serpina1L	5'-AGAGTGTCTCGGGTTCTCCA-3'	5'-ATGCTCATGGTGCTGTCCTC-3'	164	NCBI Primer Blast
	shoc2	5'-GGGCCTGTCTGAAGAGAACA-3'	5'-CGCCGGGATTCACATCCTTT-3'	113	NCBI Primer Blast
	snai2	5'-ACCGAATTATAGTGAACTGGAGA-3'	5'-ACTGTTATGGGATTGTACGCC-3'	126	Bickers et al., 2018
	sned1	5'-CAGACCGCTTCCACCTCAAA-3'	5'-AGTGCTCTTTACTGGTATGGAAA-3'	309	NCBI Primer Blast
	sox9a	5'-TCAGCAAAACTCTGGGAAAAC-3'	5'-CTGGAGCGCTTTGAAGATG-3'	221	Crowder et al., 2018
	twist1a	5'-CGCGTTTTCTGTGTGGAGAA-3'	5'-CCGAGAATCATGCTGCATCA-3'	93	Mahmaoud et al., 2016
Human	*cxcl10*	AGCAGTTAGCAAGGAAAGGTCT	GGAGGATGGCAGTGGAAGTC	482	NCBI Primer Blast
	edn1	CCCGTTAAAAGGGCACTTGGG	CGGAACAACGTGCTCGGG	386	NCBI Primer Blast
	gapdh	GGTGGTCTCCTCTGACTTCA	GTTGCTGTAGCCAAATTCGT	127	Kim et al., 2017
	nppb	TCTGGCTGCTTTGGGAGGAAGA	CCTTGTGGAATCAGAAGCAGGTG	592	Jiang et al., 2022
	sema3e	GCACTTCGGAACTGTGCTTTC	AATTTGCACATTCACCCGCA	496	NCBI Primer Blast
	sfrp2	CCACCGAGGAACGTCCAAA	GCCACAGCACCGATTTCTTC	225	NCBI Primer Blast
	shoc2	TCAGTGGTGTATAGGCTGGATTCT	GCTACATCCAGCGTAATGAGGT	182	Geng et al., 2020

Table 2.1 Primers for qPCR analysis

CHAPTER 3. SHOC2 CONTROLS ERK1/2-DRIVEN NEURAL CREST DEVELOPMENT BY BALANCING COMPONENTS OF THE EXTRACELLULAR MATRIX

(This chapter is a manuscript that has been submitted for publication.)

Contributing authors: Rebecca G. Norcross[1], Lina Abdelmoti[1], Eric C. Rouchka[2,3], Kalina Andreeva[3,4,5], Olivia Tussey[1], Daileen Landestoy[1], Emilia Galperin[1*]

[1]Department of Molecular and Cellular Biochemistry, University of Kentucky, Lexington, KY 40536. [2]Department of Biochemistry and Molecular Genetics, University of Louisville, Louisville, KY 40292. [3]KY INBRE Bioinformatics Core, University of Louisville, Louisville, KY 40292. [4]Department of Neuroscience Training, University of Louisville, Louisville, KY 40292. [5]Department of Genetics, Stanford University, Palo Alto, CA 94304

*To whom correspondence should be addressed:

Emilia Galperin, University of Kentucky Department of Molecular and Cellular Biochemistry, 741 S Limestone St, Lexington, KY 40536. Phone 859-323-1796. Email: emilia.galperin@uky.edu

AUTHOR CONTRIBUTIONS: E.G. conceptualized and supervised the project; K.A. and E.C.R. analyzed all the RNA sequencing data, L.A. performed the microinjection and western blot experiments. R.G.N. performed in situ experiments and analysis, PH3 immunostaining, RT-qPCR experiments and analyses; D.L. performed *in situ* experiments, O.T. performed in situ analysis; R.G.N. and E.G. wrote the manuscript with inputs from all authors.

Abstract

The extracellular signal-regulated kinase (ERK1/2) pathway is essential in embryonic development. The scaffold protein Shoc2 is a critical modulator of ERK1/2 signals, and mutations in the *shoc2* gene lead to the human developmental disease known as Noonan-like syndrome with loose anagen hair (NSLH). The loss of Shoc2 and the shoc2 NSLH-causing mutations affect the tissues of neural crest (NC) origin. In this study, we utilized the zebrafish model to dissect the role of Shoc2-ERK1/2 signals in the development of NC. These studies established that the loss of Shoc2 significantly altered the expression of transcription factors regulating the specification and differentiation of NC cells. Using comparative transcriptome analysis of NC-derived cells from shoc2 CRISPR/Cas9 mutant larvae, we found that Shoc2-mediated signals regulate gene programs at several levels, including expression of genes coding for the proteins of extracellular matrix (ECM) and ECM regulators. Together, our results demonstrate that Shoc2 is an essential regulator of NC development. This study also indicates that disbalance in the turnover of the ECM may lead to the abnormalities found in NSLH patients.

Introduction

The Ras-ERK1/2 canonical signaling pathway is activated by multiple extracellular cues and promotes cell proliferation, cell cycle progression, and a myriad of other cellular functions. The pleiotropic role of the ERK1/2 signals in various tissues has been well described by a large body of literature. Mutations in genes of the Ras-ERK1/2 signaling pathway can result in congenital disorders that are collectively termed RASopathies [6, 163]. Individual RASopathies display considerable variability within their clinical phenotypes. The hallmarks of RASopathies include distinct facial features, cardiac defects, growth delays, neurologic issues, and gastrointestinal difficulties [64, 164]. Given the universal significance of the ERK1/2 pathway in all cell types, it is somewhat surprising that the clinical hallmarks of RASopathies are very specific. Thus, to develop therapeutic avenues for minimizing these diseases, it is essential to understand the precise etiology and pathogenesis of individual malformation syndromes. This requires an in-depth understanding of the functional developmental roles played by genes that are mutated in specific disorders.

NSLH is a relatively rare RASopathy with an estimated incidence of 1:50000 live births [66]. The majority of NSLH patients carry autosomal dominant mutations in the *shoc2* gene that encodes the non-enzymatic leucine-rich repeat scaffold protein Shoc2 [67]. To develop therapeutic avenues for minimizing these diseases, it is essential to understand the precise etiology and pathogenesis of individual malformation syndromes. This requires an in-depth understanding of the functional developmental roles played by genes that are mutated in specific disorders.

Studies from several labs demonstrated that to modify ERK1/2 signals Shoc2 assembles an intricate protein machinery [165]. Yet, the question of what biological activities are regulated by the Shoc2-transmitted signals remains elusive. The ablation of Shoc2 in mice leads to early embryonic lethality and partial embryo absorption at E8.5 [166]. The loss of Shoc2 in zebrafish induced an array of developmental defects [103]. Interestingly, the most prominent deficiencies in morphogenesis of the Shoc2 *null* zebrafish mutants were in the tissues of NC origin: facial cartilage, bone, and pigment [103]. These and other studies indicated that NCCs exhibit a specific threshold sensitivity to the deficiencies in ERK1/2 signals during morphogenesis. Yet, a clear mechanistic link between any RASopathy-causing mutations and the resulting developmental defect is still missing.

Here, we leveraged the power of the zebrafish model to delineate the role of Shoc2 in the development of the NC. We establish that Shoc2 deficiency affects early NC gene expression and demonstrate that Shoc2-guided signals are critical for the cell fate determination. The loss of Shoc2 affects NC-derived precursors as well as differentiated populations of craniofacial cartilage and cranial ganglia. We found that Shoc2 is critical for the differentiation of pigment cells and myelinated Schwann cells. Moreover, we observed that transcriptional circuits of *sox10*-positive cells derived from CRISPR/Cas9 Shoc2 *null* mutants were markedly altered. The loss of Shoc2 leads to perturbations in the expression of the extracellular matrix (ECM) components and proteins associated with ECM. These perturbations are likely to be responsible for the cranio-skeletal defects observed in the Shoc2 CRISPR/Cas9 *null* mutants. Most significantly, our results point to a role for Shoc2 as a novel regulator of NC and early embryonic cell fate programming.

Results

3.1 Loss of Shoc2 alters neural plate border gene expression

Our earlier studies characterized the overall developmental abnormalities of two Shoc2 mutant zebrafish lines generated by CRISPR/Cas9 mutagenesis: *shoc2Δ22* and *shoc2Δ14* [103]. These studies demonstrated that the developmental abnormalities found in CRISPR/Cas9 shoc2 mutants were in several neural crest (NC) derived tissues, including malformations of multiple cartilage elements, bone, and pigment (**Fig. 3.1A**). Here we investigate the effect of Shoc2-mediated signals on the development of NC further. Homozygous *shoc2* CRISPR/Cas9 mutant embryos are phenotypically distinguishable from their control siblings only at 5 days post fertilization (dpf), likely due to the contribution of the maternal *shoc2* mRNA. Thus, we utilized a targeted morpholino oligonucleotide (MO)-mediated knock-down for an acute depletion of Shoc2. The efficacy of the *shoc2* MO to interfere with the translation of *shoc2* mRNA was validated by Western blot analysis using an anti-Shoc2 antibody. The results of these experiments were analogous to what we reported earlier [49] (**Fig. 3.1B**). The specificity of the shoc2 MO was also validated in our earlier studies, when co-injection of wildtype (WT) human *shoc2* mRNA with *shoc2* MO partially rescued *shoc2* MO-induced deficits [49, 103].

First, we analyzed whether the loss of Shoc2 affects the expression of genes involved in the definition of the neural plate border (NPB) territory that gives rise to the NC precursors[109, 110]. The expression of transcription factors specific to the NPB, PR domain containing 1a, with the ZNF domain (*prdm1a*) and paired box 7 (*pax7*) [113, 116, 117, 119, 167] was examined at the 2-somite stage, when NC progenitors are present in the anterior portion of the embryos, using whole body in situ hybridization (WISH). In the

shoc2 morphant embryos, the *prdm1a* expression pattern was altered and the lateral edge of the neural plate was farther apart from the adaxial cells adjacent to the midline compared to control larvae (**Fig. 3.2A, E**). The *shoc2* morphants also had a mild alteration in the expression pattern of pax7 (**Fig.3.2B, E**). Furthermore, cells expressing the forkhead-box transcription factor *foxd3*, an essential "NC specifier", were spaced farther from the midline in the *shoc2* morphants than in control embryos. The expression of *foxd3* was also reduced in the posterior region (**Fig. 3.2C, E**). Although, the loss of *shoc2* mildly effected the expression pattern of the pan-neural marker SRY-box transcription factor 2 (sox2), the *sox2* domain was wider in the *shoc2* morphants than in control larvae (**Fig. 3.2D, E**). We have not detected changes in the major-to-minor axis ratio of the *shoc2* morphants at 11 hours post fertilization (hpf), suggesting that convergent extension cell movement during gastrulation was largely unaffected. Thus, it is possible that the expression of Shoc2 is required in the very early steps of NC development- the definition of the NPB territory.

3.2 Shoc2 is necessary for induction of neural crest

To understand whether the loss of Shoc2 affects the specification of cells in the NPB to the NC fate, we used WISH to analyze the expression of the "neural crest specifiers" foxd3, snail family zinc finger 2 (*snai2*), and SRY-box transcription factors *sox10*, and *sox9a* at 5 somites, before the onset of NC migration [110, 168, 169]. We found that cells expressing *foxd3* (**Fig. 3.3A, F**) and *sox10* (**Fig. 3.3B, F**) were shifted more laterally from the midline in embryos injected with Shoc2 MO. The expression levels of *sox10* appeared to be reduced (**Fig. 3.3B, F**). The loss of Shoc2 also affected the expression patterns of *snai2* and *sox9a* (**Fig. 3.3C, D and F**). Moreover, we found a marked reduction in

expression of *crestin*, a pan-NC marker [127, 170] in the anterior portion of NPB of *shoc2* morphants (**Fig. 3.3E, F**). These findings suggest that the NC is specified in the *shoc2* morphants, but is not patterned correctly.

3.3 Shoc2 effect on the migratory neural crest cells

Following NC induction and specification, the NCCs transition to become actively migrating mesenchymal cells [109]. This gradual transition requires the regulation of many effector genes and relies on transcription factors that are also involved in NCC fate specification, such as *foxd3* and *snai2* [115, 171]. Thus, we assessed whether expression of *foxd3* and *snai2* was affected by the loss of Shoc2 at the 18-somite stage (ss). In *shoc2* morphant larvae, the spatiotemporal migratory paths of cells expressing *foxd3* and *snai2* were altered in both the cranial and trunk NC of 18-somite *shoc2* morphants (**Fig. 3.4A, C**). The expression of *foxd3* was decreased in somites, in the cranial NC around the otic vesicle and the late migrating NC precursors. We also detected reduced expression of *snai2* in migrating NC precursors. Consistent with reduced expression of *foxd3* and *snai2* in migratory NCCs, a significant loss in NCCs expressing *crestin* was detected in the first trunk segments of the migrating ventral streams between the neural keel and somites of *shoc2* morphants (**Fig. 3.4A, C (bottom panels))**. Together, our findings point to either a loss in migratory NCCs or to defects in the premigratory NCC maintenance of the *shoc2* morphants.

To better understand the extent of Shoc2 loss of function on the specification of non-ectomesenchymal NC derivatives and their migration, the expression of the transcription factors *sox10* and *sox9a* was assessed [140]. Compared to control larvae, *shoc2* morphants

exhibited irregular distribution of the anterior rostal-to-caudal *sox10*-positive NCCs with a greatly diminished area of cells positive for the expression *sox9a* (**Fig. 3.4B, C**). The 18 ss of zebrafish development generally correlates with initial migration of cranial NCCs. Examination of the expression of transcription factor distal-less homeo-box 2 (*dlx2a*) demonstrated that in *shoc2* morphants three streams of mature cranial NCCs migrating towards the prospective pharyngeal arches (Sperber et al., 2008) were noticeably diminished (**Fig. 3.4B, C** (**bottom panels)).**

Mesenchymal transition of NCCs also involves cell surface changes, dissolution of cadherin-mediated adherens junctions and a "cadherin switch" from E-cadherin to N-cadherin [172]. While the pre-migratory NCCs in zebrafish mostly express E-cadherin (*cdh1*), migratory NCCs predominantly express N-cadherin (*cdh2*) [133, 134]. The impact of the Shoc2 loss on the migratory properties of the NCCs was determined by analyzing the expression of *cdh1*, *cdh2* and additional genes expressed in NCCs at the time of epithelial-to mesenchymal transition, *twist1a* and *snai2*, using qRT-PCR. Data in **Fig. 3.5A** establish that at 24 hpf the expression of *chd1*, *cdh2*, and *twist* were significantly reduced in *shoc2* morphants. This suggests that while *shoc2* function is necessary to control expression of *chd1*, *cdh2*, and *twist1a*, it does not seem to be necessary to control a "cadherin switch". Importantly, differences in expression of genes regulating migration of NCCs also coincided with a dramatic decrease in migrating *crestin*- and *foxd3*- positive cells (**Fig. 3.5B-E** and **Fig. 3.4A**). Together, our data suggest that loss of Shoc2 leads to defective NCC specification and migration, which, in turn, could underlie other developmental defects observed in zebrafish *shoc2* mutants.

3.4 Shoc2 signals in the development of pigment cells

Zebrafish NCCs are fate-restricted from an early stage, and individually labeled premigratory NCCs typically produce differentiated cells of only a single class [109]. NCCs differentiate into the cells of the peripheral nervous system, the craniofacial osteocytes and chondrocytes, and three major pigment cells types: xanthophores, iridophores, and melanocytes [109] . Our earlier studies reported that ablation of Shoc2 affected the pigmentation pattern of Shoc2 *null* larvae and, at 6 dpf, *shoc2* mutants lost the regularity of melanophore patterning and presented with overlapping lentigines [103]. Here, we demonstrate additional deficiencies in the development of pigment cells resulting from the loss of Shoc2. Compared to WT larvae, numbers of iridophores in Shoc2 *null*s were reduced substantially, particularly in the trunk and tail, at 120 hpf (**Fig. 3.6A, B**), indicating defects in the differentiation of pigment NC lineage.

3.5 Shoc2 and the peripheral nervous system

Neurogenic derivatives of NCCs are generated at all axial levels (Rocha et al., 2020). In the cranial region, NCCs contribute to the cranial ganglia, Schwann, and satellite cells, while in the trunk they give rise to sensory neurons of the dorsal root ganglia (DRG), sympathetic neurons, and Schwann cells [173]. To determine the extent of Shoc2 requirement for the development of the peripheral nervous system, we evaluated the expression of the transcription factor *foxd3* at 48 hpf when it is required for the proper specification of the peripheral neurons of DRG, enteric neuron, and the cranial ganglia precursors [174] (**Fig. 3.7A, E**). In control larvae, *foxd3* expression was easily detected in the cranial ganglia-associated glia of the developing trigeminal ganglion, the pre- and post-

otic ganglia, and the trunk satellite glia associated with DRG. However, in the embryos injected with *shoc2* MO, the expression of *foxd3* was greatly diminished in the ganglia-associated glia (**Fig. 3.7A, E**). The *shoc2* morphants also had irregular *foxd3*-positive ventral streams of NCCs and the DRG structures, including abnormal ectopic expression patterns of precursors of the peripheral nervous system (**Fig. 3.7A, inset**).

To assess further whether Shoc2-mediated signals are required for the late-forming neural progenitors (neurons and glia) in the trunk, we examined the expression of the *sox10* gene at 48 hpf (**Fig. 3.7B, E**). The loss of Shoc2 resulted in a dramatic reduction of glial cells and NC-derived sensory neurons of DRGs in zebrafish embryos. We found that, similarly to *foxd3*, *sox10* expression was lost in segmentally arranged lines of cells laying adjacent to the notochord (the precursors of the peripheral nervous system) in the trunk of the *shoc2* morphants (**Fig. 3.7B (inset), E**). The loss in expression of *foxd3* and *sox10* in *shoc2* morphant larvae indicates that Shoc2 contributes to the specification of the NC peripheral neurogenic progenitor population.

To understand better the role of Shoc2 in the development of the peripheral nervous system, we assessed a subset of the glia, the Schwann cells, that surround the ganglia of the lateral line and ensheath the lateral line nerves [175]. We examined the expression of transcription factor *krox20*, which, together with *sox10*, regulates terminal differentiation by controlling expression of another marker of glial differentiation, myelin basic protein (*mbp*). Compared to controls (**Fig. 3.7C, E**), the *shoc2* morphants showed a decrease in overall *krox20* expression which was particularly clear along the lateral line (**Fig. 3.7C**). Likewise, we found a dramatic reduction in expression of mbp in the anterior (all) and

posterior lateral line (pll), cranial ganglia and central nervous system of *shoc2* morphants at 3 dpf (**Fig. 3.7D, E**).

To determine if overall reduction in the differentiation of NCCs into glial and pigment derivatives was due to increased apoptosis, TUNEL labelling was carried out. In contrast to control larvae, which exhibited limited staining, embryos injected with the *shoc2* MO showed an increase in apoptosis along the trunk (at 24 hpf) and in the hindbrain region (at 48 hpf) (**Fig. 3.8A-C**). We also assessed cell proliferation by labeling larvae with anti-phospho-Histone H3 antibody and Alexa Fluor 488 dye at 24 hpf. We have not detected changes in numbers of GFP- positive cells, indicating that Shoc2 signals do not affect cell proliferation (**Fig. 3.8D, E**). These data suggest that increased apoptosis may partially account for the reduction of *foxd3* and *sox10* expression in specified NCCs cells. The increase in apoptotic cells in *shoc2* morphants also suggest that Shoc2 signals contribute to the survival of certain cell populations.

3.6 Shoc2 regulates the expression of cranial NCC (cNCC) specific genes in the posterior pharyngeal arches

One of the strongest abnormalities of the Shoc2 CRISPR/Cas9 mutants is the defects in the cartilaginous structures of the viscerocranium (**Fig. 3.1A**) [103]. Data in **Fig. 3.4B** strongly indicate that *dlx2a*-positive NCCs fated to become CNCCs do not migrate properly in *shoc2* morphant embryos, possibly affecting formation of the cartilaginous structures of the viscerocranium. Moreover, we also found that chondrocyte stacking within the cartilaginous elements of *shoc2* morphants was not as orderly arrayed as in controls (**Fig. 3.9A**). Thus, to better understand the craniofacial phenotypes of Shoc2 mutant larvae, we examined the differentiation of post-migratory CNCCs into

chondrocytes. WISH was used to analyze the expression of the NC and prechondrogenic marker *sox9a* critical for cartilage morphogenesis and chondrocyte stacking (Yan et al., 2005). Compared to embryos injected with the control MO, in which the *sox9a* expression was readily detectable in cranial structures and in fin buds, *sox9* expression was decreased in various cranial structures of *shoc2* morphants and was mostly absent from the pectoral fin (**Fig. 3.9B**). In contract to the decreased *sox9a* expression in cranial structures, sox9a expression was elevated in the trunk of the *shoc2* morphant embryo. These data, validated by the qPCR analysis (**Fig. 3.9C**), suggest that loss of Shoc2 has region-specific effects on *sox9* gene expression, and that the cartilage abnormalities of *shoc2* mutants are likely due to the defective specification and migration of cranial NCCs or chondrocytes.

Sox9a directly activates the expression of the alpha I chain of type II collagen (*col2a1*), the major collagen in cartilage and marker of differentiating chondrocytes in zebrafish [176]. When the expression of *col2a1* was compared in control and *shoc2* morphant larvae, dramatic changes in *col2a1* expression were detected in *shoc2* morphants at 3 dpf (**Fig. 3.9D, E**). Embryos injected with *shoc2* MO exhibited a reduction in *col2a1* staining in the Meckel cartilage, ethmoid plate and ceratobranchial arches (**Fig. 3.9D, E**). Other cartilage genes regulated by *sox9a* and required both for proper cartilage formation in the development and maintenance of mature cartilage include proteoglycans aggrecan a and b (*acana* and *acanb*) [123, 139]. Similar to *col2a1*, we found dramatic changes in patterns and expression levels of acana, and acanb in larvae injected with *shoc2* MO (**Fig. 3.10A, B**). The expression of acana and acanb was limited to the ethmoid plate from the bilateral cranial NCC streams of the anterior maxillary, Meckel's cartilage and ceratobranchials elements of *shoc2* morphant larvae (**Fig. 3.10A, B** and **Fig. 3.11A**). qPCR

analysis (**Fig. 3.10C**) further demonstrated that *shoc2* loss leads to the misregulation of *sox9a* signals, thereby affecting the expression of proteins needed for cartilage maturation.

To address the extent to which bone ossification is affected in *shoc2* morphants, we assayed the expression of runt-related transcription factors *runx2a* and *runx2b*. *Runx2a* and *runx2b* regulate the maturation from immature chondrocytes to hypertrophic chondrocytes and osteoblast differentiation during the process of endochondral ossification [177, 178]. In embryos injected with control MO, *runx2a* and *runx2b* were expressed in hypertrophic chondrocytes and dermal ossification centers (**Fig. 3.10D, E**). *Runx2a* was expressed in the cleithrum, dentary, maxilla, operculum, pharyngeal arches and parasphenoid, whereas *runx2b* expression was detected in differentiating osteoblasts of the branchiostegial ray, cleithrum, operculum, palatoquadrate, parasphenoid, and pharyngeal arches (**Fig. 3.10D, E** and **Fig. 3.11A**). Yet, in *shoc2* morphant embryos, *runx2a* and *runx2b* expression was greatly reduced or absent in presumptive cartilaginous elements of the viscerocranium at 3 dpf, indicating that endochondral ossification was practically absent (**Fig. 3.10F**). These results were consistent with our earlier findings demonstrating a dramatic reduction in calcification of craniofacial bones visualized by Alizarin Red S staining [103] (**Fig. 3.1A**). Overall, these results demonstrate that Shoc2 function is required for the proper execution of the chondrocyte differentiation program.

3.7 Shoc2 knock-out affects gene expression of the *sox10*-positive cells

Our previous studies established that Shoc2 is expressed in *sox10*-positive cells at 6 dpf [103]. Thus, to gain more insight into the transcriptional changes that NC-derived cells experience in the absence of Shoc2, we performed comparative transcriptome analysis of

the *sox10*-positive cells. In order to prevent experimental variability associated with MO injections, in these experiments we utilized our CRISPR/Cas9 *shoc2Δ22*$^{+/-}$ mutant [103] and Tg(*sox10:RFP*) transgenic reporter lines to generate Tg(*sox10*:RFP; *shoc2Δ22*$^{+/-}$) fish. *Sox10*-expressing and *sox10*-derived cell populations were then isolated from 200 embryonic Tg(*sox10:RFP* or Tg(*sox10:RFP; shoc2Δ22*) transgenic zebrafish larvae at 6 dpf. Pooled embryos were dissociated and *sox10:RFP*$^{+}$ cells were isolated immediately using fluorescence-activated cell sorting (FACS) followed by mRNA isolation and RNA-seq analysis (**Fig. 3.12A**).

RNA-seq reads were aligned to the *Danio rerio* GRCz11 reference genome (GRCz11.fa) using STAR (version 2.6) [179], followed by the assembly and merging using Cufflinks software package [180].The number of mapped reads ranged from 27.3 million to 30.3 million per sample and resulted in an overall mapping rate of approximately 97%. Taken together, this indicates both a depth and breadth of sequencing coverage allowing for comprehensive analysis of differentially expressed genes (DEG).

To identify DEGs, data were analyzed using DESeq2 (Love et al., 2014) and CuffDiff (Trapnell et al., 2012). DEGs were then ranked using a false discovery rate (FDR) < 0.05 and fragments per kilobase of exon per million reads mapped (FPKM) ranking resulting in 351 differentially expressed genes, with 188 upregulated and 163 downregulated. The Log_2fold changes for the obtained gene set are highlighted on the volcano plot (**Fig. 3.13**).

Further analysis of DEGs for gene ontology biological processes (GO: BP) and KEGG pathways [181] identified significant enrichment in biological terms, including “skeletal tissue development”, “cartilage morphogenesis”, “connective tissue

development", and "cartilage development" (**Fig. 3.12A**). Other significant biological terms included "immune response" and "antigen processing and presentation". Further analysis of the DEGs by the Protein Analysis Through Evolutionary Relationships (PANTHER) resource separated DEGs into PANTHER protein classes, with "metabolite interconversion enzymes", "cytoskeletal protein", "protein modifying enzyme" and "ECM proteins" being the top enriched classes (**Fig. 3.12B, Table 3.1**). Together, these analyses suggested that deficiencies in the development of the NC-derived cartilage and bone observed in *shoc2* CRISPR mutants are potentially due to changes in expression of ECM-related proteins. *Sox10*-RFP positive cells from shoc2 mutant larvae showed robust changes in the expression of ECM proteins (e.g. *acana*, *acanb*, *sned1*, *matn1*, *hapln1b*), collagens (e.g. *col6a3*, *col9a1*, *col2a1*, *col11a2/a1*, *col7a*, *col5a*, etc.), ECM-affiliated proteins (e.g. *anxa1*, *snorc*), ECM regulators (e.g. *mmp13*, *serpinh1*), and other genes associated with ECM remodeling (e.g. *pcolce2*, *loxl4*) (**Fig. 3.12B**). Importantly, many of the DEGs identified in this screen have previously been implicated in being aberrantly expressed in developmental diseases of cartilage or related NC-derived tissues [182].

Several relatively abundantly expressed genes (i.e. *acana*, *acanb*, *mmp13a*, *mmp13a*, *hapln1*, and *matn1*) were selected for additional confirmation by qRT-PCR using mRNA isolated from *sox10:RFP*$^{+}$ cells (**Fig. 3.12C**). All of the analyzed genes showed consistent expression patterns (Log2fold change) between RNA-seq and qRT-PCR analysis. Comparable changes in expression were also observed when the whole larvae were utilized for qRT-PCR analysis (**Fig. 3.12D**). Interestingly, we found that the expression of ISG15 ubiquitin-like modifier related to the interferon response [183] was significantly upregulated. ISG15 and MMP13 were previously associated with a population of mature-

hypertrophic chondrocytes [184]. Due to the limited availability of antibodies recognizing zebrafish proteins, we examined the protein expression of MMP13a and Collagen 2a1 only. Results in **Fig. 3.12E** confirmed that increased mRNA expression of *mmp13* and *col2a1* corresponded to elevated protein levels of processed and unprocessed forms of MMP13 and Collagen 2a1.

Surprisingly, these findings were in contrast to what we observed at 3 dpf, where *shoc2* loss led to a significant decrease in the expression *col2a1*, *acana*, *acanb*, and *sox9a* (**Figs. 3.9 and 3.10**). These observations prompted the hypothesis that Shoc2-mediated signals affect the temporal aspect of protein expression during embryonic development. To test this hypothesis, we first established temporal patterns of expression for *col2a1*, *acana* and acanb in WT larvae. The qRT-PCR analysis demonstrated that *col2a1*, *acana*, and *acanb* expression raises significantly around 3 dpf followed by a sharp decrease in RNA expression by 6 dpf, when compared to the expression levels at 2 dpf (**Fig. 3.11B**). However, when mRNA expression of *col2a1*, *acana* and *acanb* was examined in Shoc2 *null* larvae, we found that the expression levels of *col2a1*, *acana* and *acanb* were increasing gradually, when compared to WT larvae at 5 and 6 dpf (**Fig. 3.12G**). Likewise, we also found the expression of *sox9a* in Shoc2 *null*s was much higher than in WT larvae at 6 dpf (**Fig. 3.12F**). Of note, the expression of *col2a1*, *acana* and *acanb* in Shoc2 *null* larvae at 6 dpf was still much lower than their expression levels detected at 3 dpf of WT larvae (**Fig. 3.11C**).

An additional DEG evaluated in this study was the structural ECM glycoprotein, SNED1 (Sushi, Nidogen and EGF-like Domains 1). Sned1 is broadly expressed during development, in particular, in NC and mesoderm derivatives [185], and was previously

implicated in multiple aspects of mouse embryonic development, including the formation of craniofacial structures [186]. Zebrafish SNED1 protein orthologue shares 64% identity with its human counterpart and preserves protein domains found in human SNED1 [185]. *Sned1* expression was easily detectable in cranial structures of control 3 dpf larvae by WISH, but, was reduced considerably in *shoc2* morphants (**Fig. 3.12H, I and Fig. 3.11D**). Of note, our data in **Fig. 3.12D** show that the expression of sned1 at 6 dpf was somewhat elevated in *shoc2 null* larvae (**Fig. 3.12D).** These data indicate that, in the absence of Shoc2, ERK1/2 signals regulating the expression of ECM-related proteins are delayed, further supporting our hypothesis that Shoc2 signals control temporal expression programs during development.

We conclude that Shoc2-controlled signals regulate the expression of master transcription factors in the gene regulatory network governing the NC developmental program. Aberrantly activated ERK1/2 signaling at the early embryonic stages caused in disbalance extracellular matrix turnover either by decreased matrix synthesis and/or increased matrix degradation which in its turn may drive long lasting defects in organ development (**Fig. 3.14**).

3.8 Tables and figures, Ch. 3

ensemble N	Description	PANTHER Subfamily: ECM proteins
ENSDARG00000095901	Endostatin domain-containing protein;col18a1b;ortholog	COLLAGEN ALPHA-1(XVIII) CHAIN (PTHR24023:SF1034)
ENSDARG00000068516	Hyaluronan and proteoglycan link protein 1b;hapln1b;ortholog	HYALURONAN AND PROTEOGLYCAN LINK PROTEIN 1 (PTHR22804:SF10)
ENSDARG00000012422	Fibrillar collagen NC1 domain-containing protein;col11a2;ortholog	COLLAGEN ALPHA-2(XI) CHAIN (PTHR24023:SF509)
ENSDARG00000101816	Fibrillar collagen NC1 domain-containing protein;col5a3b;ortholog	FIBRILLAR COLLAGEN NC1 DOMAIN-CONTAINING PROTEIN (PTHR24023:SF1050)
ENSDARG00000030215	Matrilin 1;matn1;ortholog	CARTILAGE MATRIX PROTEIN (PTHR24020:SF16)
ENSDARG00000035891	Aggrecan a;acana;ortholog	AGGRECAN A (PTHR22804:SF55)
ENSDARG00000024032	Cochlin;coch;ortholog	COCHLIN (PTHR24020:SF36)
ENSDARG00000037845	Elastin;col9a3;ortholog	COLLAGEN ALPHA-3(IX) CHAIN (PTHR24023:SF866)
ENSDARG00000069245	Matrilin 3a;matn3a;ortholog	MATRILIN-3 (PTHR24020:SF12)
ENSDARG00000091602	Si:dkey-163f14.6;si:dkey-163f14.6;ortholog	SI:DKEY-163F14.6 (PTHR24034:SF137)
ENSDARG00000098294	Fibrillar collagen NC1 domain-containing protein;col5a3a;ortholog	MACROPHAGE RECEPTOR MARCO (PTHR24023:SF897)
ENSDARG00000060893	C1q domain-containing protein;col8a2;ortholog	COLLAGEN ALPHA-2(VIII) CHAIN (PTHR24023:SF855)
ENSDARG00000024492	Procollagen, type IX, alpha 2;col9a2;ortholog	COLLAGEN IV NC1 DOMAIN-CONTAINING PROTEIN-RELATED (PTHR24023:SF1046)
ENSDARG00000073699	Collagen, type IX, alpha 1a;col9a1a;ortholog	COLLAGEN, TYPE IX, ALPHA 1A (PTHR24023:SF996)
ENSDARG00000094324	EGF-containing fibulin extracellular matrix protein 2a;efemp2a;ortholog	EGF-CONTAINING FIBULIN-LIKE EXTRACELLULAR MATRIX PROTEIN 2 (PTHR24034:SF96)
ENSDARG00000076623	Collagen, type XIV, alpha 1b;col14a1b;ortholog	COLLAGEN ALPHA-1(XIV) CHAIN (PTHR24020:SF15)
ENSDARG00000102395	Uncharacterized protein;ENSDARG00000102395;ortholog	HYALURONAN AND PROTEOGLYCAN LINK PROTEIN 1 (PTHR22804:SF10)
ENSDARG00000069415	Collagen, type XVII, alpha 1a;col17a1a;ortholog	COLLAGEN ALPHA-1(XVII) CHAIN-RELATED (PTHR24023:SF891)
ENSDARG00000058960	C1q domain-containing protein;otol1b;ortholog	OTOLIN-1 (PTHR24023:SF914)
ENSDARG00000026165	Fibrillar collagen NC1 domain-containing protein;col11a1a;ortholog	FIBRILLAR COLLAGEN NC1 DOMAIN-CONTAINING PROTEIN (PTHR24020:SF73)
ENSDARG00000003903	Hapln2 protein;hapln2;ortholog	HYALURONAN AND PROTEOGLYCAN LINK PROTEIN 2 (PTHR22804:SF8)

Table 3.1 Differentially expressed genes in PANTHER protein classes

The following genes were differentially expressed and separated into the classes: “metabolite interconversion enzymes”, “cytoskeletal protein”, “protein modifying enzyme” and “ECM proteins

ensemble N	Description	PANTHER Subfamily: Metabolite interconversion enzymes
ENSDARG00000099860	Pyruvate kinase;pkmb;ortholog	PYRUVATE KINASE (PTHR11817:SF115)
ENSDARG00000005913	Transglutaminase 1-like 3;tgm1l3;ortholog	PROTEIN-GLUTAMINE GAMMA-GLUTAMYLTRANSFERASE K (PTHR11590:SF49)
ENSDARG00000040535	Hexosyltransferase;csgalnact1a;ortholog	CHONDROITIN SULFATE N-ACETYLGALACTOSAMINYLTRANSFERASE 1 (PTHR12369:SF19)
ENSDARG00000025089	Lysyl oxidase homolog;loxl4;ortholog	LYSYL OXIDASE HOMOLOG 4 (PTHR45817:SF5)
ENSDARG00000061248	Peptide O-xylosyltransferase 1;xylt1;ortholog	XYLOSYLTRANSFERASE 1 (PTHR46025:SF2)
ENSDARG00000103277	Cytochrome P450, family 24, subfamily A, polypeptide 1;cyp24a1;ortholog	1,25-DIHYDROXYVITAMIN D(3) 24-HYDROXYLASE, MITOCHONDRIAL (PTHR24291:SF5)
ENSDARG00000014179	ATP-dependent 6-phosphofructokinase;pfkma;ortholog	ATP-DEPENDENT 6-PHOSPHOFRUCTOKINASE (PTHR13697:SF58)
ENSDARG00000045414	Elongation of very long chain fatty acids protein 2;elovl2;ortholog	ELONGATION OF VERY LONG CHAIN FATTY ACIDS PROTEIN 2 (PTHR11157:SF16)
ENSDARG00000099517	Adenylosuccinate synthetase isozyme 1;adss1;ortholog	ADENYLOSUCCINATE SYNTHETASE ISOZYME 1 (PTHR11846:SF2)
ENSDARG00000033832	AMP deaminase;ampd1;ortholog	AMP DEAMINASE 1 (PTHR11359:SF1)
ENSDARG00000111240	Dehydrogenase/reductase (SDR family) member 13a, tandem duplicate 2;dhrs13a.2;ortholog	DEHYDROGENASE/REDUCTASE SDR FAMILY MEMBER 13 (PTHR43157:SF44)
ENSDARG00000020711	Ribonucleoside-diphosphate reductase subunit M2;rrm2;ortholog	RIBONUCLEOSIDE-DIPHOSPHATE REDUCTASE SUBUNIT M2 (PTHR23409:SF20)
ENSDARG00000045190	Cholesterol 25-hydroxylase-like protein;ch25h;ortholog	CHOLESTEROL 25-HYDROXYLASE (PTHR11863:SF213)
ENSDARG00000034470	Fructose-bisphosphate aldolase;aldoab;ortholog	FRUCTOSE-BISPHOSPHATE ALDOLASE A (PTHR11627:SF1)
ENSDARG00000011934	Glycogenin 1;gyg1a;ortholog	GLYCOGENIN-1 (PTHR11183:SF164)
ENSDARG00000089233	Hexosyltransferase;csgalnact1b;ortholog	CHONDROITIN SULFATE N-ACETYLGALACTOSAMINYLTRANSFERASE 1 (PTHR12369:SF19)
ENSDARG00000042983	Hyaluronan synthase 1;has1;ortholog	HYALURONAN SYNTHASE 1 (PTHR22913:SF4)
ENSDARG00000056151	Tyrosinase-related protein 1b;tyrp1b;ortholog	5,6-DIHYDROXYINDOLE-2-CARBOXYLIC ACID OXIDASE (PTHR11474:SF3)
ENSDARG00000028098	Alpha-1,3-fucosyltransferase 9D;fut9d;ortholog	4-GALACTOSYL-N-ACETYLGLUCOSAMINIDE 3-ALPHA-L-FUCOSYLTRANSFERASE 9 (PTHR11929:SF10)
ENSDARG00000001971	Collagen triple helix repeat-containing 1b;cthrc1b;ortholog	COLLAGEN TRIPLE HELIX REPEAT-CONTAINING PROTEIN 1 (PTHR11903:SF18)
ENSDARG00000092660	Cytochrome P450 27C1;cyp27c1;ortholog	CYTOCHROME P450 27C1 (PTHR24291:SF9)
ENSDARG00000059231	Hephaestin-like 1a;hephl1a;ortholog	FERROXIDASE HEPHL1 (PTHR11709:SF233)
ENSDARG00000010276	Cyclooxygenase-2;ptgs2b;ortholog	PROSTAGLANDIN G/H SYNTHASE 2 (PTHR11903:SF8)
ENSDARG00000036893	Coagulation factor XIII, A1 polypeptide b;f13a1b;ortholog	COAGULATION FACTOR XIII A CHAIN (PTHR11590:SF42)
ENSDARG00000055518	Alpha-1,4 glucan phosphorylase;pygma;ortholog	ALPHA-1,4 GLUCAN PHOSPHORYLASE (PTHR11468:SF11)
ENSDARG00000040565	Creatine kinase;ckmb;ortholog	CREATINE KINASE (PTHR11547:SF60)
ENSDARG00000013856	Alpha-amylase;amy2a;ortholog	ALPHA-AMYLASE (PTHR43447:SF51)
ENSDARG00000007715	Lengsin, lens protein with glutamine synthetase domain;lgsn;ortholog	LENGSIN (PTHR43407:SF1)
ENSDARG00000099420	Nucleoside diphosphate kinase;nme2b.2;ortholog	NUCLEOSIDE DIPHOSPHATE KINASE B (PTHR11349:SF57)

Table 3.1 (Continued) Differentially expressed genes in PANTHER protein classes

The following genes were differentially expressed and separated into the classes: “metabolite interconversion enzymes”, “cytoskeletal protein”, “protein modifying enzyme” and “ECM proteins

ensemble N	Description	PANTHER Subfamily: cytoskeletal proteins
ENSDARG00000067990	Myosin, heavy polypeptide 1.1, skeletal muscle;myhz1.1;ortholog	MYOSIN-4 (PTHR45615:SF44)
ENSDARG00000058656	Desmin a;desma;ortholog	DESMIN (PTHR45652:SF2)
ENSDARG00000103459	Envoplakin b;evplb;ortholog	ENVOPLAKIN (PTHR23169:SF7)
ENSDARG00000012944	Myosin, heavy polypeptide 2, fast muscle-specific;myhz2;ortholog	MYOSIN-4 (PTHR45615:SF44)
ENSDARG00000030270	Fast skeletal muscle troponin T;tnnt3a;ortholog	TROPONIN T, FAST SKELETAL MUSCLE (PTHR11521:SF4)
ENSDARG00000076075	Myosin, heavy chain 7B, cardiac muscle, beta a;myh7ba;ortholog	MYOSIN-7B (PTHR45615:SF29)
ENSDARG00000099197	Actin alpha cardiac muscle 1b;actc1b;ortholog	ACTIN ALPHA CARDIAC MUSCLE 1B (PTHR11937:SF184)
ENSDARG00000055618	Actin;acta1b;ortholog	ACTIN (PTHR11937:SF389)
ENSDARG00000053254	Mylz2 protein;mylpfa;ortholog	MYOSIN REGULATORY LIGHT CHAIN 2, SKELETAL MUSCLE ISOFORM (PTHR23049:SF10)
ENSDARG00000099974	LIM domain-binding 3b;ldb3b;ortholog	LIM DOMAIN-BINDING PROTEIN 3 (PTHR24214:SF9)
ENSDARG00000090268	Keratin type 1 c19e;krtt1c19e;ortholog	KERATIN 17-RELATED (PTHR23239:SF367)
ENSDARG00000094041	Keratin 17;krt17;ortholog	KERATIN 17-RELATED (PTHR23239:SF367)
ENSDARG00000033683	Tropomyosin alpha-1 chain;tpma;ortholog	TROPOMYOSIN ALPHA-3 CHAIN (PTHR19269:SF38)
ENSDARG00000070835	Fast skeletal muscle troponin C;tnnc2;ortholog	FAST SKELETAL MUSCLE TROPONIN C (PTHR23064:SF58)
ENSDARG00000067997	Myosin, heavy polypeptide 1.3, skeletal muscle;myhz1.3;ortholog	MYOSIN-4 (PTHR45615:SF44)
ENSDARG00000036832	Type I cytokeratin, enveloping layer,-like;cyt1l;ortholog	KERATIN 17-RELATED (PTHR23239:SF367)
ENSDARG00000002589	Myosin light chain, phosphorylatable, fast skeletal muscle b;mylpfb;ortholog	MYOSIN REGULATORY LIGHT CHAIN 2, SKELETAL MUSCLE ISOFORM (PTHR23049:SF10)
ENSDARG00000035438	Myosin heavy chain 4;myhc4;ortholog	MYOSIN-4 (PTHR45615:SF44)
ENSDARG00000115956	Uncharacterized protein;unassigned;ortholog	DESMOPLAKIN (PTHR23169:SF26)
ENSDARG00000013755	Actinin alpha 3a;actn3a;ortholog	ALPHA-ACTININ-3 (PTHR11915:SF432)
ENSDARG00000017441	Fast skeletal muscle myosin light polypeptide 3;mylz3;ortholog	FAST SKELETAL MUSCLE MYOSIN LIGHT POLYPEPTIDE 3 (PTHR23048:SF38)
ENSDARG00000014196	Myosin, light chain 1, alkali_ skeletal, fast;myl1;ortholog	MYOSIN, LIGHT CHAIN 1, ALKALI_ SKELETAL, FAST (PTHR23048:SF10)
ENSDARG00000000212	Keratin 97;krt97;ortholog	KERATIN 97-RELATED (PTHR23239:SF374)
ENSDARG00000067995	Myosin, heavy polypeptide 1.2, skeletal muscle;myhz1.2;ortholog	MYOSIN-4 (PTHR45615:SF44)
ENSDARG00000068457	Tnnt3b protein;tnnt3b;ortholog	TROPONIN T, FAST SKELETAL MUSCLE (PTHR11521:SF4)
ENSDARG00000092947	Type I cytokeratin;cyt1;ortholog	KERATIN 17-RELATED (PTHR23239:SF367)
ENSDARG00000101043	Periplakin;ppl;ortholog	PERIPLAKIN (PTHR23169:SF10)
ENSDARG00000029069	Troponin I type 2a (skeletal, fast), tandem duplicate 4;tnni2a.4;ortholog	TROPONIN I TYPE 2A (SKELETAL, FAST), TANDEM DUPLICATE 3-RELATED (PTHR13738:SF31)

Table 3.1 (Continued) Differentially expressed genes in PANTHER protein classes

The following genes were differentially expressed and separated into the classes: “metabolite interconversion enzymes”, “cytoskeletal protein”, “protein modifying enzyme” and “ECM proteins

ensemble N	Description	PANTHER Subfamily: protein modifying enzymes
ENSDARG00000079618	Non-specific serine/threonine protein kinase;sik2a;ortholog	SERINE/THREONINE-PROTEIN KINASE SIK2 (PTHR24343:SF154)
ENSDARG00000073742	Serine protease 59, tandem duplicate 2 (Fragment);prss59.2;ortholog	TRYPSINOGEN (PTHR24264:SF6)
ENSDARG00000098108	Dual specificity protein phosphatase;dusp2;ortholog	DUAL SPECIFICITY PROTEIN PHOSPHATASE 2 (PTHR10159:SF109)
ENSDARG00000052057	Procollagen C-endopeptidase enhancer b;pcolceb;ortholog	PROCOLLAGEN C-ENDOPEPTIDASE ENHANCER B (PTHR24251:SF32)
ENSDARG00000100691	Protease, serine, 35;prss35;ortholog	INACTIVE SERINE PROTEASE 35 (PTHR15462:SF17)
ENSDARG00000020761	Arrestin domain-containing 2;arrdc2;ortholog	ARRESTIN DOMAIN-CONTAINING PROTEIN 2 (PTHR11188:SF48)
ENSDARG00000099889	Serine/threonine/tyrosine-interacting-like protein 2;styxl2;ortholog	SERINE/THREONINE/TYROSINE-INTERACTING-LIKE PROTEIN 2 (PTHR45682:SF4)
ENSDARG00000078683	RBR-type E3 ubiquitin transferase;zmp:0000000524;ortholog	E3 UBIQUITIN-PROTEIN LIGASE RNF14 (PTHR11685:SF371)
ENSDARG00000069529	Dual specificity protein phosphatase;zgc:153981;ortholog	DUAL SPECIFICITY PROTEIN PHOSPHATASE (PTHR45682:SF12)
ENSDARG00000100794	Collagenase 3 (Fragment);mmp13b;ortholog	COLLAGENASE 3 (PTHR10201:SF165)
ENSDARG00000102525	Tyrosine-protein kinase;lck;ortholog	TYROSINE-PROTEIN KINASE LCK (PTHR24418:SF39)
ENSDARG00000052578	Metalloendopeptidase;c6ast4;ortholog	METALLOENDOPEPTIDASE (PTHR10127:SF779)
ENSDARG00000042993	Serine protease 1;prss1;ortholog	RIKEN CDNA 2210010C04 GENE (PTHR24264:SF15)
ENSDARG00000007276	Elastase 3-like;ela3l;ortholog	CHYMOTRYPSIN-LIKE ELASTASE FAMILY MEMBER 3B (PTHR24257:SF22)
ENSDARG00000099509	Bloodthirsty-related gene family, member 23;btr23;ortholog	BLOODTHIRSTY-RELATED GENE FAMILY, MEMBER 1-RELATED (PTHR25465:SF32)
ENSDARG00000103308	Macrophage stimulating 1 (Hepatocyte growth factor-like);mst1;ortholog	HEPATOCYTE GROWTH FACTOR-LIKE PROTEIN-RELATED (PTHR24261:SF12)
ENSDARG00000055172	Si:ch211-256m1.8;si:ch211-256m1.8;ortholog	SI:CH211-256M1.8 (PTHR10188:SF42)
ENSDARG00000019130	Serine/threonine-protein kinase PLK;plk2b;ortholog	SERINE/THREONINE-PROTEIN KINASE PLK2 (PTHR24345:SF44)
ENSDARG00000021339	Carboxypeptidase A5;cpa5;ortholog	CARBOXYPEPTIDASE A1 (PTHR11705:SF94)
ENSDARG00000021859	Aminopeptidase;erap1b;ortholog	ENDOPLASMIC RETICULUM AMINOPEPTIDASE 1 (PTHR11533:SF156)
ENSDARG00000017314	Chymotrypsin-like elastase family member 1, tandem duplicate 6;cela1.6;ortholog	CHYMOTRYPSIN-LIKE ELASTASE FAMILY MEMBER 1 (PTHR24257:SF0)
ENSDARG00000090428	Chymotrypsinogen B1;ctrb1;ortholog	CHYMOTRYPSINOGEN B1-RELATED (PTHR24250:SF59)
ENSDARG00000093844	Similar to chymotrypsinogen B1;LOC562139;ortholog	CHYMOTRYPSINOGEN B1-RELATED (PTHR24250:SF59)

Table 3.1 (Continued) Differentially expressed genes in PANTHER protein classes

The following genes were differentially expressed and separated into the classes: “metabolite interconversion enzymes”, “cytoskeletal protein”, “protein modifying enzyme” and “ECM proteins

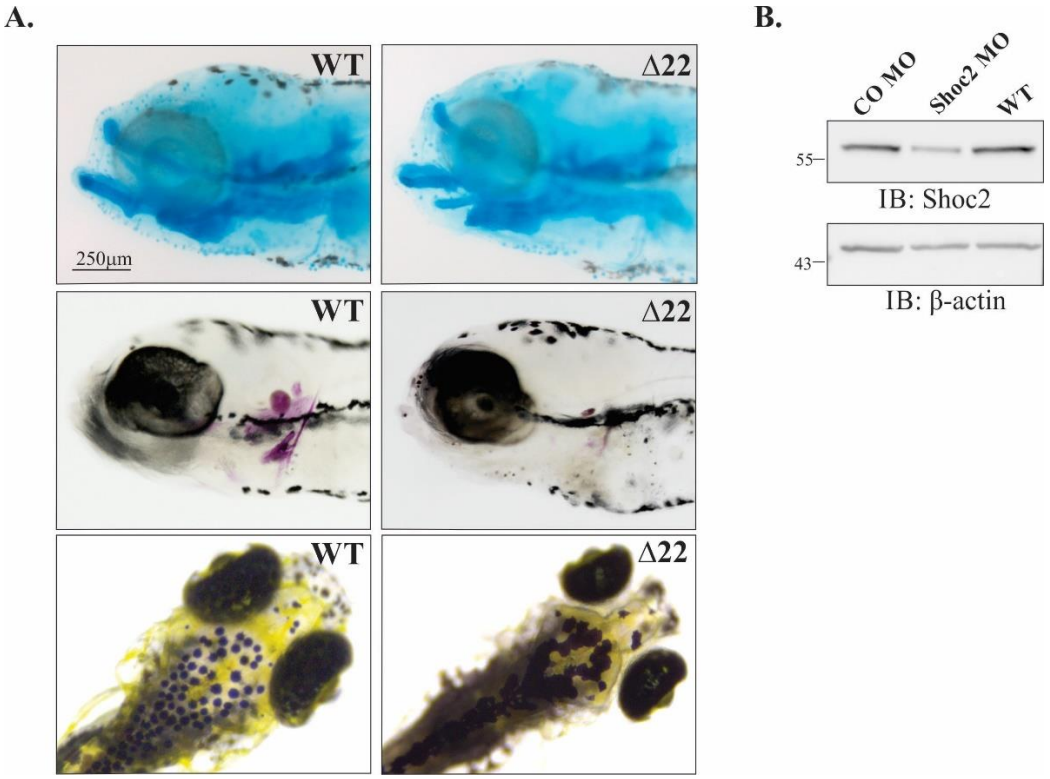

Figure 3.1 Developmental impairments in CRISPR/Cas9 *shoc2* mutants and loss of Shoc2 expression in morphant embryos

(**A**) Developmental impairments found in CRISPR/Cas9 shoc2 mutants. Lateral view of 6 dpf WT and *shoc2Δ22*-crispant larvae show significant differences in craniofacial cartilage (Alcian blue staining), cranial bone formation (Alizarin Red S staining) and melanocytes patterning. (**B**) Shoc2 protein expression is reduced upon morpholino injection. Embryos injected with shoc2 and control MO were harvested for immunoblotting at 48 hpf. The expression of indicated proteins was analyzed using specific antibodies.

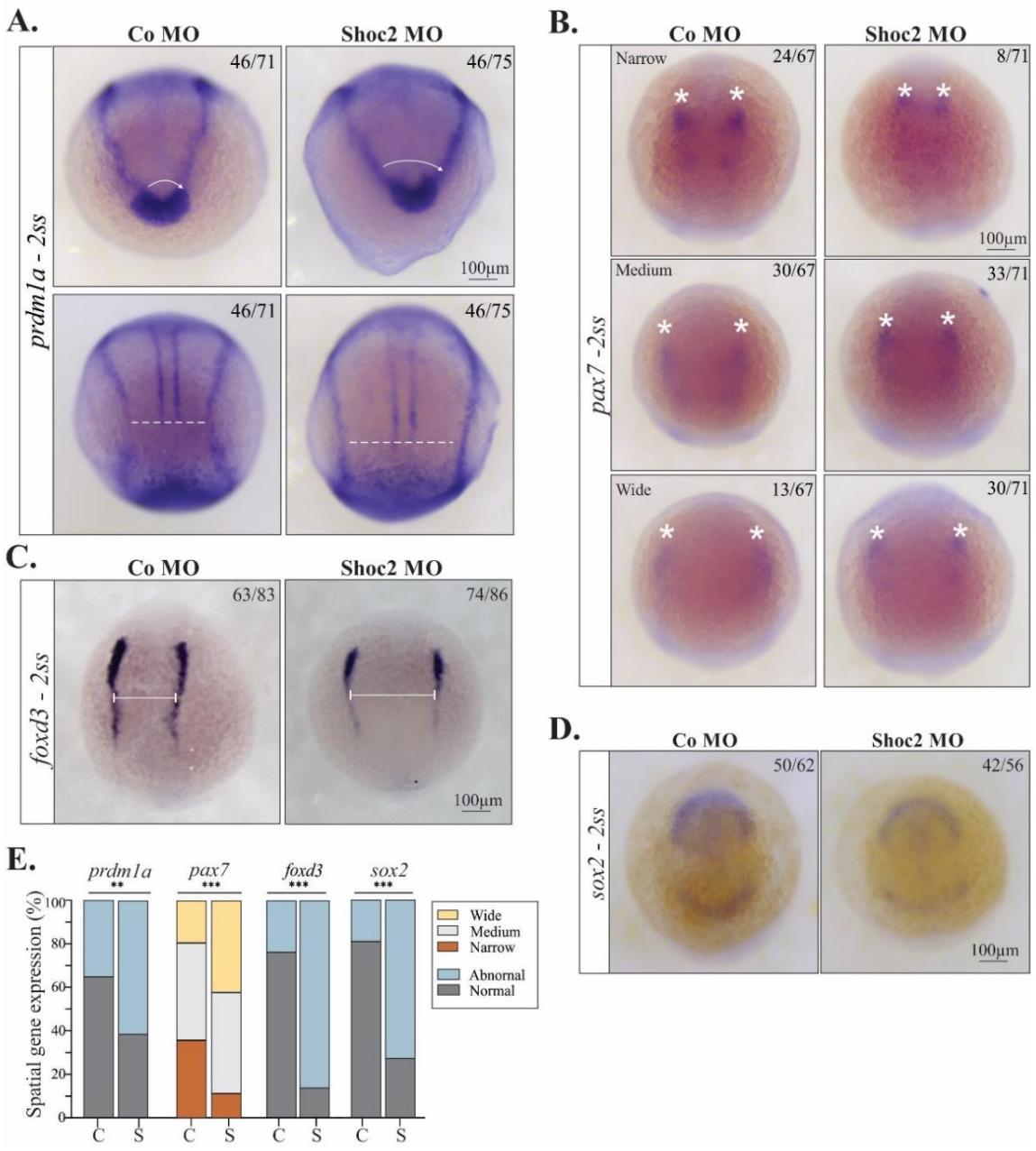

Figure 3.2 Analysis of gene expression at NPB of *shoc2* morphants

Dorsal views of control and *shoc2* morphant embryos showing expression of *prdm1a* (A), *pax7* (B), *foxd3* (C), and *sox2* (D) in 2-somite-stage embryos. Aberrant expression patterns of *prdm1a*, *pax7*, *foxd3*, and *sox2* are evident in *shoc2* morphants. Arrows, lines, and asterisks indicate parameters that were assessed to determine the abnormal expression

patterns. The categorical spatial distribution of *pax7* was determined empirically. The groupings “narrow”, “medium”, and “wide” are relative terms created to classify the embryos’ *pax7* gene distribution of the embryos used within this study’s replicates. The graph (E) shows the frequency of observed patterns from at least three independent experiments. The total number of embryos is indicated on each image. Statistically significant differences between *shoc2* MO and control MO according to the Pearson’s chi-squared test are indicated by *$p<0.05$, **$p<0.01$, ***$p<0.001$

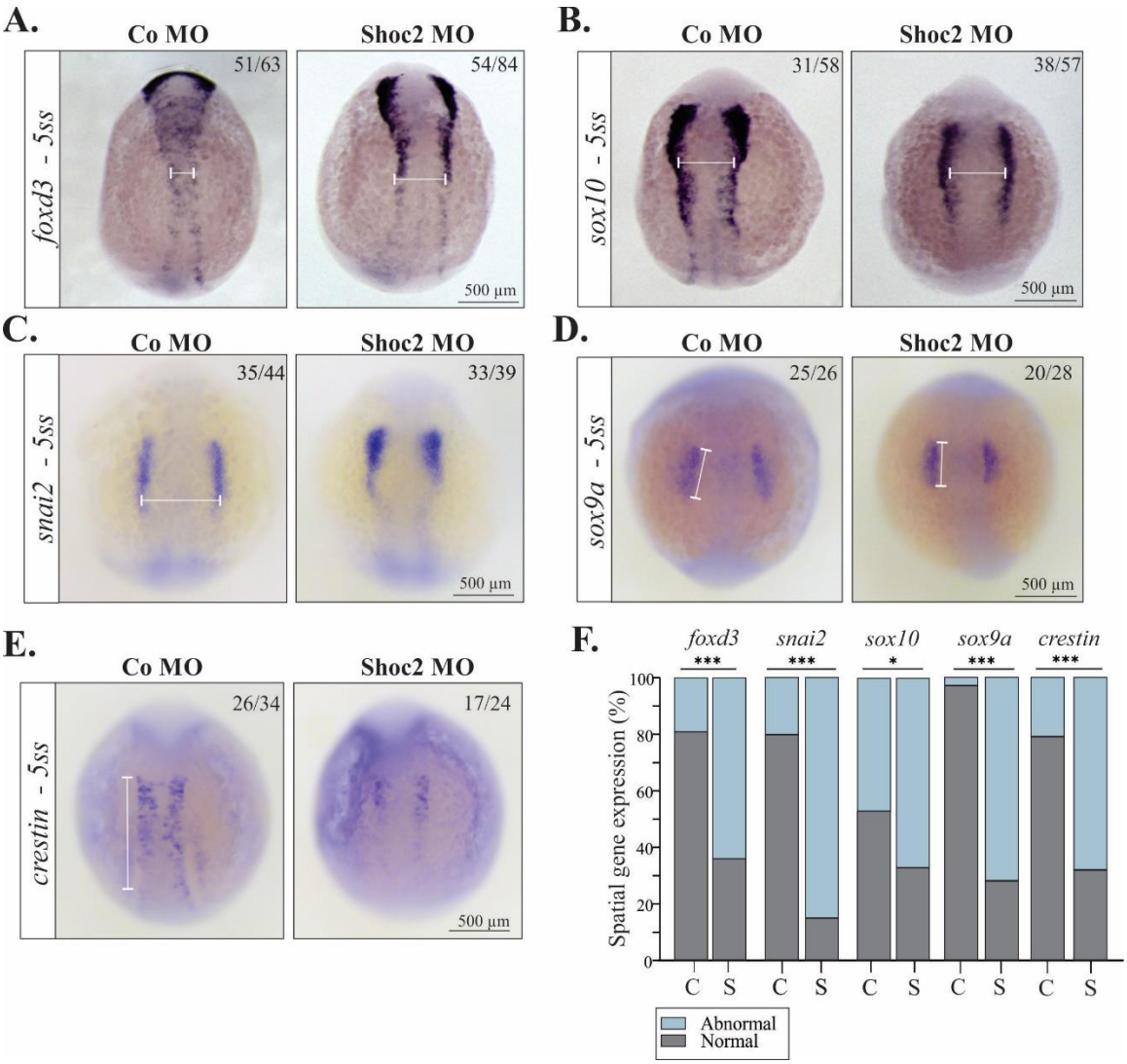

Figure 3.3 Molecular defects in NC specification in *shoc2* morphants

Dorsal views of control and *shoc2* morphant embryos show expression of NC specifiers *foxd3* (**A**), *sox10* (**B**), *snai2* (**C**), *sox9a* (**D**) and *crestin* (**E**) in 5-somite-stage embryos. White lines indicate the parameters that were assessed to determine the changes in expression of *foxd3*, *sox10*, *snai1*, *sox9a* and *crestin*. The graph (**F**) shows the frequency of observed expression patterns (C) from at least three independent experiments. The total number of embryos used in the statistical analysis is indicated on each image. Statistically significant differences between *shoc2* MO and control MO according to the Pearson's chi-squared test are indicated by *p<0.05, **p<0.01, ***p<0.001.

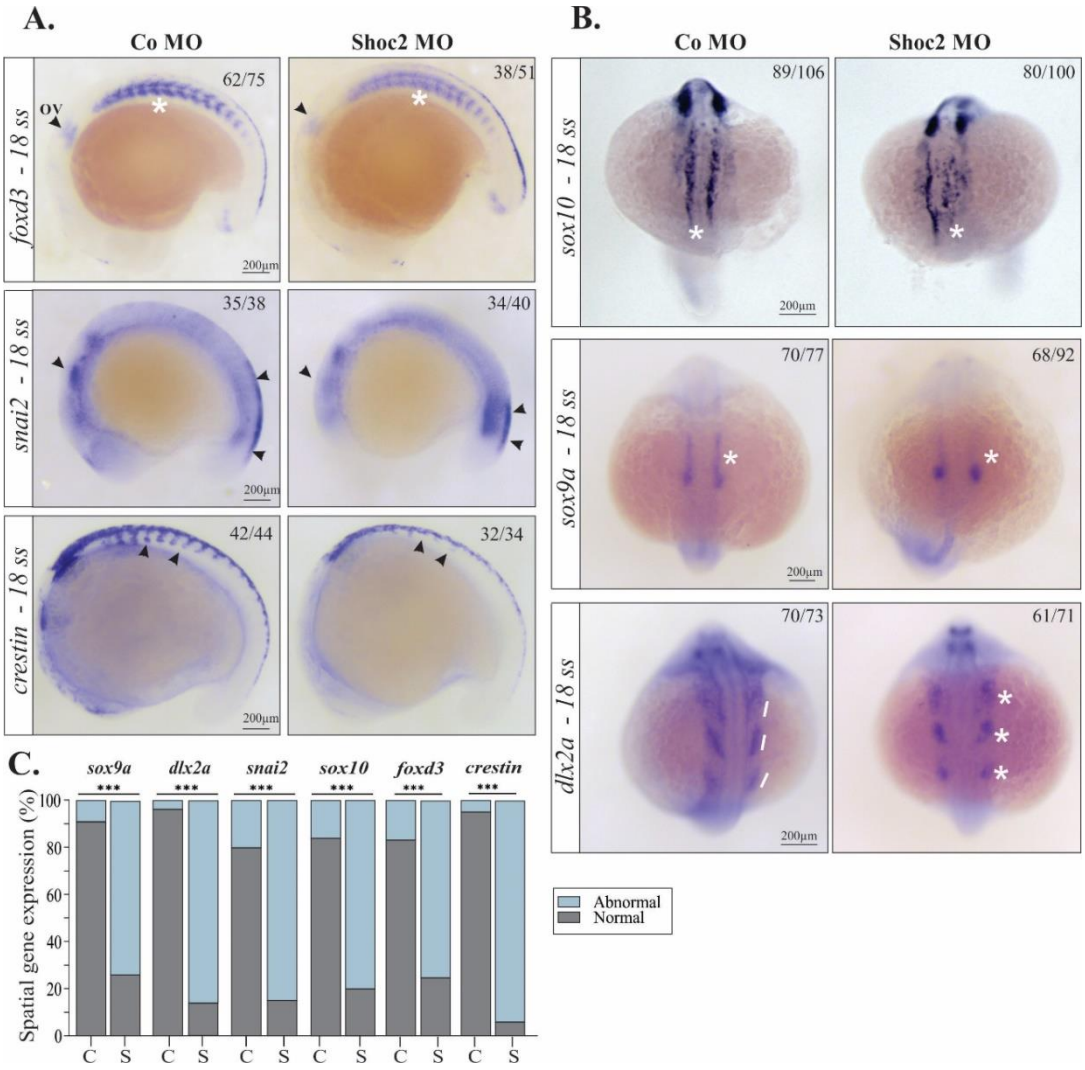

Figure 3.4 Gene expression abnormalities in early migrating NCCs in *shoc2* morphants

Lateral views of control and *shoc2* morphant embryos showing expression of (**A**) *foxd3, snai2,* and *crestin* at the 18-somite stage. (**B**) Dorsal views of control and *shoc2* morphant embryos showing expression of *sox10, sox9a,* and *dlx2a*. Arrows, asterisks, and lines indicate the parameters that were assessed to determine the abnormal expression patterns. The graph (**C**) shows the frequency of observed abnormal patterns after injection of *shoc2* MO or a control MO from at least three independent experiments. The total number of embryos assessed is indicated in each image. Statistically significant differences between

shoc2 MO and control MO according to the Pearson's chi-squared test are indicated by *p<0.05, **p<0.01, ***p<0.001. ov: otic vesicle.

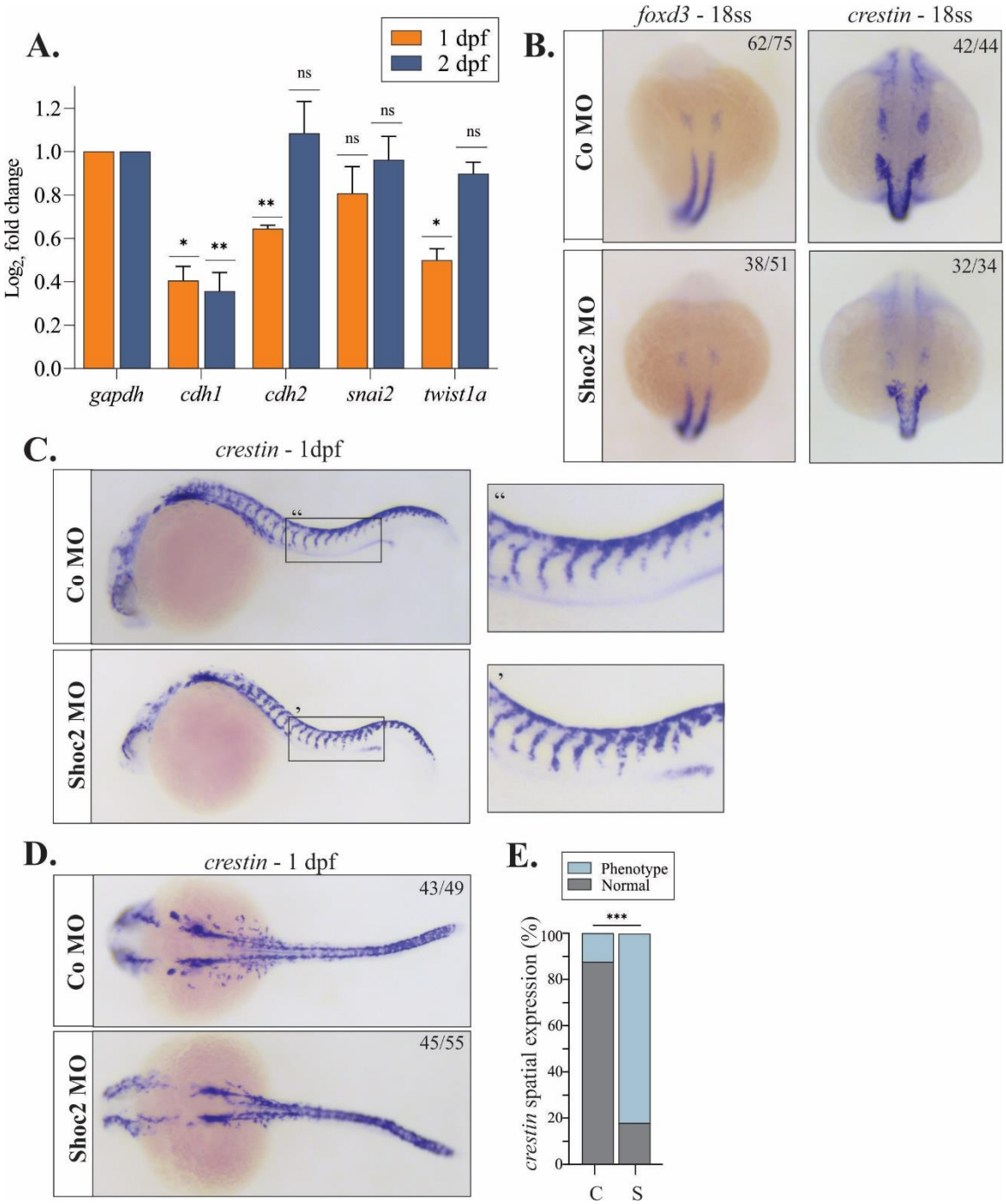

Figure 3.5 NC cell expression and EMT regulatory genes are misregulated in *shoc2* morphants

(**A**) Total RNA was extracted from 1 and 2 dpf morphant larvae and levels of mRNA was quantified by qPCR. The data are presented as the Log_2fold change of the mRNA levels in

the *shoc2 null* larvae normalized to WT larvae. *gapdh* is a control mRNA gene. The results represent an average of three biological replicas. Error bars indicate means with SEM. *p<0.05, ** p<0.01, *** p<0.001 (Student's t-test). (**B**) Dorsal view of control and *shoc2* morphant embryos showing expression of *foxd3* and *crestin* at 18 ss. The reduced expression of *foxd3* and *crestin* in morphant larvae is evident. The frequency of abnormal expression patterns after injection of *shoc2* MO or a control MO was quantified from at least three independent experiments. The total number of embryos is indicated on each image. (**C**) Lateral and dorsal views of control and *shoc2* morphant embryos showing expression of crestin at 1 dpf. (**D)** Changes in the crestin expression are apparent in the dorsal projection. The graph (**E**) shows the frequency of observed abnormal expression patterns after injection of *shoc2* MO or control MO from at least three independent experiments. The total number of embryos used in the statistical analysis is indicated. Statistically significant differences between *shoc2* MO and control MO according to the Pearson's chi-squared test are indicated by *p<0.05, **p<0.01, ***p<0.001.

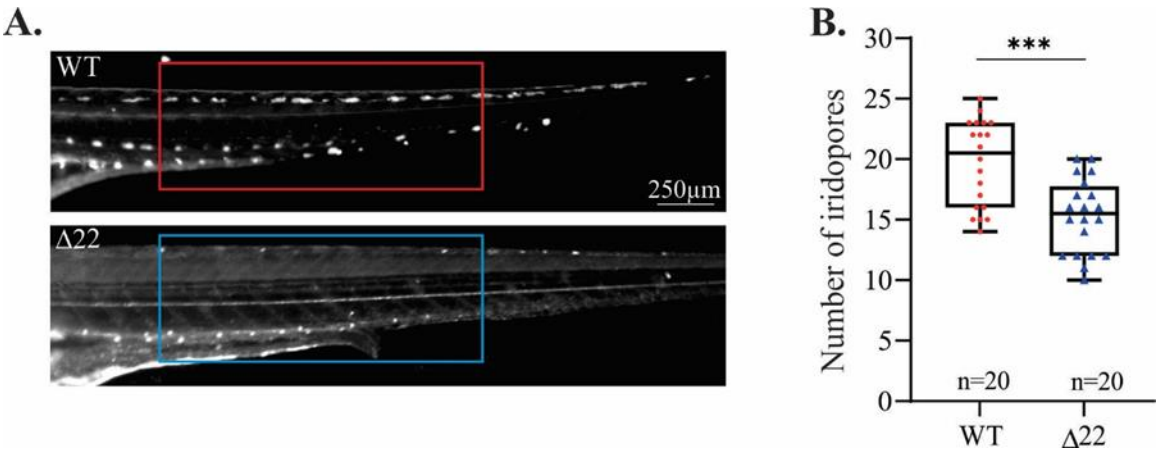

Figure 3.6 Reduced numbers of iridophores in Shoc2 *null* larvae

(**A**) 5 dpf embryos were imaged using incident light (lateral view) and all iridophores in a 1350µm long region in the tail (spanning approximately 11 somites) were quantified. Shoc2 *null* larvae display a significantly lower number of iridophores. (**B**) The box and whiskers plot shows the frequency of iridophores in WT and Shoc2 *null* larvae. The results represent an average of three biological replicas. Error bars indicate means with SEM. *p<0.05, ** p<0.01, *** p<0.001 (Student's t-test).

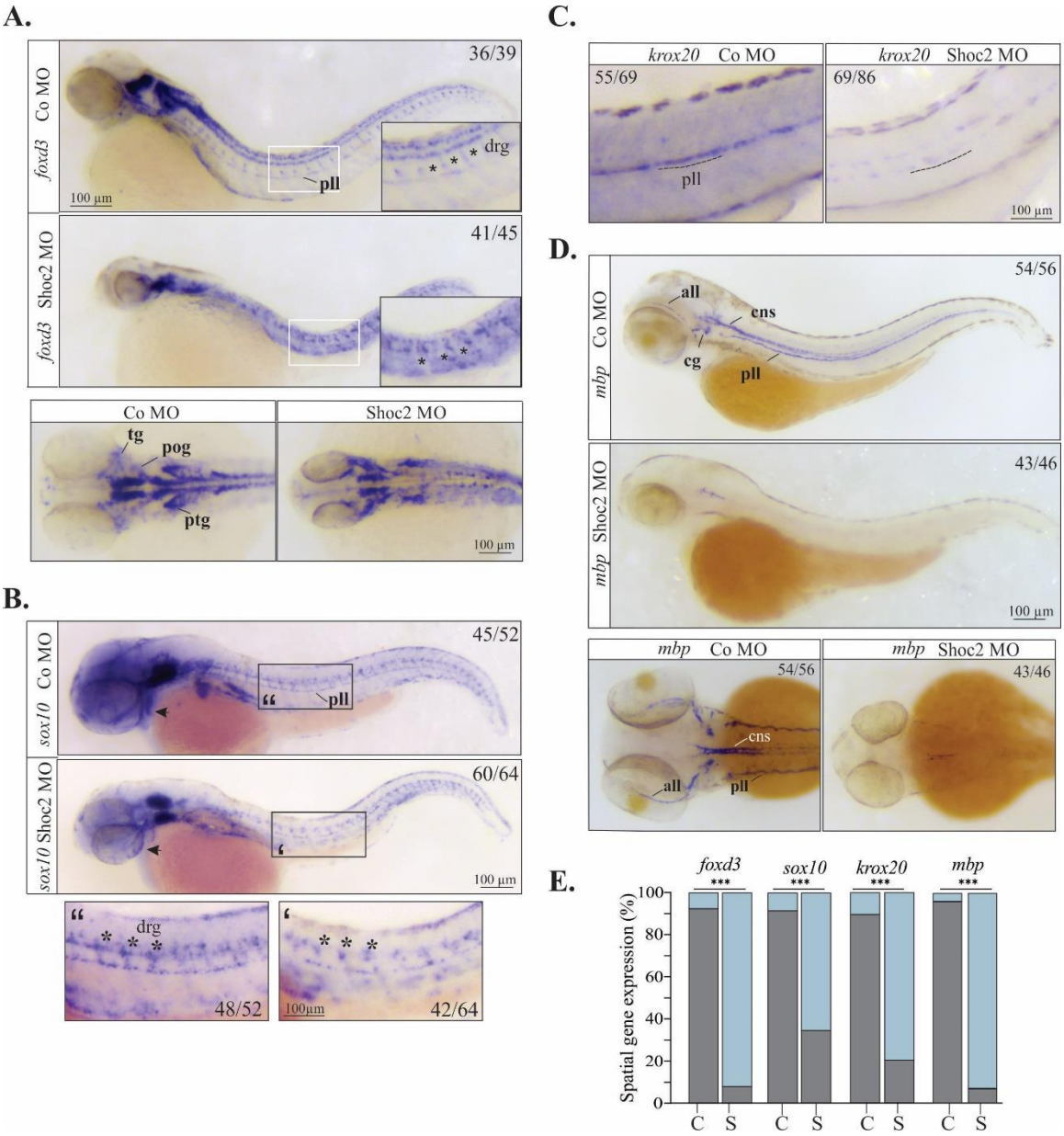

Figure 3.7 Molecular defects in NC specification and differentiation in *shoc2* morphants

Lateral and dorsal views of control and *shoc2* morphant embryos show the expression of *foxd3* (**A**) and *sox10* (**B**) at 2 dpf, and *krox20* (**C**) and *mbp* (**D**) at 3 dpf. Asterisks and lines indicate the parameters that were assessed to determine the abnormal expression patterns. The graph (**E**) shows the frequency of abnormal patterns from at least three independent

experiments. The total number of embryos assessed is indicated in each image. Statistically significant differences between *shoc2* MO and control MO according to the Pearson's chi-squared test are indicated by *p<0.05, **p<0.01, ***p<0.001. all: anterior lateral line. cns: central nervous system. pll: posterior lateral line. cg:cranial ganglia. drg: dorsal root ganglia. pog: preotic ganglia; ptg: postotic ganglia; tg: trigeminal ganglia

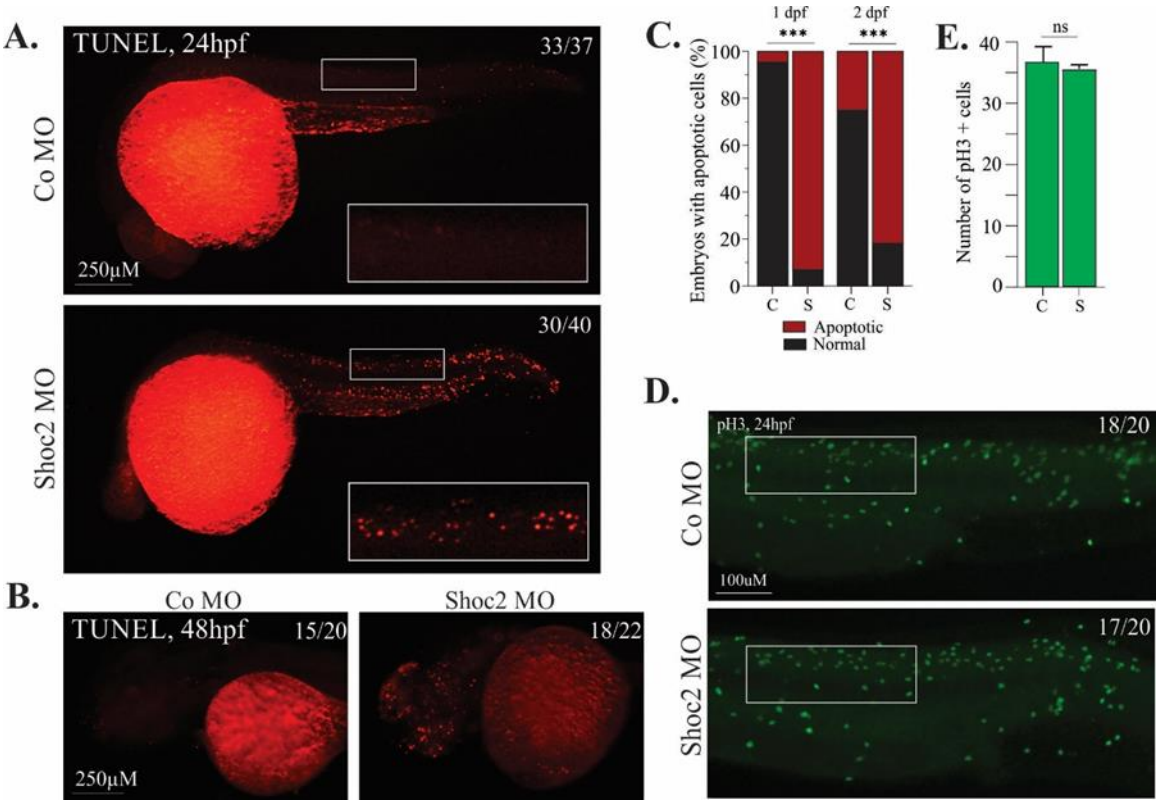

Figure 3.8 Loss of Shoc2 induces cell apoptosis but does not affect proliferation

(A, B) Lateral views of control and *shoc2* morphant larvae of cells labeled using TUNEL assay at 24 and 48 hpf. Apoptotic cells were found in the cranium and trunk/tail region at 24 and 48 hpf, respectively. The total number of embryos used in the statistical analysis is indicated on each image. (C) The graph shows the frequency of apoptotic cells after injection of *shoc2* MO or control MO from at least three independent experiments. Analysis by Pearson's chi-square test are indicated by *p<0.05, **p<0.01, ***p<0.001. (D) Control and *shoc2* morphant embryos are stained for phosphohistone H3 (pH3) as a marker of cell proliferation. Images of larvae trunk region were taken at 24 hpf. For statistical analysis, the total number of pH3 positive cells in 25,000 µm2 area from six embryo trunk regions were quantified for each injection group. (E) Graph shows the average number of positively stained pH3 cells per embryo after injection of shoc2 MO or

control MO from at least three independent experiments. Error bars indicate means with SEM. *$p<0.05$, ns: nonsignificant according to the Student's t-test.

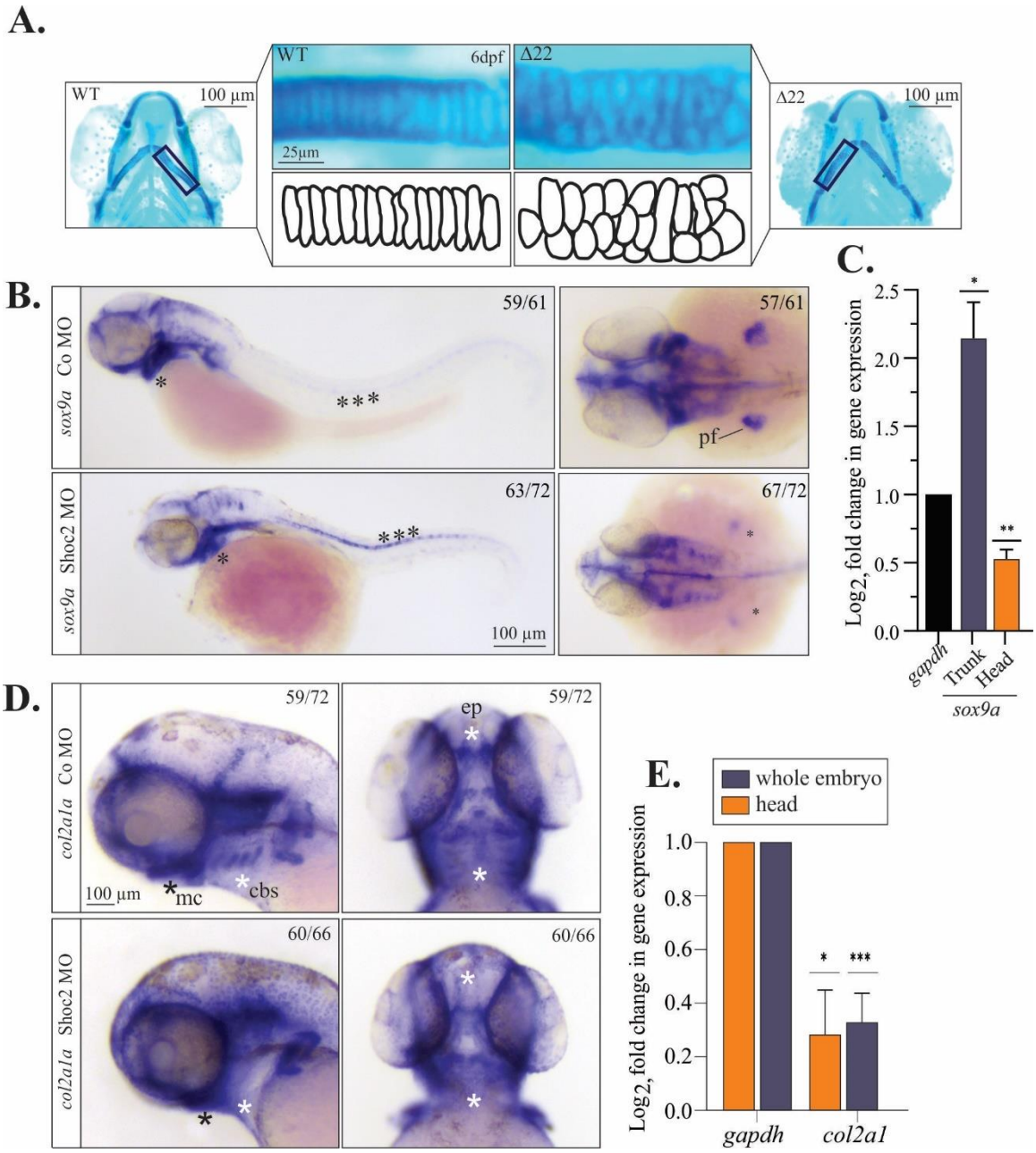

Figure 3.9 Molecular defects in craniofacial development and chondrocyte morphology in Shoc2 depleted embryos

(A) Flat mounts of WT and shoc2(Δ22) mutant 6 dpf larvae stained with Alcian blue. The lower panels show individual chondrocytes outlined in black, highlighting the differences in cell morphology of the ceratohyal cartilage. (B) Lateral and dorsal views of control and

shoc2 morphant larvae show the *sox9a* expression of 2 dpf larvae. Asterisks show areas of altered *sox9a* expression in the control and *shoc2* morphants. (C) Total RNA was extracted from dissected 3 dpf control and *shoc2* morphant larvae. The levels of *sox9a* mRNA expression were quantified by qPCR. *gapdh* is a control mRNA. The data are presented as the Log2fold change of the mRNA levels in morphant larvae normalized to control. The results represent an average of three biological replicas. Error bars indicate means with SEM. *p<0.05, ** p<0.01, *** p<0.001 (Student's t-test). (D) Lateral and dorsal views of control and *shoc2* morphant embryos show the *col2a1* expression in 3 dpf larvae. Asterisks mark areas of reduced col2a1 expression in *shoc2* morphants. (E) Total RNA was extracted from dissected 3 dpf control and *shoc2* morphant larvae and levels of *col2a1* mRNA expression were quantified by qPCR. The data are presented as the Log_2fold change of the mRNA levels in morphant larvae normalized to control. *gapdh* is a control mRNA. The results represent an average of three biological replicas. Error bars indicate means with SEM. *p<0.05, ** p<0.01, *** p<0.001 (Student's t-test). pf: pectoral fin. mc: Meckel's cartilage. cbs: ceratobranchials. ep: ethmoid plate.

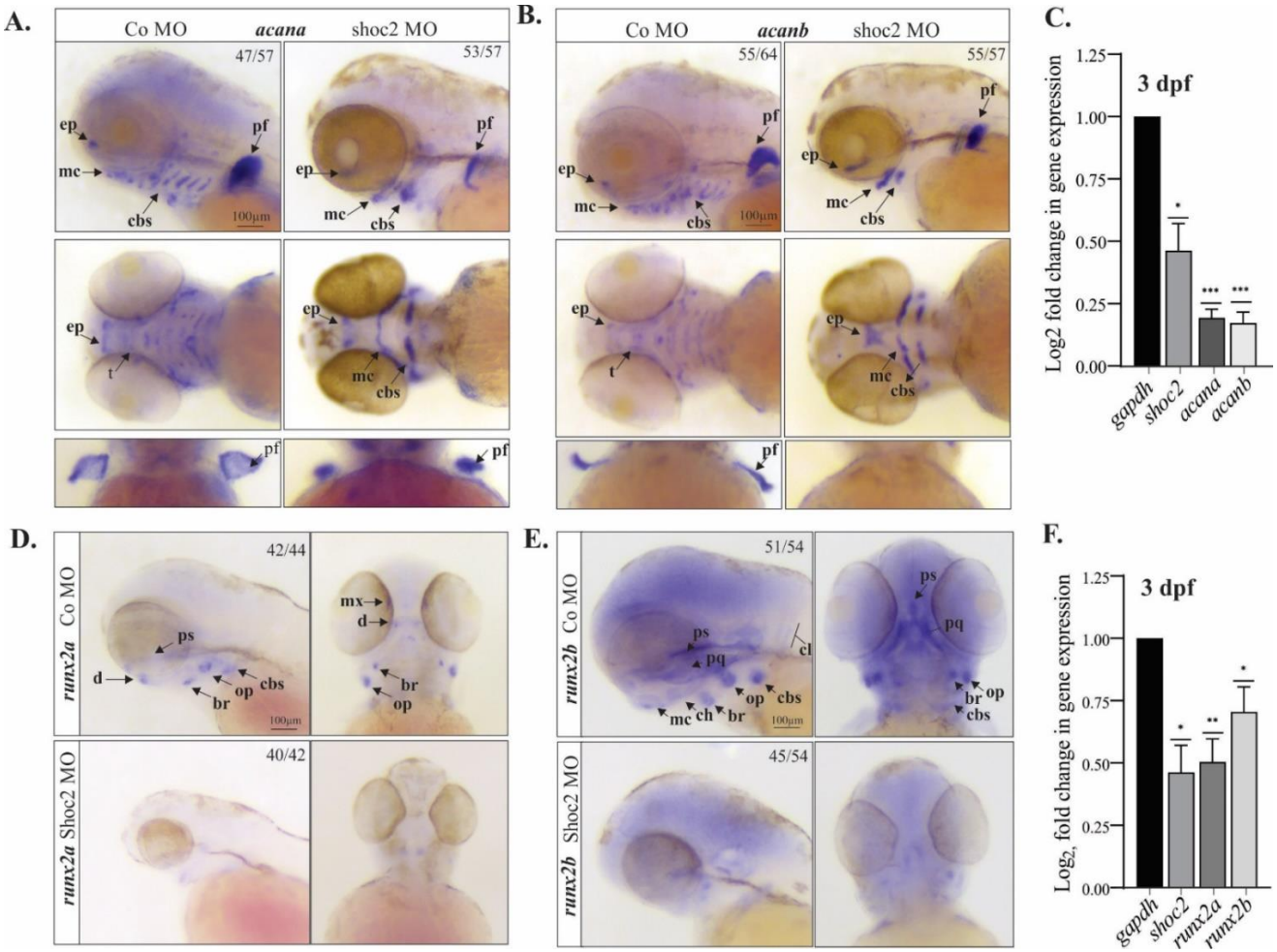

Figure 3.10 Extracellular matrix and bone pre-cursor genes are deficient in craniofacial cartilage and bone structures in *shoc2* morphants

Lateral and ventral views of control and *shoc2* morphant embryos show expression of the extracellular matrix proteoglycan acana (A) and acanb (B) at 3 dpf. Arrows indicate sites of reduced or lost expression. The total number of embryos used in the statistical analysis is indicated on each image. (C) Total RNA was extracted from control and *shoc2* morphant larvae at 3 dpf and levels of *shoc2*, *acana* and *acanb* mRNA expression were quantified by qPCR. *gapdh* is a control mRNA. The data are presented as the Log_2fold change of the mRNA levels in morphant larvae normalized to control. The results represent an average of three biological replicas. Error bars indicate means with SEM. *$p<0.05$, ** $p<0.01$, *** $p<0.001$ (Student's t-test). Lateral and ventral views of control and *shoc2* morphant embryos show expression of the runx2a (D) and runx2b (E) at 3 dpf Arrows indicate sites of reduced or lost expression. The total number of embryos used in the statistical analysis is indicated on each image. (F) Total RNA was extracted from control and *shoc2* morphant larvae at 3 dpf and levels of shoc2, runx2a and runx2b mRNA expression were quantified by qPCR. gapdh is a control mRNA. The results represent an average of three biological replicas. The data are presented as Log2fold change of the mRNA levels in morphant larvae normalized to control. Error bars indicate means with SEM. *$p<0.05$, ** $p<0.01$, *** $p<0.001$ (Student's t-test). ep: ethmoid plate. mc: Meckel's cartilage. cbs: ceratobranchials. pf: pectoral fin. t: trabeculae. d: dentary. ps: parasphenoid. br: branchiostegal ray. op: opercle. mx: maxilla. pq: palatoquadreate. cl: cleithrum. ch: ceratohyal

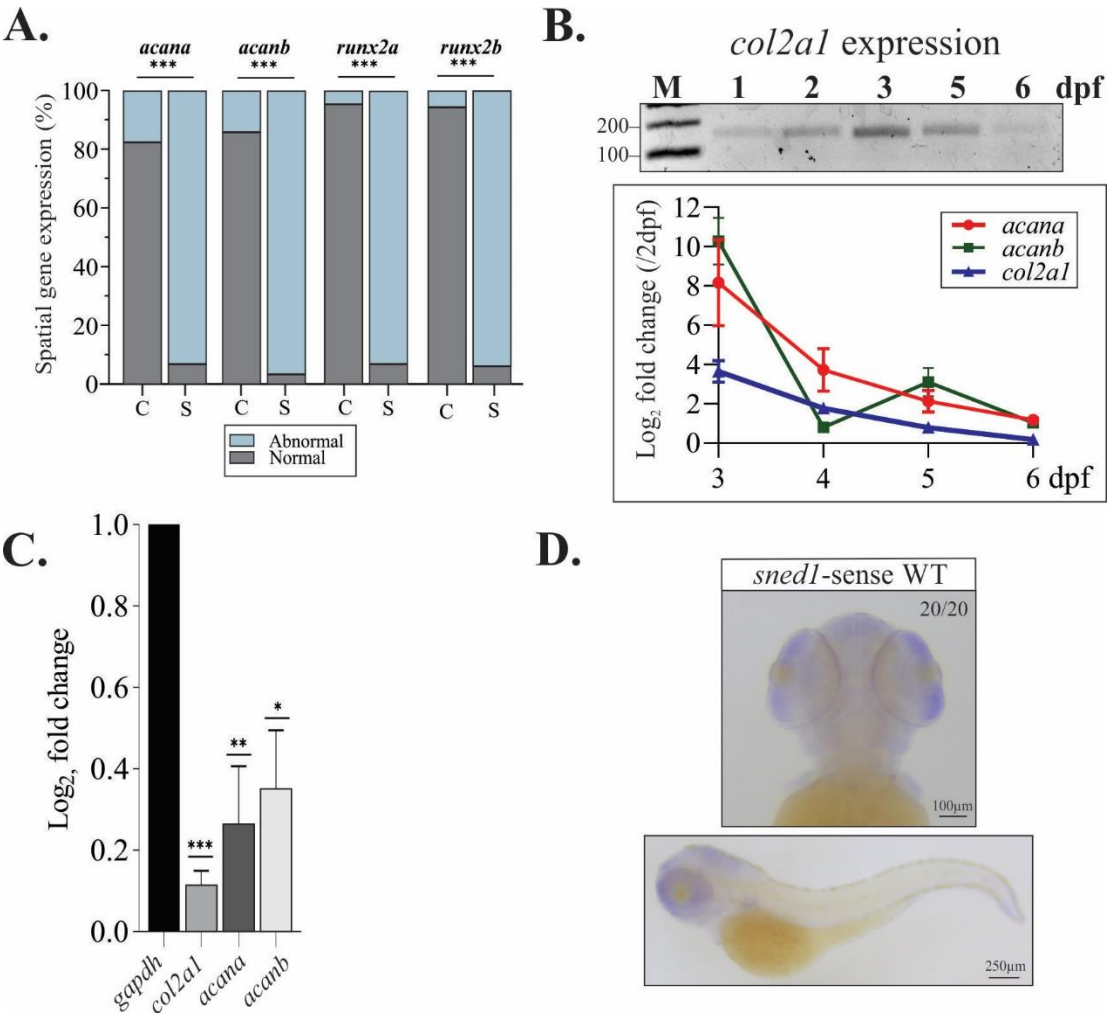

Figure 3.11 mRNA expression analysis

(A) The graph shows the frequency of abnormal patterns from at least three independent experiments. The total number of embryos assessed is indicated in each image. Statistically significant differences between shoc2 MO and control MO according to the Pearson's chi-squared test are indicated. (B) Total RNA was extracted from WT larvae at 1, 2, 3, 5, and 6 dpf. The levels of col2a1 expression were examined using semiquantitative RT-PCR (25 cycles) and visualized using agarose gel. The expression levels of col2a1, acana and acanb in WT larvae was then analyzed using qPCR. The data presented as the Log2fold change of the mRNA levels were normalized to mRNA levels at 2 dpf. The results represent an average of three biological replicas. (C) Total RNA was extracted from 3 dpf WT and 6

dpf Shoc2 *null* larvae and levels of mRNA were quantified by qPCR. The data are presented as the Log2fold change of the mRNA levels in the Shoc2 *null* larvae normalized to WT larvae. gapdh is a control mRNA gene. The results represent an average of three biological replicas. Error bars indicate means with SEM and statistically significant differences are indicated (Student's t-test). (D) Lateral and ventral view of WT embryos examined with sense probes for sned1 at 3 dpf. No apparent background staining presented. Statistically significant differences are indicated by *$p<0.05$, **$p<0.01$, ***$p<0.001$.

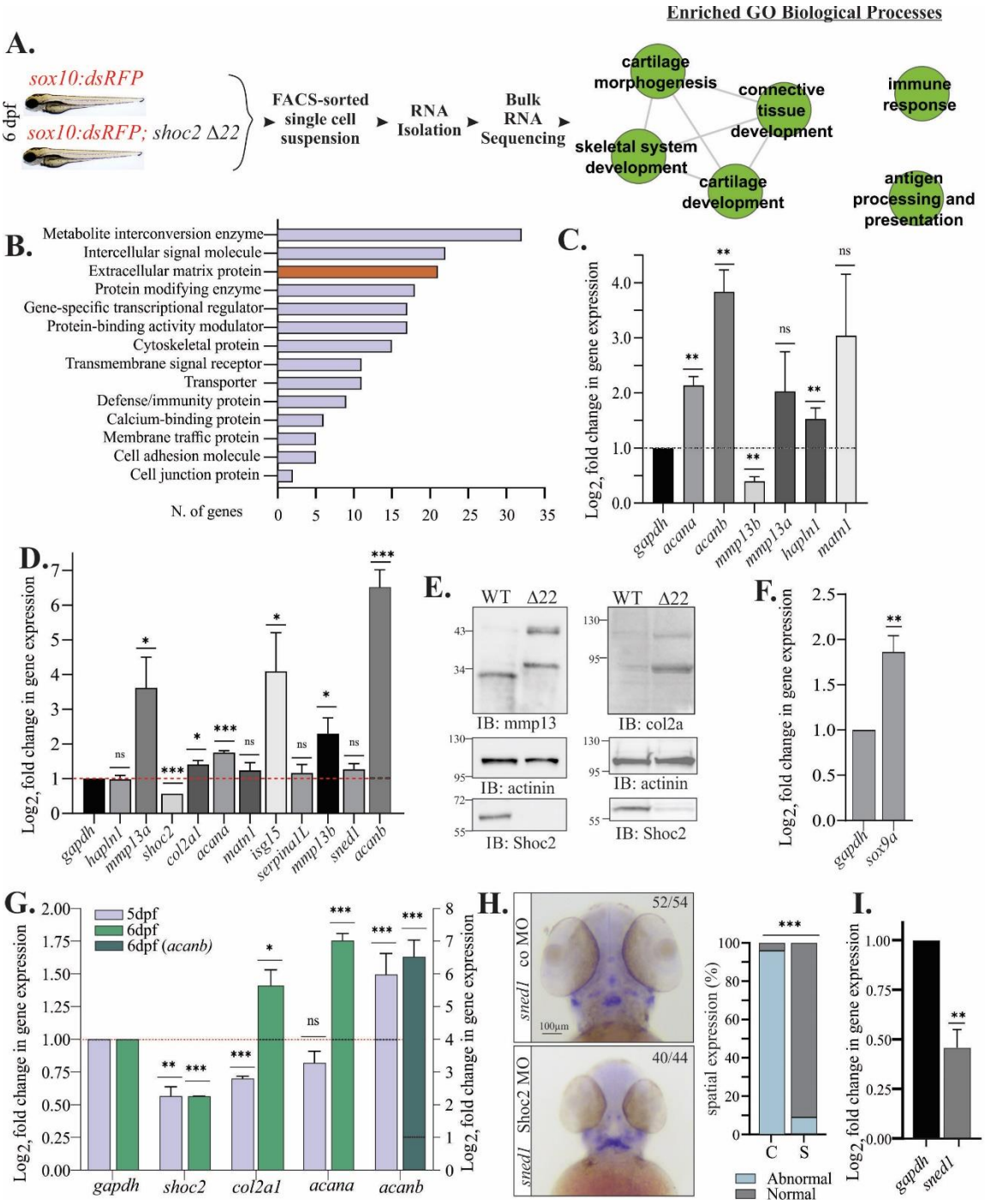

Figure 3.12 Shoc2 knock-out affects gene expression of the Sox10-positive cells

(A) Cartoon illustrating the workflow used to analyze transcriptome of sox10: RFP + cells. Total RNA was isolated from the FACS-sorted sox10: RFP + cells, followed by RNA-seq

analysis. Data was profiled to identify Enriched GO Biological Processes from Category Compare (Flight et al., 2014). Nodes represent enriched annotation of DEGs. Edges represent relationship between annotation sharing high number of genes with p-value cutoff 0.001 and edge weight greater than 0.90. (B) The top 15 protein classes of 351 differentially expressed genes (FDR≤ 0.05) analyzed with PANTHER pathway analysis. (C) DEGs were selected from the protein class of "Extracellular matrix proteins". Total RNA was extracted from sox10:dsRed + cells of control and shoc2 *null* larvae at 6 dpf and mRNA expression were quantified by qPCR. gapdh is a control mRNA. The results represent an average of three biological replicas. The data are presented as the Log2fold change of the mRNA levels in the shoc2 *null* larvae normalized to WT larvae. Error bars indicate means with SEM. *p<0.05, ** p<0.01, *** p<0.001 (Student's t-test). (D.) DEGs were selected from the protein class of Extracellular Matrix Proteins. Total RNA extracted from sox10:dsRed + control and shoc2 *null* larvae at 6 dpf and levels mRNA expression were quantified by qPCR. The data are presented as the Log2fold change of the mRNA levels in the shoc2 *null* larvae normalized to WT larvae. gapdh is a control mRNA. The results represent an average of three biological replicas. Error bars indicate means with SEM. *p<0.05, ** p<0.01, *** p<0.001 (Student's t-test). (E) Control and shoc2 *null* larvae were harvested for immunoblotting at 6 dpf. The expression of indicated proteins was analyzed using specific antibodies by WB. (F.) Total RNA extracted from WT and shoc2 *null* larvae at 6 dpf. mRNA expression of sox9a was quantified by qPCR at 6 dpf. The data are presented as the Log2fold change of the mRNA levels in the shoc2 *null* larvae normalized to WT larvae. Gapdh is a control mRNA. The results represent an average of three biological replicas. Error bars indicate means with SEM. *p<0.05, ** p<0.01 (Student's t-test). (G) Total RNA extracted from control and shoc2 *null* larvae. mRNA expression was quantified by qPCR at 5 or 6 dpf. The data are presented as the Log2fold change of the mRNA levels in the shoc2 *null* larvae normalized to WT larvae. Gapdh is a control mRNA. The results represent an average of three biological replicas. Error bars indicate means with SEM. *p<0.05, ** p<0.01 (Student's t-test). (H) Ventral view of WT and *shoc2* morphant embryos showing expression of sned1 in 3 dpf larvae. Aberrant expression patterns of sned1 are evident in *shoc2* morphants. The graph shows the frequency of abnormal patterns. The total number of embryos used in the statistical analysis

is indicated. The results represent an average of three biological replicas. Statistically significant differences between shoc2 MO and control MO according to the Pearson's chi-squared test are indicated by *$p<0.05$, **$p<0.01$, ***$p<0.001$. (I) Total RNA was extracted from control and shoc2 *null* larvae at 6 dpf. The levels of sned1 mRNA expression were quantified by qPCR at 5 and 6 dpf. The data are presented as the Log_2fold change of the mRNA levels in the *shoc2* morphant larvae normalized to control larvae. gapdh is a control mRNA. The results represent an average of three biological replicas. Error bars indicate means with SEM. *$p<0.05$, ** $p<0.01$ (Student's t-test).

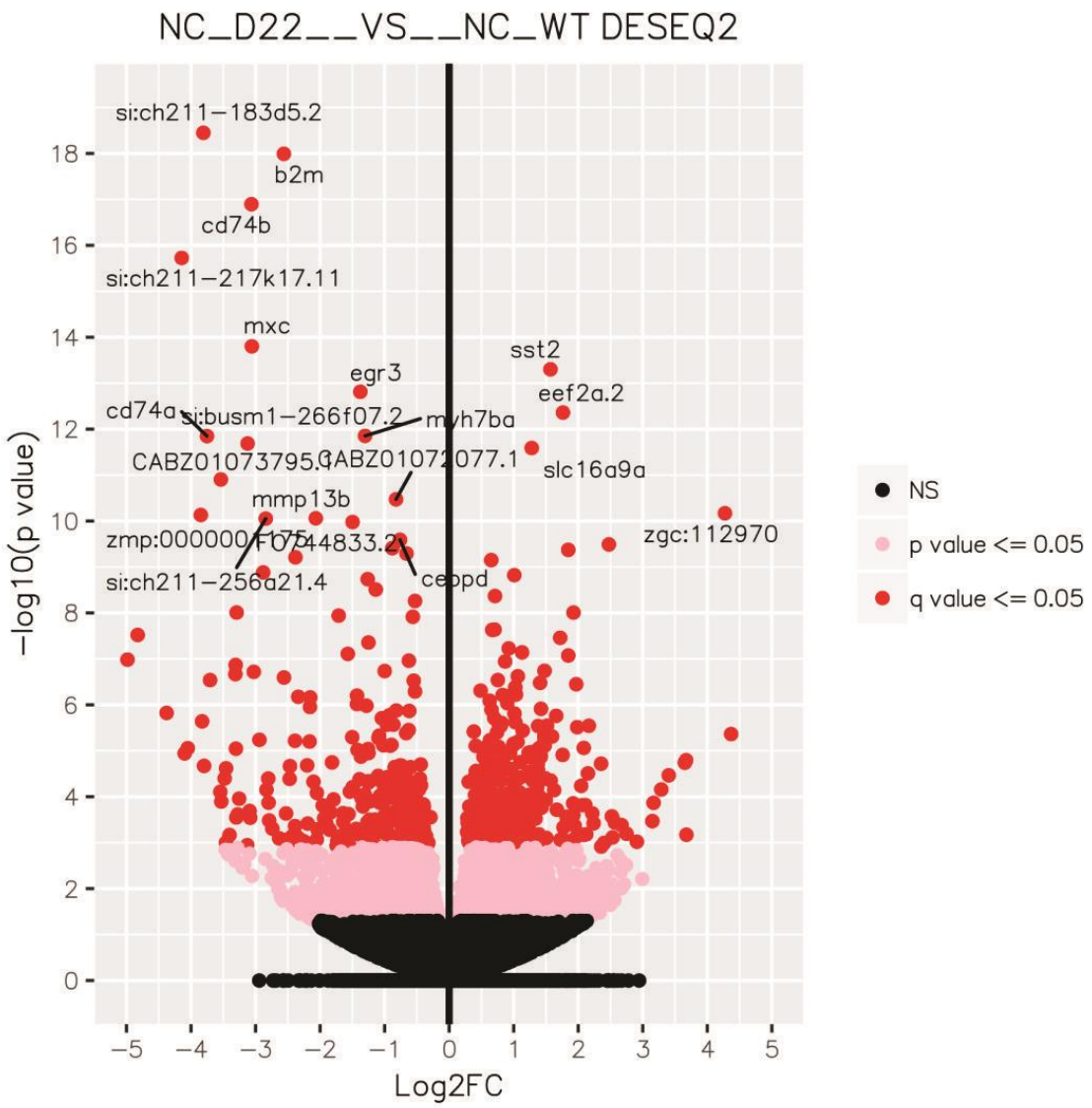

Figure 3.13 DESeq2 Volcano plot

Volcano plot was created to examine the distribution of Log2 fold change at different significance levels. Log2 fold change on the x-axis is plotted against – log10 (p-value) on the y-axis. NS- non-significant.

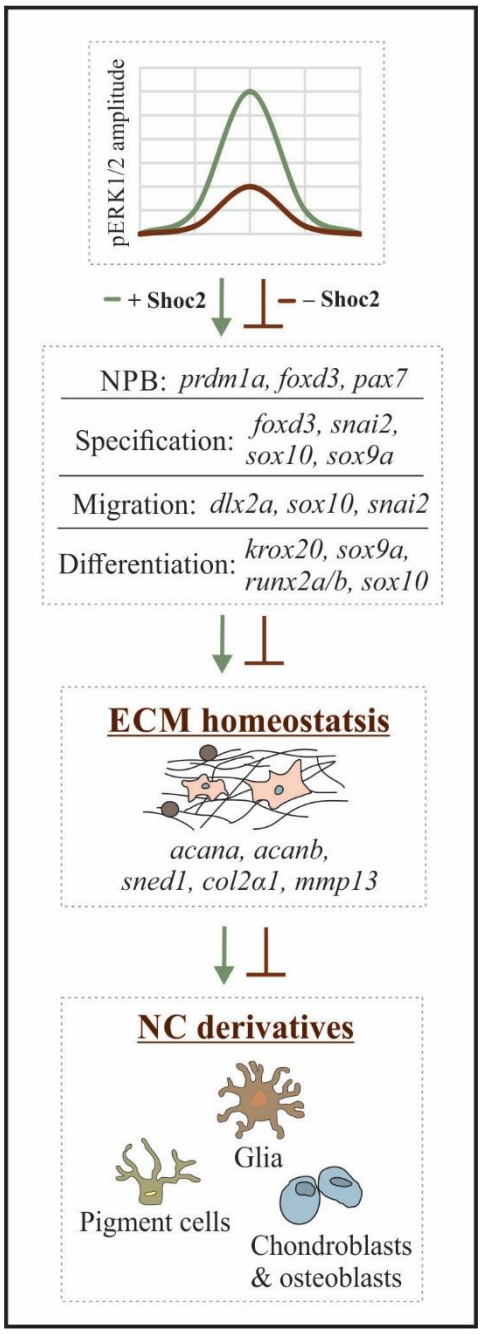

Figure 3.14 Schematic diagram showing the working model depicting what is currently understood for the role of Shoc2 embryonic development

Shoc2 amplifies and modulates ERK1/2 signaling during early stages of NC development. Lack of Shoc2 followed by the changes in dynamics of ERK1/2 signals (e.g. reduction in

signals amplitude) affects expression of key transcription factors essential for NCCs specification, migration and differentiation. Defects in early stages of NC development lead to aberrant expression of downstream effector genes, including proteins regulating homeostasis and remodeling of ECM, ultimately leading to the profound defects in multiple NCC derivatives.

CHAPTER 4. CHARACTERIZATION OF THE SHOC2 SA24200 MUTANTS

Abstract

To study the role of Shoc2 in development, the Galperin lab has developed several zebrafish models. One of these models, *shoc2* Δ22, was utilized in the studies above (**Figures 3.9-3.13**) [103]. For these models, the *shoc2* gene was edited using CRISPR/Cas9 methodology to introduce a premature stop codon in the protein-coding sequence of Shoc2. An additional model was obtained from the Zebrafish International Resource Center (ZIRC) [154]. Here, ENU methodology was utilized for random mutagenesis. In this zebrafish line the mutation was introduced in c.1546G>A disrupting the splice site between exons five and six. In this study, we further characterize the *shoc2* (sa24200) model and determine that the splice site mutation leads to an insertion of 31 nucleotides of intronic sequences thereby disrupting Shoc2 protein coding. Moreover, we established that zebrafish embryos homozygous for c.1546G>A substitution are embryonic lethal. Importantly, severe morphological defects observed in homozygous c.1546G>A larvae were identical to those of the homozygous *shoc2* Δ22 mutants demonstrating the feasibility of sa24200 model for future studies.

Introduction

Similar to other species, N-Ethyl-N-Nitrosourea (ENU) treatment introduces high rates of random mutagenesis in zebrafish [154, 187]. To generate or expand a mutant line depository, random mutagenesis by ENU treatment is often utilized as a broad, "shotgun" approach [154, 187]. For example, The Wellcome Trust Sanger Institute Zebrafish Mutation Project generated a mutant depository of over 40,000 mutant zebrafish alleles covering more than 60% of all zebrafish protein coding genes [188]. Among these mutations, the *shoc2* mutant zebrafish (sa24200) was recovered through mutation screens after ENU treatment. The sa24200 line was subsequently obtained by the Galperin lab from the Zebrafish International Resource Center [154]. The induced point mutation (c.1546G >A) was reported within a predicted consensus splice site. However, no additional validation or information was performed.

Although the ENU-induced random mutagenesis approach effectively generates many mutant lines, ENU treated organisms may acquire additional, undetected mutations within genes. Therefore, prior to use for scientific experimentation, these mutant lines must be thoroughly examined and characterized to prevent aberrant data. The study presented in this chapter shows the characterization of the *shoc2* sa24200 homozygous mutant $sa^{24200/24200}$.

Results

4.1 *Shoc2* c.1546G>A mutation leads to zebrafish embryonic lethality

The ENU-induced *shoc2* homozygous F2 male mutant, *shoc2*+/sa^{24200}, zebrafish (sa24200, *shoc2*, c. 1546G>A) was acquired from ZIRC (**Figure 4.1A**). The c.1546G>A substitution obliterates a restriction site for Hph1 endonuclease (5'…G<u>G</u>TGA$(N)_8$…3' (the

1546th nucleotide underscored) (**Figure 4.1A**). Thus, to identify the c.1546G>A mutation, the substitution's flanking region was amplified by PCR using the primers: Forward 5'-TCCCTTTTGGCATTTTCTCTCG-3' and Reverse 5' -GAGTTTGTTCAGCCAGCATCC-3'. The PCR product was then digested with Hph1 enzyme (**Figure 4.1B**). The *shoc2*+/sa^{24200} adults were selected based on the results of a PCR followed by the failure of a Hph1 restriction enzyme digest. The *shoc2*+/sa^{24200} adult fish are viable, fertile, and displayed no overt phenotypes. To avoid potential non-specific ENU-induced mutations, *shoc2*+/sa^{24200} zebrafish were outcrossed with WT AB fish to obtain generation F5.

To generate homozygous *shoc2* mutant larvae (sa^{24200}/sa^{24200}), heterozygous *shoc2*+/sa^{24200} adults were incrossed. The sa24200 line was reported to contain the *shoc2* mutation at the first intronic nucleotide after exon 5. Here, the nucleotide residue of interest is underlined and the functional consensus splice site is: 5'… MAG<u>G</u>TRAGT…3' ; where M = A or C and R = A or G. To validate aberrant splicing, cDNA was generated from 6 dpf *shoc2* sa^{24200}/sa^{24200} larvae. We found that cDNA amplified using mRNA isolated from sa^{24200}/sa^{24200} mutants was larger than a similar fragment amplified from WT control (**Figure 4.2A**). The defect in the exon-intron splicing was confirmed by sequencing. The primers' sequences for cDNA fragment amplification were located in exon four and six to fully incorporate the region of interest (Forward (exon 4): 5'-CGGTTTTACCAGAGGGGCTT-3' and reverse (exon 6) 5' -CCACCATACTGGTCCACGTC -3'. The mutant *shoc2* sa24200 allele incorporates 31 intronic nucleotides into the mRNA transcript resulting in a longer amplicon (289 nucleotides) as compared to WT's fragment (258 nucleotides) (**Figure 4.2B**).

To determine whether defects in RNA splicing affects the mRNA expression levels, qPCR was performed (**Figure 4.3A**). We found that *shoc2* mRNA levels were dramatically lower than in the control larvae. To visualize changes in expression levels, semi-quantitative PCR was performed by limiting the PCR amplification cycles to 26. Resulting cDNA fragments were resolved by agarose gel (**Figure 4.3B**). Additionally, *shoc2* mRNA expression was assessed using WISH. We found that 23% of the embryos from incrossed *shoc2*+/sa^{24200} zebrafish exhibited reduced *shoc2* staining, consistent with expected Mendelian ratios. The intensity of WISH *shoc2* staining corresponded to the genotypes in all larvae (**Figure 4.3 C-E**).

4.2 S*hoc2* c.1546G>A embryos are Shoc2-*null*, edemic, and lethal

To examine the Shoc2 protein expression in *shoc2* sa^{24200}/sa^{24200} larvae, a western blot analysis was performed. Protein expression analysis using an antibody against Shoc2 confirmed the loss of Shoc2 protein expression in *shoc2* sa^{24200}/sa^{24200} (**Figure 4.4**). Similar to *shoc2*$^{\Delta 22}$ homozygous mutants, sa^{24200}/sa^{24200} larvae are not viable (**Figure 4.5**). When *shoc2* +/sa^{24200} were incrossed, no severe morphological defects were detected in the progeny prior to 4 dpf. However, at later stages of development, pleiotropic effects on larval morphology became progressively more severe and were observed in the *shoc2* sa^{24200}/sa^{24200} larvae beginning at 4 dpf (**Figure 4.6A, B**). By 6 dpf, 72% of *shoc2* sa^{24200}/sa^{24200} larvae developed edema of the heart cavity, along the trunk, yolk sac/extension, and around the eyes (**Figure 4.6B**). Similar to the *shoc2Δ22* and *shoc2Δ14* lines, the sa24200 swim bladders were underinflated and larvae were lethargic. Of note, the sa^{24200}/sa^{24200} larvae initially began to developed edemas a day earlier (4 dpf) than

previously observed by the *shoc2Δ22* homozygous mutants (5 dpf). Furthermore, the severity of the *shoc2* sa^{24200}/sa^{24200} induced edemas was worse as compared to *shoc2Δ22* mutant edemas. Further quantitative survival studies indicated that at 6 dpf *shoc2* sa^{24200}/sa^{24200} larvae began to die with none surviving beyond 11 dpf. All of WT and heterozygous larvae survived to 11 dpf and displayed the expected Mendelian ratio for homozygous WT versus heterozygous genotypes (1:2) (**Figure 4.6B**).

Similar severe edema was observed for the compound mutant of *shoc2Δ22* and *shoc2* +/sa^{24200} (**Figure 4.6C**). Of note, 18% of embryos that developed edema were *shoc2* +/sa^{24200} suggesting that some *shoc2* +/sa^{24200} embryos may also develop abnormalities. Furthermore, from an additional *shoc2* +/sa^{24200} and *shoc2*Δ^{22} compound mutant outcross, on 6 dpf, 10 edemic embryos were selected, genotyped, and determined to be *shoc2* sa^{24200}*/Δ22*. (**Figure 4.6D**). This further emphasizes that the edemic phenotype is *shoc2* mutant specific. Taken together, these data suggest that c.1546G>A nucleotide substitution in the fifth intronic splice site destabilizes *shoc2* mRNA thereby affecting Shoc2 protein levels.

4.3 *Shoc2* c.1546G>A mutation affects development of NC-derived tissues

In addition to edemas, *shoc2* sa^{24200}/sa^{24200} larvae also display craniofacial abnormalities including hypoplastic closure of the Meckel's Cartilage (**Figure 4.**7). Morphological analyses of Alcian blue stained embryos showed that *shoc2* sa^{24200}/sa^{24200} mutants presented a prominent defect in their Meckel's cartilage (**Figure 4.**7). S*hoc2* sa^{24200}/sa^{24200} mutants' Meckel's cartilage curved downwards and did not extend as far rostrally as compared to the WT. Additionally, careful examination revealed that the *shoc2*

sa^{24200}/sa^{24200} larvae exhibited hypoplastic closure of the Meckel's cartilage. These changes indicate that Shoc2-mediated signaling is required for craniofacial structure development.

During early development intramembranous (dermal) and cartilage bones make up three ossified teeth, other ossified bone structures (including parasphenoid, opercle, ceratobranchial, cleithrum), and contribute to the pharyngeal arches. Alizarin Red S staining detects calcified cells of the osteogenic lineage present by 6 dpf. In sa^{24200}/sa^{24200} larvae, Alizarin Red S staining visualized a strong reduction in the calcification of craniofacial bones compared to WT (**Figure 4.8**). These data suggest that bone formation and/or remodeling requires Shoc2 mediated signaling.

In addition to craniofacial deficiencies, *shoc2* sa^{24200}/sa^{24200} mutants also displayed abnormal pigmentation patterning shown as a loss of iridophores (**Figure 4.9A & B**) and irregular melanocyte patterning (**Figure 4.9 C**). At 6 dpf WT larvae displayed a consistent pattern of *de novo* iridophores along the dorsal and ventral aspects of the lateral trunk. However, the total number of iridophores presented on *shoc2* sa^{24200}/sa^{24200} mutants was reduced as compared to WT (**Figure 4.9 A, B**). Additionally, WT larvae displayed a distinct, uniform patterning of melanophores on the head and along the lateral stripe (**Figure C**). However, *shoc2* sa^{24200}/sa^{24200} mutants present irregular melanophore patterning with overlapping lentigines.

In summary, the findings of the *shoc2* sa^{24200}/sa^{24200} mutant embryos are consistent with our data from the *shoc2* Δ*22* and Δ*14* zebrafish lines. *Shoc2* sa^{24200}/sa^{24200} are Shoc2-*null*, display mutant-specific edemas, and present deficient craniofacial development (impaired cartilage and bone formation). They exhibit irregular pigmentation presented as a reduced number of iridophores and displayed abnormal melanophore patterning.

4.4 Ch. 4 Tables and figures

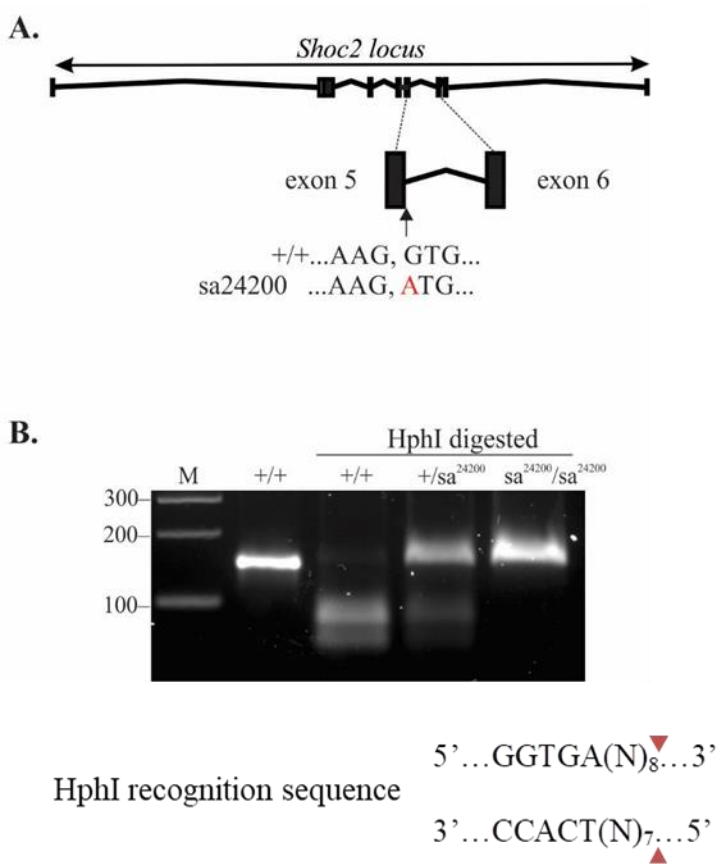

Figure 4.1 Detection of heritable shoc2 point mutation

(A) Schematic representation of *shoc2* loci and the ENU-induced c.1546G>A point mutation in *shoc2* sa24200 fish.

(B) PCR analysis from genomic DNA and subsequent restriction enzyme (HphI) digestion allows for sensitive detection of *shoc2* WT and mutant alleles in individual larvae. *Shoc2* c.1546 G>A alters the HphI recognition sequence (WT) 5'…G<u>G</u>TGA$(N)_8$…3' at the 1546th nucleotide residue shown underlined inhibiting HphI digestion of the WT *shoc2* region of interest. Agarose gel electrophoresis shows amplicons of WT, heterozygous, and homozygous *shoc2*. Primers used for *shoc2* amplification are reported in **Table 2.1.**

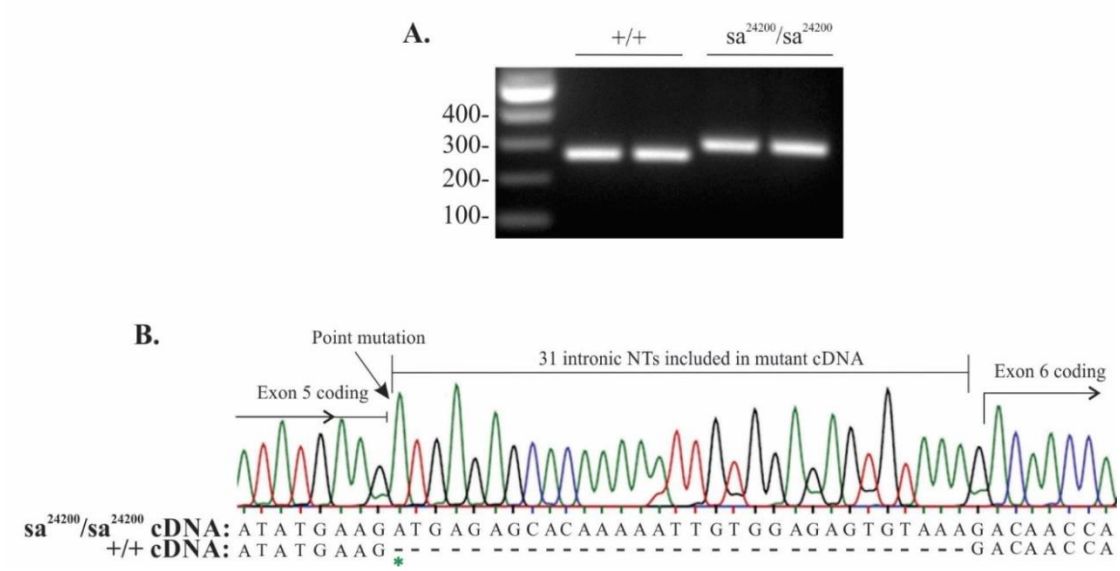

Figure 4.2 Analysis of the shoc2 mutant transcripts

A) RT-PCR analysis allows for sensitive detection of WT and *shoc2* mutant RNA in individual larvae. Agarose gel electrophoresis shows PCR amplicons of WT and *shoc2* sa^{24200} mutant.

(B) Sequencing chromatogram from cDNA from *shoc2* sa^{24200}/sa^{24200} mutant embryo. The sequencing result confirms the reported mutation. (Asterisk indicates the G>A point mutation induced by ENU treatment).

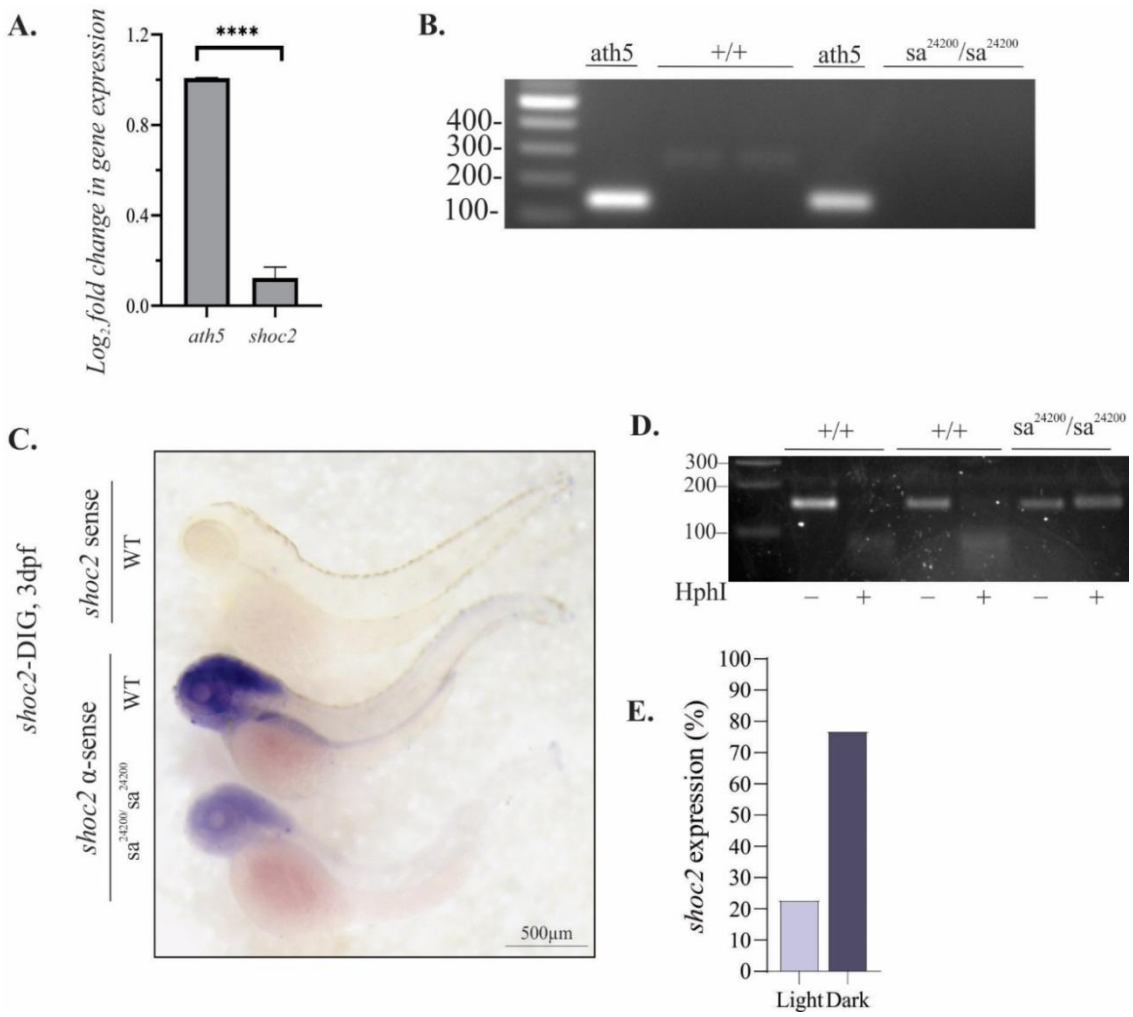

Figure 4.3 Homozygous shoc2 mutant RNA stability analysis

(A) The relative changes in the expression of *shoc2* were evaluated in *shoc2* sa^{24200}/sa^{24200} mutants. Total RNA was extracted from 6 dpf WT and *shoc2* sa^{24200}/sa^{24200} larvae and levels of mRNA expression were quantified by qPCR. The data are presented as the fold change of the mRNA levels in WT larvae verses the mRNA levels in mutant larvae. *ath5* is a control mRNA. Primer sets are provided in **Table 2.**1. The results represent an average of three biological replicas. Error bars indicate means with SEM. ****P<0.0005 at 95% confidence interval (Student's t-test).

(B) Determination of the exponential range of amplification for *shoc2* from WT and sa^{24200}/sa^{24200} *shoc2* embryos. *ath5* was used as a control gene. Samples were completed in independent duplicates. Amplification was limited to 26-cycles. Agarose gel electrophoresis shows amplicons *shoc2* fragments.

(C) RNA whole *in situ* hybridization was completed on 3 dpf embryos using sense and anti-sense probes for *shoc2*. The lateral view of WT and *shoc2* sa^{24200}/sa^{24200} larvae is shown. Loss of *shoc2* staining is evident in *shoc2* sa^{24200}/sa^{24200} embryos. No staining was detected in the negative control *shoc2*-sense stained embryos. The results represent an average of three biological replicas.

(D) PCR analysis of genomic DNA (isolated from post-WISH embryos shown in **Figure 4.3C**) and subsequent restriction enzyme (HphI) digestion for sensitive detection of *shoc2* WT and mutant alleles in individual larvae. *shoc2* c.1546 G>A permits HphI digestion in the region of interest. Agarose gel electrophoresis shows amplicons of WT, heterozygous, and homozygous *shoc2* carriers.

(E) The graph shows the frequency of the staining intensity (**Figure 4.3C**) from at least three independent experiments. 20 of 87 (23%) embryos displayed reduced staining.

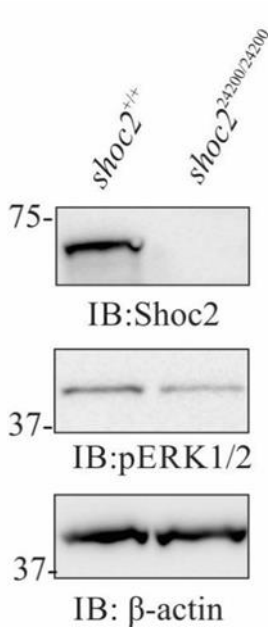

Figure 4.4 Western blot analysis of shoc2 sa24200/sa24200 larvae

Immunoblot analysis of Shoc2 WT and sa24200 larvae. Larvae were harvested at 6 dpf. Protein expression was analyzed using specific antibodies. β-actin was used as a loading control.

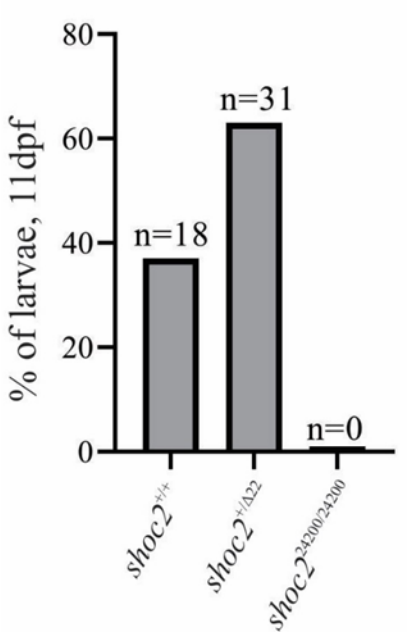

Figure 4.5 PCR analysis of genomic DNA of shoc2 +/sa24200 incrossed larvae

PCR analysis of genomic DNA from inbred *shoc2* $^{+}$/sa^{24200} fish. Larval progeny from three independent experiments were genotyped. All surviving larvae at 11 dpf genotyped as either *shoc2* WT or *shoc2* +/sa^{24200}.

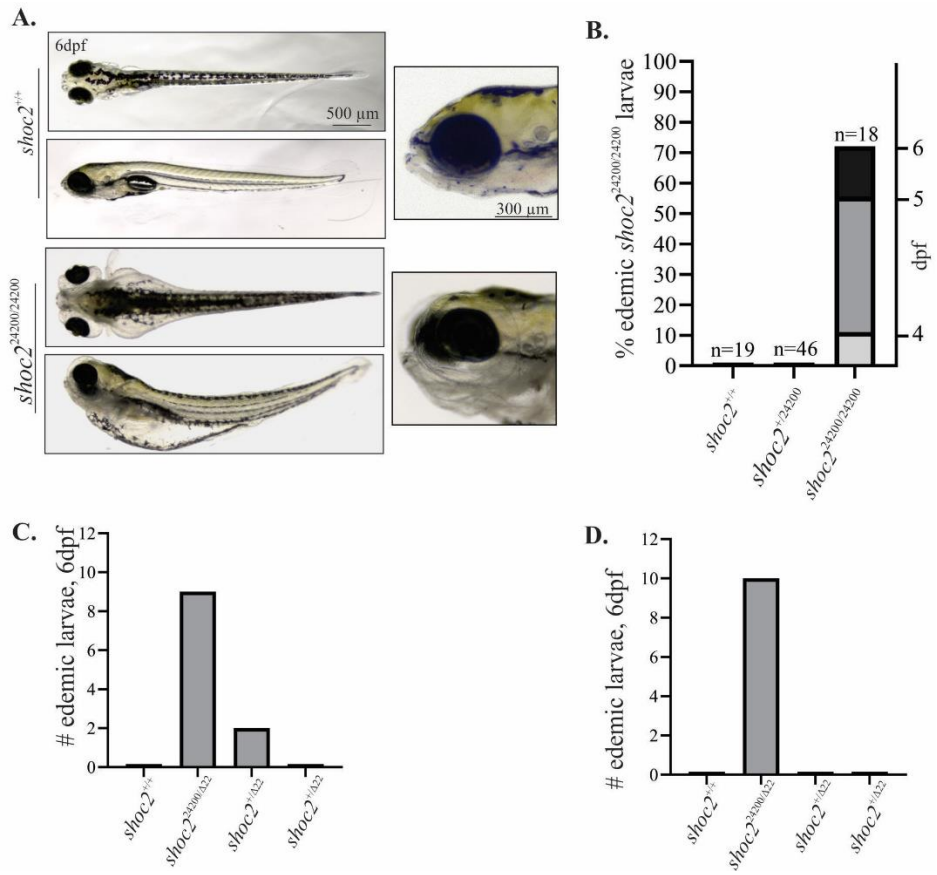

Figure 4.6 Shoc2 sa24200/24200 mutants and compound mutants (sa24200/Δ22) develop edemic phenotype

(A) Severe edemas are evident in 6 dpf *shoc2* sa^{24200}/sa^{24200} larvae. Edemas form around larvae eyes and in their trunks. The most severe edemas induce the embryos to bow inward causing a concave spine.

(B) PCR analysis of genomic DNA from 6 dpf +/sa^{24200} inbred larvae. Progeny from inbred *shoc2* +/sa^{24200} adults were selected for upon edema formation and subsequently genotyped. On day 6 after all edemic embryos were collected, all remaining embryos were also genotyped.

(C) *shoc2* +/sa^{24200} and *shoc2* +/Δ^{22} adult fish were bred to generate *shoc2* sa^{24200}/Δ^{22}compound mutants. PCR analysis of genomic DNA confirmed all edemic embryos as *shoc2* sa^{24200}/Δ^{22} or *shoc2* +/sa^{24200}.

(D) *shoc2* +/sa^{24200} and *shoc2* +/Δ^{22} adult fish were inbred to generate *shoc2* sa^{24200}/Δ^{22}compound mutants. On 6 dpf, 10 edemic embryos were selected and

genotyped. All edemic embryos were *shoc2* homozygous compound mutants (*shoc2* sa^{24200}/Δ^{22}).

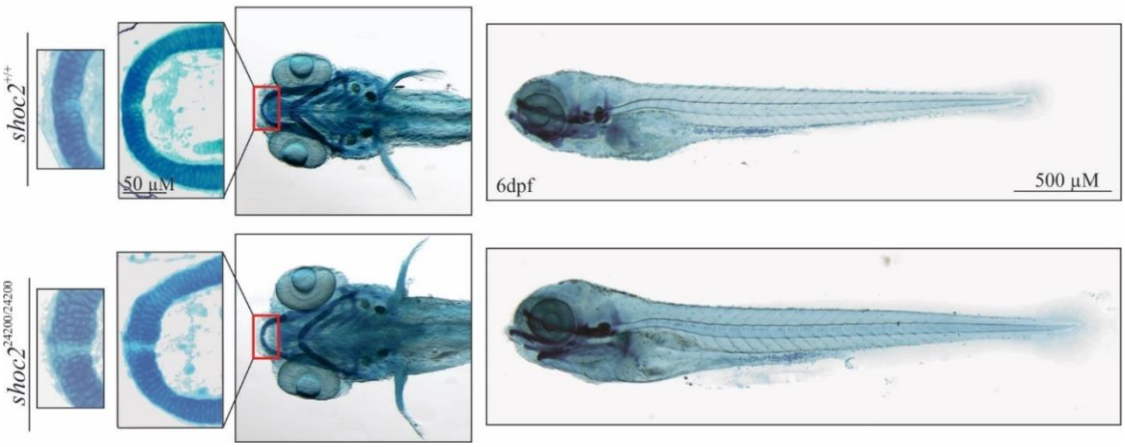

Figure 4.7 Loss of Shoc2 leads to defects in cartilage formation

Lateral and ventral view of 6 dpf WT or *shoc2* sa^{24200}/sa^{24200} larvae stained with Alcian blue. Mutant larvae show significant changes in head cartilage. The Meckel's Cartilage was dissected and mounted prior to imaging to highlight the hypoplastic closure in *shoc2* sa^{24200}/sa^{24200} larvae.

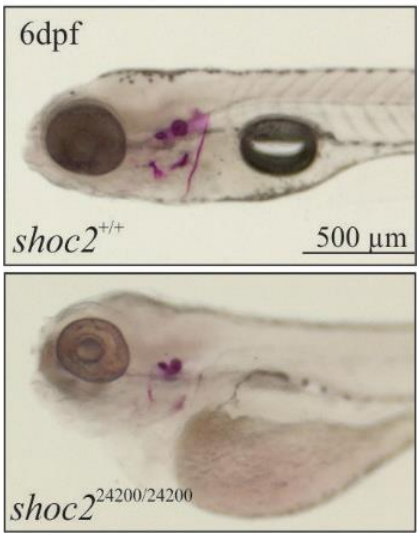

Figure 4.8 Bone development is impaired in shoc2 sa24200/sa24200 larvae

Lateral view of a 6 dpf WT or *shoc2* sa^{24200}/sa^{24200} larvae stained with Alizarin Red S. Mutant larvae show significant differences in cranial bone formation.

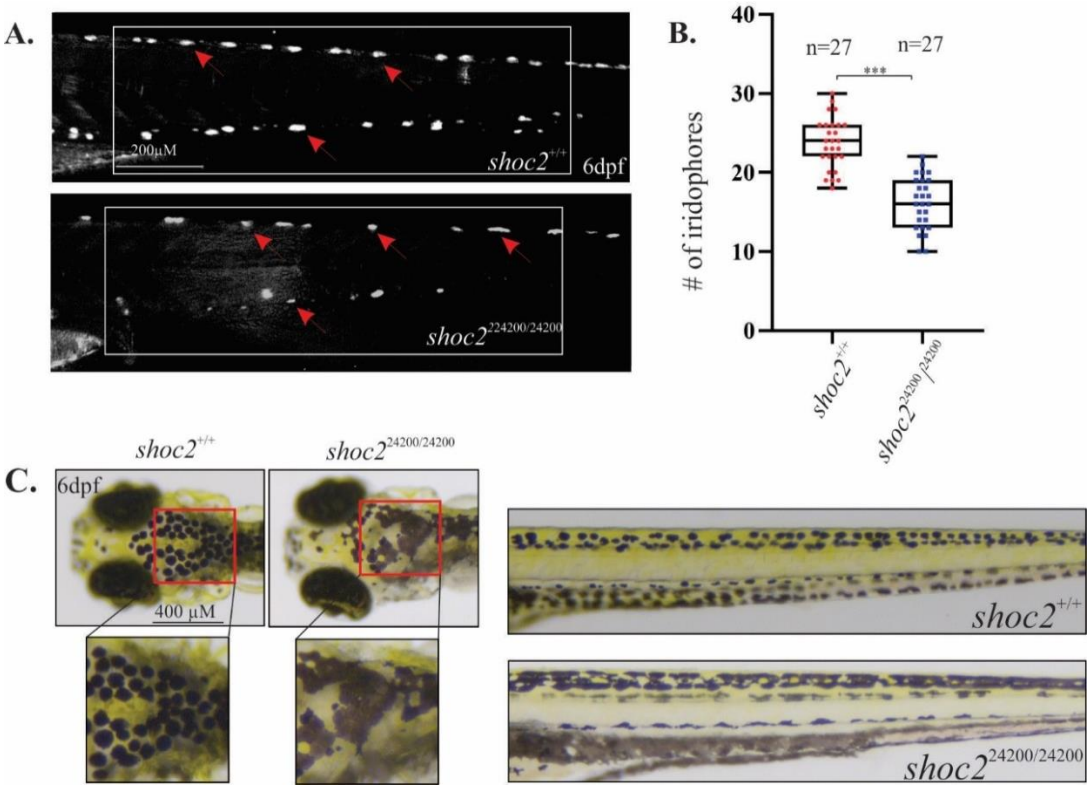

Figure 4.9 Pigmented cell development is impaired in shoc2 sa24200/sa24200 larvae

(A) Iridophores from 6 dpf WT *shoc2* sa^{24200}/sa^{24200} larvae were detected using iridescent light and quantified.

(B) Quantification of iridophores (**Figure A)** from three biological replicas. ***P<0.001 at 95% confidence interval (Student's t-test).

(C) Dorsal (head) and lateral (trunk) views of 6 dpf WT and *shoc2* sa^{24200}/sa^{24200} larvae. WT larvae show concisely patterned melanophores. Unlike WT larvae, *shoc2* sa^{24200}/sa^{24200} *shoc2* larvae present closed gaps in pigmentation patterning on both the head and lateral stripe.

CHAPTER 5. SHOC2 IS ESSENTIAL FOR LYMPHATIC VESSEL DEVELOPMENT

Abstract

Pathogenic variants in the ERK1/2 pathway are associated with abnormal development of the lymphatic system. Although the clinical symptoms vary between RASopathy patients, lymphatic abnormalities often manifest as increased nuchal translucency, chylothorax, and lymphedema. Moreover, NSLH patients with Shoc2 mutations have higher risks of developing lymphatic problems later in life. Yet, the mechanistic connection between Shoc2 pathogenic mutations and lymphatic abnormalities remains unknown. A number of zebrafish transgenic reporter lines differentiating between blood and lymphatic vessels have been developed in recent years providing powerful tools for imaging and studying lymphatic development. To define the role Shoc2 plays in the development of the zebrafish lymphatic system, we utilized transgenic reporter lines specifying blood and lymphatic vasculature (Tg*(mrc1a:egfp)y251* and Tg*(kdrl:mcherry)y171*) in conjunction with the Shoc2 *null* zebrafish model *shoc2* sa^{24200}/sa^{24200} (reported in chapter four). We found that Shoc2-mediated signals are critical for the development of the major lymphatic structures such as the parachordal line and thoracic duct. Our studies using primary human LEC also determined that loss of Shoc2 dramatically affect the transcriptional program. Together, our preliminary findings highlight the requirement of Shoc2 for proper lymphatic development.

Introduction

Cellular interstitial fluid originates from fluid seeping out of high-pressured arterial capillary walls. Lymphatic capillaries are integrated throughout interstitial spaces and are highly permeable due to their micro-valve like, loosely overlapping, single-cell thick walls [189] (**Figure 1.9**). Fluid enters lymphatic capillaries (now termed "lymph") through their one-way valves when the pressure in the interstitial space is greater than within lymphatic vessels. Lymph moves through enlarging lymphatic vessels until it is returned to the blood circulatory system through a venous vessel at a low-pressure site. Aberrant lymphatic vessel development and the subsequent loss of lymphatic homeostasis can result in excess interstitial fluid accumulation causing edemas [190].

The rapid and complex process of lymphatic vasculature development is coordinated by signals of Protein kinase B (Akt) and ERK1/2 pathways. ERK1/2 and Akt promote cell survival, proliferation, and migration – all of which are vital to lymphangiogenesis. Akt and ERK1/2 signaling cascades are both activated by vascular endothelial growth factor -C (VEGF-C) stimulation inducing vascular endothelial growth factor receptor 3 (VEGFR-3) dimerization. The dimerization of a VEGFR-3/VEGFR-2 complex activates Akt signaling, whereas VEGFR-3/VEGFR-3 homo-dimerization activates ERK1/2 signaling [191]. VEGFR-3 is a crucial regulator of lymphangiogenesis. Inactivation of VEGFR-3 led to severe defects in the sprouting of lymphatic vessels and to the loss of ERK1/2 signals [192]. Conversely, expression of the constitutively-active RAF1S259A mutant or the loss of GAPs rasa4 and rasal3 resulted in excessive LEC proliferation and enlarged lymphatic vessels [191]. Together, these data showed that balanced ERK1/2 signaling is critical for lymphangiogenesis. Although lymphedemas and

other related abnormalities are often found in RASopathies, the molecular mechanisms underlying these defects are not well understood.

Similar to humans, zebrafish have a closed circulatory system and their lymphatic system shares many of the molecular and functional characteristics of lymphatic vessels in other vertebrates [148]. Transgenic reporter lines have provided powerful tools for imaging and studying vascular development in the optically clear zebrafish embryo *in vivo*. For example, the pan-endothelial *Tg(fli1a:egfp)* (the promotor *fli1* drives the expression of eGFP) transgene line is utilized to visualize the development of all vasculature (arterial, venous, and lymphatic) [193]. A number of double-transgenic lines are used to differentiate between blood and lymphatic vessels, including *Tg(fli1a:egfp)*^{y1}, *Tg(kdrl:Hsa.HRAS-mCherry)* and *Tg(flt1:yfp), Tg(kdrl:mcherry)* double transgenics and the *Tg(fli1a:egfp)*^{y1}, *Tg(kdrl:mcherry)* line [152]. The transgene combination of these and other lines permits reliable distinction between blood and lymphatic vessels. In this study, we utilized three transgenic zebrafish lines, *Tg(fli1a:egfp)*^{y1}, *Tg(mrc1a:egfp)*^{y251}, and *Tg(kdrl:mcherry* to visualize lymphangiogenesis. The reporter line *Tg(mrc1a:egfp)*^{y251} uses the *mrc1a* promoter to drive robust EGFP expression in all venous derived endothelial cells (venous and lymphatic vessels) while the v*ascular endothelial growth factor receptor kdr-like* (*kdrl*) promotor drives mCherry expression in only arterial vessels.

To investigate the role Shoc2 plays in lymphangiogenesis, the *shoc2* sa24200 zebrafish line (discussed in **chapter 4**) was crossed onto the double transgenic reporter line Tg(*mrc1a*:*egfp*)y^{251}; Tg(*kdrl*:*mcherry*)y^{171} generously provided by Dr. Brant Weinstein (NIH) as well as onto the pan-endothelial line Tg(*fli*:egfp) obtained from Dr. Ann Morris.

Presented are preliminary results and ongoing experimentation that investigate misregulated Shoc2-signaling and the induction of NSLH fetal hydrops. As previously discussed, the *shoc2* sa24200 line presents edemas earlier and more severely than the Δ*22* and Δ*14 shoc2* mutant lines. Therefore, this model is optimum for determining the etiology of edemas in Shoc2 *null* embryos.

We found that the parachordal line (PL) and its derivative, the thoracic duct ((TD, the most major lymphatic vessel in zebrafish), are both severely impaired in homozygous *shoc2* sa24200 embryos. Furthermore, we also found aberrant levels of Shoc2 in lymphatic endothelial cells (LEC) disrupts the transcription of multiple genes. Thus, these novel preliminary findings are a premise for exciting studies that will delineate Shoc2 signals in the development of the lymphatic system.

Results

5.1 Inflammatory response and vasculature permeability are not affected in Shoc2 *nulls*

Edemas observed in Shoc2 *null* fish were reminiscent of oedemic swellings resulting from an immune response from aberrant Shp1 and Shp2 proteins (associated with Noonan syndrome) in zebrafish larvae [194, 195]. Thus, we first explored a possible innate immune response. Glucocorticoids are widely used as an anti-inflammatory treatment that can alleviate interstitial fluid accumulation. Here, glucocorticoid treatment was administered to determine if an inflammatory immune response drives the formation of Shoc2 *null* associated edemas. Dechorionated embryos (48hpf) were treated with the anti-inflammatory glucocorticoids betamethasone valerate or dexamethasone. The media containing the drug was changed daily and the development of edemas was closely

monitored starting at 3 dpf. However, I surprisingly found that both glucocorticoid treatments enhanced larval edema formation in the Shoc2 *null* embryos sooner than DMSO control treated embryos and exacerbated the severity of the swelling. By 4 dpf, we observed more edemic *shoc2* sa^{24200}/sa^{24200} embryos undergoing a glucocorticoid treatment than *shoc2* sa^{24200}/sa^{24200} embryos that were incubated in a corresponding concentration of DMSO (**Fig. 5.1A**). The adverse effect was surprising, yet, an enhanced inflammatory effect after glucocorticoid treatment has previously been reported in zebrafish [194, 195]. Therefore, the augmented edema phenotype under glucocorticoid treatment coupled with prior data indicating that Shoc2 *null* larvae have an overall reduced number of circulating blood cells, [103] suggests that an immune response is unlikely to be the source of swelling.

The Galperin lab previously identified that *shoc2* morphants present defective vascular angiogenesis at 3 dpf [103]. Furthermore, edema formation can arise from leaky vasculature. As compared to arteries, both veins and lymphatic vessels reside under chronically low fluid pressure. They maintain unidirectional fluid flow by their intraluminal, bicuspid valves. When under pressure from fluid accumulation, their lumen valves open allowing fluid passage and subsequently close. Efficient transport of lymph and deoxygenated blood depends on the competency of this gated mechanism.

The loss of luminal vasculature valves can lead to extraluminal fluid and edema formation. Thus, to investigate potential leaky vasculature, we utilized the Evan's Blue Dye (EBD) assay to detect potential aberrant albumin outside of vasculature [159, 160]. Permeable vasculature permits the concurrent secretion of a small, but prominent blood protein, albumin, with the exuding fluid. EBD has a high affinity for albumin and therefore

can be used to detect aberrant vasculature secretions. EBD was co-injected with fluorescein isothiocyanate (FITC) into *shoc2* WT and *shoc2* mutant Tg(kdrl:mCherry)^{y171} (labeling arterial endothelial cells) embryos' common cardinal vein at 4 dpf (not shown) and 6 dpf (**Fig. 5.1B**). No florescence (no vasculature leakage) was detected outside of the peripheral blood vasculature 4-6 hours post-injection. This indicates that the blood vessels maintain their integrity and are impermeable to blood albumin.

5.2 Shoc2 is essential for lymphangiogenesis

We next examined whether the development of the lymphatic system in zebrafish embryo was affected by the loss of Shoc2. Here, we utilized pan-endothelial cell marker transgenic line, Tg(fli:eGFP); *shoc2* +/sa^{24200} and the more recently established double transgenic zebrafish line Tg(mrc1a:eGFP)^{y251} (labeling venous and lymphatic EC) and Tg(kdrl:mCherry)^{y171} (labeling arterial EC) crossed onto the *shoc2* +/sa^{24200} line. Unlike wildtype embryos, *shoc2* sa^{24200}/sa^{24200} mutants do not develop a parachordal line by 3 dpf (**Figure 5.2A, B**) Furthermore, the thoracic duct, (normally derived from the parachordal line by 5 dpf) also does not form in Shoc2 *null* embryos (**Figure 5.2A**). By this, we identified that deregulated Shoc2-mediate ERK1/2 signaling results in aberrant lymphangiogenesis. Specifically, Shoc2 is required for the development of two critical lymphatic vessel components, the parachordal line and the thoracic duct.

5.3 Lymphatic endothelial cell differential gene analysis

To gain insight into the transcriptional changes that endothelial cells experience in the absence of Shoc2, a comparative transcriptome analysis of the LEC was performed.

We utilized lymphatic endothelial cells (LEC) stably depleted or over-expressing Shoc2 using lentivirus delivery method. To examine the Shoc2 protein expression in LECs, a western blot analysis was performed. Protein expression analysis using an antibody against Shoc2 confirmed both the loss of and overexpression of Shoc2 in respective samples (**Figure 5.3A**). mRNA was isolated from LEC samples and RNAseq was completed. Preliminary data (not presented) indicates that 28 ECM coding genes are misregulated including: 8 types of collagen, *thrombospondin* 1b (known for angiogenesis), *matrix metallopeptidase 17b* (degrades collagen), and *elastin microfibril interface 1b* (associated in the ECM of lymph vasculature aiding in elastin fiber fusion). RT-qPCR was completed against five of the upregulated genes validate RNAseq analysis results (**Figure 5.3B**). During angiogenesis the ECM provides essential support and aids key signaling events for endothelial cell migration, invasion, and proliferation [196, 197]. Together, these preliminary results (by RNAseq and qPCR) (**Figure 4.3B**) suggest that the loss of Shoc2 misregulates the ECM thereby inhibiting lymphangiogenesis. However, additional analysis is required.

5.4 Figures, Ch. 5

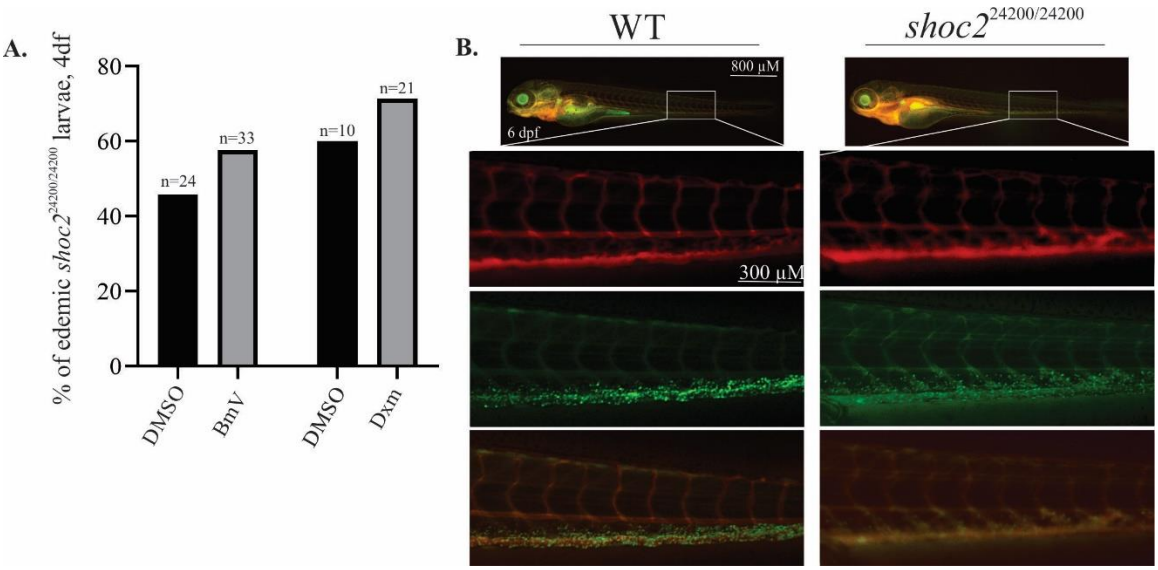

Figure 5.1 Inflammatory response and vasculature permeability analysis

(A) Incrossed *shoc2* +/sa^{24200} larvae were dechorionated at 48hpf embryos and incubated in E3 media containing the glucocorticoids betamethasone valerate (BmV, 1µM) or dexamethasone (Dex., 100µM). Embryos were evaluated daily for edema formation. Upon edema detection, embryos were removed and PCR analysis of genomic DNA was completed. At 4 dpf, after edemic embryos were selected, all remaining embryos were also genotyped. **(B)** Evans Blue dye and FITC were mixed and co-injected into the circulation 6 dpf live AB/WT embryos at the pericardial area into the CCV. Images were acquired 4-6 hours post-injection. Larvae were anaesthetized with 0.2µg/mL tricaine prior to injection.

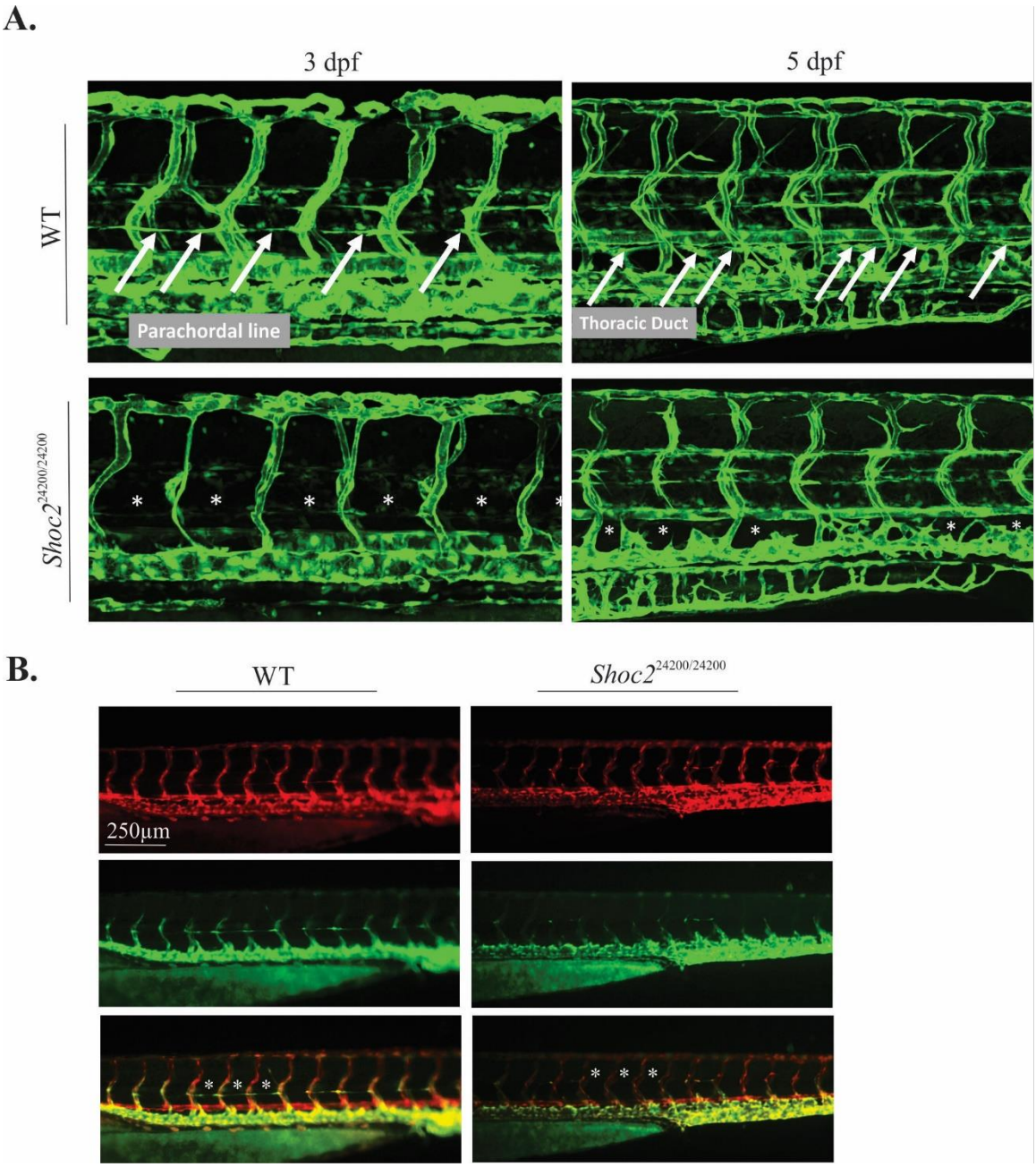

Figure 5.2 Loss of Shoc2 inhibits lymphatic vessel formation

Loss of Shoc2 inhibits lymphatic vessel development. (**A**) Confocal images of larvae from incrossed pan-endothelial cell marker transgenic reporter line, Tg(fli:eGFP); *shoc2* +/sa^{24200}, raised to 3 or 5 dpf. (**B**) Florescence images of larvae from venous and arterial-

specific derived endothelial cells, Tg(mrc1a:eGFP; kdrl:mcherry); *shoc2* +/sa^{24200} raised to 3 dpf.

All images (rostral left) are lateral views of the trunk region. Asterisks indicate the loss of the and thoracic duct (**A**) and parachordal line (**A, B**).

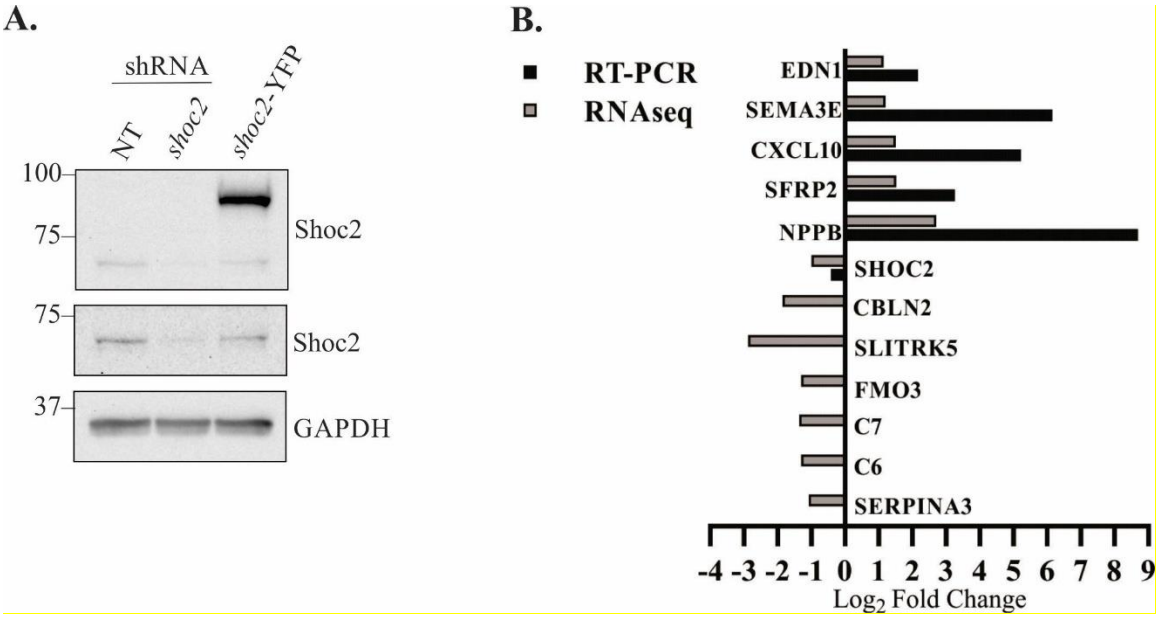

Figure 5.3 Gene expression analysis in LEC

Differentially expressed gene validation by qPCR from total RNA isolated from LEC with knocked down or overexpressed Shoc2. **(A)** Western blot analysis of lentiviral infected LEC. Cells were infected with Shoc2 shRNA, nontargeting (NT) shRNA or expressing Shoc2-YFP. The expression of Shoc2 and GAPDH was determined to confirm Shoc2 knockdown and overexpression**. (B)** Total mRNA was extracted from the LEC shRNA NT and *shoc2* samples from (A) and levels of differentially expressed genes were quantified by qPCR. The data are presented as the Log_2fold change of the mRNA levels in NT infected cells. The results represent an average of three biological replicas. Primers are presented in **Table 2.1**.

CHAPTER 6. DISCUSSION AND FUTURE DIRECTIONS OF THE ROLE OF SHOC2 FOR EMBRYONIC DEVELOPMENT

6.1 Discussion

In this study, we identified the role of Shoc2 for the development of NC during embryogenesis and made the novel discovery that Shoc2 is required for lymphangiogenesis. First, to analyze how Shoc2 affects the expression of the key regulatory genes participating in the various stages of NC development, we depleted *shoc2* by injecting *shoc2* MO thereby blocking the translation from both maternal and zygotic *shoc2* mRNAs. MO depletion uncovered developmental deficits obscured by the maternal RNA in the CRISPR/Cas9 Shoc2 *null* mutants [103]. We found that the loss of Shoc2 affected the expression of the key NPB regulators *sox2*, *pax7*, and *prdm1a* at the stage when cells at the NPB commit to the NC fate (**Fig. 3.2**). Although we have not detected changes in the major-to-minor axis ratio of the *shoc2* morphants, we cannot rule out that Shoc2 signals influence the coordinated convergent extension cell movements during zebrafish gastrulation. Yet, early abnormalities of Shoc2 MO larvae varied from the phenotypes of the zebrafish injected with ERK1 and ERK2 MOs [60]. Injection of the ERK1 and ERK2 MO severely altered anterior-posterior extension of the dorsal body axis and caused easily detectable deficits in cell movement during gastrulation and low survival rates at 24 hpf [60]. Future studies will determine whether differences in the observed phenotypes are due to the specificity of the Shoc2-mediated signals or simply changes in the ERK1/2 amplitude.

The loss of Shoc2 also affected the expression patterns of the NC specifier required for the NCCs formation in the NPB, *foxd3* [114, 115, 198]. The changes in the expression

of *foxd3* concurred with the altered expression of other NCC specifiers, *snai2* [199], *sox9a*, and *sox10* [120, 121, 200], as well as a pan-neural crest marker *crestin* [127, 170] (**Fig. 3.3**). NCC specification is dependent on precise spatial development of the NPB. Furthermore, NPB formation requires a balanced gradient of inducers, inhibitors, and transcription factors such as BMP, Wnt, chordin, and noggin [201, 202]. For example, epidermal fate and neural specification are stimulated by high and low BMP concentration respectively, while intermediate BMP induces the formation of the NPB. Therefore, it is possible that the loss of NCC specifier expression is due to cells at the NPB receiving an aberrant BMP signal gradient. Regardless of the mechanism, the loss of *shoc2* impairs the expression of NCC specifiers.

As determined by the limited migration of *dlx2a* positive cells and the decreased expression of *sox9a, sox10, snai2,* and *crestin* at the 18 ss stage, Shoc2 loss also affects the migration of NCCs (**Fig. 3.4**). Our data suggest that changes in the expression of the central players regulating the specification of NC (e.g. *foxd3, sox9a,* and *sox10)* likely triggers changes in transcriptional programs responsible for cytoskeletal rearrangement. As a result, NCC motility and the epithelial-to-mesenchymal transition (EMT) (e.g. expression *twist, chd1, chd2*) are influenced. These findings are well-aligned with the results of earlier studies demonstrating that signals of the Shoc2-ERK1/2 axis coordinate cell adhesion and movement of cultured cells *via* controlling the expression of various proteins such as Adam12, LGALS3BP, and Col1a1 that regulate these processes [44, 203, 204]. Others suggested that M-Ras/Shoc2 signals regulate cell motility by coordinating the turnover of E-cadherin at cell-cell junctions and modulating its interaction with p120-catenin [205]. Although molecular details of how Shoc2-mediated signals regulate NCC motility are yet

to be elucidated, our study provides additional evidence for the critical role of Shoc2 in controlling cell migration.

Transcription factors *foxd3*, *sox9a*, and *sox10* also control the ability of NCC precursors to maintain their multipotency, promote survival of NC progenitors and guide the formation of multiple NC lineages [200, 206, 207]. Thus, given the dramatic changes in their expression in *shoc2* morphant larvae, it is not entirely surprising that the loss of Shoc2 hinders the development of NCC derivatives, such as chondrocytes, iridophores, Schwann cells, and neurons of the peripheral nervous system (**Figs. 3.6-3.10**). Importantly, these findings place Shoc2 ahead of *foxd3*, *sox9*, and *sox10* in the gene regulatory network underlying NC development.

The striking changes in the branchial arches, the severe loss of *crestin*-positive cells in the hindbrain at 24 hpf, and the loss of neurons and glia at 3 dpf of *shoc2* morphants could result from the specific loss of hindbrain premigratory NCCs by cell death. Shoc2 was reported to regulate the survival of neural progenitor embryonic stem cells and the maintenance of their self-renewal capacity [208]. Although we do not know the specific downstream effectors of *shoc2*-mediated cell death, our data suggest that members of the *Snail* family of transcriptional repressors are possible candidates. *Snail* proteins act as survival factors in progenitor cell populations and are often overexpressed in human cancers [171, 209-211]. A detailed understanding of the role of the Shoc2-ERK1/2 axis in cell death warrants additional studies. The broad range of affected NC lineages and the early reduction in the expression of NC specification genes suggest that Shoc2 might be required to maintain an undifferentiated pool of NC progenitors. Thus, it is tempting to speculate that when Shoc2 is depleted, and only residual ERK1/2 signals regulate NC

induction and specification, the differentiation of progenitor cell precursors stall because fewer cells of each type are formed.

One of the most unexpected discoveries is the results of the comparative transcriptome analysis of *sox10*-positive cells and our findings that the persistent changes in the expression of genes coding the various proteins associated with ECM (**Fig. 3.12**) could be a direct cause of the defects/delays in the ossification of cartilage. Shoc2 loss triggered the deregulation in the expression of many relevant chondrogenesis genes, including *col2a1, acana, acanb, hapln* and *mmp13, matn1, and sox9*. We found that the build-up in ECM proteins in *shoc2 nulls* is accompanied by the abnormal expression of ECM regulators like MMP13 and modifying enzymes like *pcolce2* and *loxl4* (**Table 3.1**). Thus, it is plausible that an accumulation of ECM collagens and glycoproteins hinders the chondrocyte potential to convert into osteoblasts. Concomitant with alterations in the intracellular signaling, metabolite interconversion, and the expression of enzymes modifying ECM proteins (**Fig. 3.12B and Table 3.1**), these data point out a global effect of Shoc2-ERK1/2 signals on ECM homeostasis and/or remodeling. Importantly, our data also suggest that during embryonic development Shoc2 scaffold modulates the parameters of ERK1/2 signaling dynamics. Future studies using different methodologies are needed to address whether marked increases in the expression of Col2a1 and Aggrecan a and b observed in 5 and 6 dpf *shoc2 null* larvae result from changes in ERK1/2 amplitude or duration.

Of note, a zebrafish model expressing a pathogenic Shoc2 nor a line that is consistently depleted of Shoc2 from fertilization though adult stages is available. Therefore, in this study, embryos either developed in the presence of *shoc2* maternal-RNA,

or with a temporary depletion of Shoc2 translation. This may have introduced experimental variability. However, extensive replication paired with the validation of many gene markers and the use of multiple methodology approaches mitigated the model's limitation.

I additionally developed and characterized a novel *shoc2* mutant line that I utilized in my studies. The sa24200 *shoc2* c.1546G>A point mutation, located within a noncoding region of *shoc2* was validated and determined to cause embryonic lethality. The loss of *shoc2* mRNA and Shoc2 protein in $sa^{24200/24200}$ mutants was detected by qPCR and western blot analysis. Sequencing confirmed that the sa24200 mutation is intronic (**Fig 4.2-4.3**). Assays to visualize the craniofacial cartilage, bone development, and pigmentation revealed deficient development of these tissues that arise from NCC (**Fig 4.7-4.9)**. Furthermore, the $sa^{24200/24200}$ larvae develop severe edemas (**Fig 4.6)**. Together, the criticality of Shoc2 for embryo viability and development is consistent with previous publications as the sa24200 mutants display phenotypes similar to the previously established Shoc2 Δ*22* mutant line [49, 103, 166].

Interestingly, the *shoc2* $sa^{24200/24200}$ mutants develop notably more severe edemas than we observe in the Shoc2 *null* larvae from either incrossed *shoc2* Δ*22* or Δ*14 shoc2* mutants. The $sa^{24200/24200}$ larvae ultimately display trunk curvature induced by the severe swellings, select individual $sa^{24200/24200}$ mutants presented edemas as early as 4 dpf, and the majority had edemas by 5 dpf (**Fig 4.6A,B)**. In comparison, the edema formation in *shoc2* Δ*22* and Δ*14* mutants was not evident until 6 dpf [103]. The molecular explanation underlying the exacerbated abnormality in the sa24200 homozygous mutants remains unknown. Regardless, due to its temporally advanced and exacerbated development of

edemas, the sa24200 model will be particularly useful for deciphering the molecular mechanism underlying the Shoc2 *null* induced edema formation.

To this end, we utilized the zebrafish line sa24200 (*shoc2* c. 4A>G) to identify the underlying causes of the edema formation. Experiments using glucocorticoid treatments or an albumin-binding fluorophore established that neither an immune response nor vasculature permeability are the factors that cause the edemic swelling in the *shoc2* $sa^{24200/24200}$ larvae. Importantly, we found that Shoc2 *null* larvae fail to develop critical lymphatic vessels. Both the parachordal line and the thoracic duct were absent at 3 and 5 dpf respectively. This data indicates that lymph abnormalities are causing the edema observed in the $sa^{24200/24200}$ larvae. Additional experiments are required to expand this data such as *in vivo* confocal imaging to further examine trunk and facial lymphatic formation, time-lapse imaging of secondary vessel sprouts, and rescue and overexpression experiments with similar imaging analysis to detect recovered and/or hyper lymphangiogenesis. Furthermore, a behavioral analysis could determine the effect of Shoc2 on EC's abilities to migrate, invade, and sprout.

Similar to Shoc2 *null* embryos, a preliminary RNAseq analysis from LECs aberrantly expressing Shoc2 revealed that multiple ECM coding genes are misregulated in LECs **(Fig 5.3)**. Given that the ECM plays a critical role in lymphangiogenesis, it is tempting to speculate that the lymphatic abnormalities in $sa^{24200/24200}$ larvae are caused by defects in the ECM [212]. Structurally, the ECM requires a specific macromolecular composition to form a complex three-dimensional assembly. Essential proteins within the ECM include integrins, hyaluronic acid, collagens, laminin, and fibronectin [145, 212]. Functionally, it facilitates interactions among the residing proteins and provides a structural

framework to promote cell migration, proliferation, and differentiation. Interestingly, both Collagen2a1, a prominent ECM collagen, and Calcium-binding EGF domain-1 (*ccbe1*) are two indispensable proteins for lymphangiogenesis in zebrafish embryos [213, 214]. The extent of the direct impact by the misregulated *col2a1* on lymphangiogenesis in Shoc2 *null* embryos is unclear and the ECM coding protein *ccbe1* has not been investigated in the Shoc2 model. Furthermore, ECM remodeling proteins (MMP13, TIMP1, and TIMP2) are abnormally expressed in induced pluripotent stem cells isolated from Costello syndrome patients' fibroblasts [215]. These cells exhibited impaired osteogenic development. Therefore, it is possible that abnormal ECM formation and homeostasis from aberrant Shoc2-mediated signaling not only inhibits NCC differentiation, but also plays a central role in the loss of embryonic lymphatic vasculogenesis. Further studies will determine whether ECM deficiencies are responsible for the defects in lymphangiogenesis observed in $sa^{24200/24200}$ larvae.

Shoc2 has additionally been suggested as a target for sensitization of the MEK inhibitors in cancer [216, 217]. Thus, our findings that Shoc2-ERK1/2 signals control ECM homeostasis/remodeling have potential implications for understanding the role of the Shoc2 in tumor progression**.** In cancer, abnormal ECM dynamics occur due to disrupted balance between ECM synthesis and secretion and altered expression of matrix-remodeling enzymes [218]. Thus, our ECM findings are directly relevant to the efforts toward novel direct therapeutics targeting the Shoc2-ERK1/2 axis.

In addition to the ECM, lymphangiogenesis critically relies on a paracrine gradient of VEGF-C for LEC's migration [219, 220]. Furthermore, VEGF-C is the primary activator of the ERK1/2 pathway for downstream lymphatic vasculature development. Thus, one can

presumptively consideration that Shoc2 has a role in lymphangiogenesis through specifically mediating VEGF-C activated ERK1/2 signaling. Of note, a subpopulation of macrophages produce large quantities of VEGF-C [221]. Interestingly, Shoc2 *null* embryos were previously determined to have reduced numbers of all blood cell types examined including macrophages [103]. This loss of macrophages may directly reduce the production of VEGF-C thereby hindering lymphangiogenesis. However, this remains to be determined. A protein expression analysis from aberrantly expressing Shoc2 LECs or Shoc2 *null* embryos will shed light on this hypothesis.

In summary, my dissertation research provokes the following two specific NSLH-patient relevant considerations. First, abnormal NC development is the underlying cause of the vertebrate-specific developmental syndromes collectively termed neurocristopathies. Although the analysis of Shoc2 *null* embryos previously indicated that the loss of Shoc2 may hinder the development of NC [103], here, for the first time, we provide substantial evidence that aberrant Shoc2-mediated ERK1/2 signaling disrupts the development of NC at multiple phases of embryogenesis. Correctly identifying developmental disorders as neurocristopathies aids physicians' patient diagnoses as well as improves their understanding of the patient's disorder's origin. Therefore, I propose that this study provides substantial evidence for the medical field to consider NSLH a neurocristopathy.

Second, NSLH patients typically live with multiple, very challenging chronic health conditions. No mortality study has been completed, yet the health problems associated with this syndrome are life threatening. NSLH is a rare disease occurring in approximately 1:50,000 infants with the majority of cases arising from just one nucleotide

mutation (*shoc2* c. 4A>G) [66]. Furthermore, within this dissertation research I identified that a single point mutation within a non-coding region of *shoc2* forces spontaneous embryonic termination in zebrafish. This highlights the sensitive molecular regulation required for the expression of Shoc2 and further emphasizes its significance for development. Taking this data together, one may postulate that the prevalence of pathogenic mutant *shoc2* in human embryos may supersede the medical field's estimated frequency of occurrence. Even still, we do not yet have a full understanding of the role of Shoc2 during embryonic development. Further experiments are required to fully resolve the etiology of NSLH and to generate a comprehensive model of the Shoc2 functions during embryonic development.

6.2 Future Directions

The data within this dissertation presents evidence that the *shoc2* deficient embryos' craniofacial deficits initially arise from reduced and aberrant expression of the transcription factor *sox9a*. Thereby, the expression of the ECM protein coding genes *col2a1*, *acana*, and *acanb* are also diminished. Furthermore, the master regulator of osteoblast differentiation and endochondral ossification, *runx2*, is downregulated in *shoc2* morphants. Considering the diverse role collagens and other ECM-related proteins play in NC migration and morphogenesis, it is tempting to speculate that other abnormalities of Shoc2 *null* zebrafish (e.g. vasculature, hematopoiesis) or even abnormalities of NSLH patients are related to the deficits in the homeostasis of the ECM [176].

The studies investigating the role of Shoc2 in development have been limited to Shoc2 *null* models. The patient relevant mechanisms by which pathogenic Shoc2 variants

misregulate ERK1/2 signaling and development as well as the regulation of the ECM have not been investigated. Additional studies are required to delineate the molecular mechanisms of pathogenic variants of *shoc2*.

The 2006 discovery of the "Yamanaka factors" (Oct4, Sox2, Klf4, c-Myc) to generate induced pluripotent stem cells (iPSCs) from somatic cells is broadly applied to many fields of research including drug treatment, individualized medicine, and tissue regeneration [222-224]. This methodology is particularly powerful for disease modeling because iPSCs can be generated from individual patient's somatic cells [215, 225, 226]. Therefore, generating iPSCs from patient samples provides the unique opportunity to investigate *shoc2* pathological variants' mechanisms of action and their effects on cells' multipotency.

Under Yamanaka transcription factor treatment, RASopathy syndrome patient-derived fibroblasts have been reverted to a pluripotent state as iPSCs [215, 225, 226].These iPSC lines were derived from patient fibroblasts harboring mutations causing Cardiofaciocutaneous syndrome (*braf)*, Costello syndrome (*H-ras*), and Noonan syndrome (*ptpn11*). The use of iPSC over skin fibroblasts is particularly beneficial for developmental studies because iPSC maintain embryonic characteristics and profiles rather than those of mature, differentiated cells [227]. The nascent iPSC lines were induced to differentiate into mesenchymal stem cells (MSC). Subsequently, the derived cells were verified as MSC by expressed known MSC surface markers.

Harnessing these established methods to generate a stable, NSLH patient-derived cell line (NSLH-iPSC), I propose the following set of investigations. First, the patient *shoc2* mutant pERK1/2 loss-of-function outcome can be unequivocally defined. A western

blot analysis from WT- and NSLH- MSC will be performed using antibodies against Shoc2, ERK1/2, pERK1/2, and GAPDH.

Next, the impact of Shoc2 pathogenic variants will be evaluated for osteogenic, chondritic, and glial differentiation. Presuming that, similar to *in vivo* (humans), Shoc2 pathogenic variants produce deficient bone development *in vitro*, it would be possible to evaluate if Shoc2 induced abnormalities are due to Shoc2-mediated signal specificity or from the general loss of the ERK1/2 signaling amplitude. To detect a differentiation rescue, ERK1/2 signaling will be artificially amplified in the NSLH-MSCs by transfection with the constitutively active M-Ras isoform (G22V) prior to differentiation [41] [228] .

iPSCs carrying RASopathy causing mutations in both *braf* and *H-ras* are reported to cause aberrant Smad pathway signaling which is typically induced by transforming growth factor -β (TGF-β) [215, 226]. Furthermore, cross-talk between the ERK pathway and TGF-β/Smad has been reported by a number of studies [229-231]. Thus, due to RASopathy syndromes common underlying dysregulation of the ERK1/2 pathway and the previously reported findings in RASopathy patient iPSC induced mesenchymal stem cells (MSC), it will be interesting to explore possible signaling effects of the Smad pathway (downstream of TGF-β ligands) in a NSLH patient derived iPSC-MSC line.

NCC's migratory abilities are an important hallmark of bonafide NCCs. Cell-to-cell contact, cell polarity, the microenvironment's ECM, and extracellular signaling cues all regulate the critical migration of NCCs [232]. Extensive NC studies and high-end imaging have been completed to investigate the mechanisms that NCCs employ for their migration [232-234]. However, NCC migration has not been studied in-depth to identify the role of Shoc2 for this process. Further studies such as live confocal imaging paired with quantified

migration measurements (total distance, end location, velocity etc.) are required to investigate misregulated Shoc2-mediated ERK1/2 signals on the migratory properties of NCC.

In summary, the studies presented in this dissertation detail the role of Shoc2-transmitted ERK1/2 signals in neural crest development, characterized a new *shoc2* mutant zebrafish model, and identified the significance of Shoc2 for lymphangiogenesis. Together, these results have a potential to open new investigative avenues for the development of improved therapeutic strategies of NSLH and possibly other RASopathies.

REFERENCES

1. Wortzel, I. and R. Seger, *The ERK Cascade: Distinct Functions within Various Subcellular Organelles.* Genes Cancer, 2011. **2**(3): p. 195-209.
2. Roskoski, R., Jr., *ERK1/2 MAP kinases: structure, function, and regulation.* Pharmacol Res, 2012. **66**(2): p. 105-43.
3. Ramos, J.W., *The regulation of extracellular signal-regulated kinase (ERK) in mammalian cells.* Int J Biochem Cell Biol, 2008. **40**(12): p. 2707-19.
4. Roberts, P.J. and C.J. Der, *Targeting the Raf-MEK-ERK mitogen-activated protein kinase cascade for the treatment of cancer.* Oncogene, 2007. **26**(22): p. 3291-310.
5. Kim, E.K. and E.J. Choi, *Pathological roles of MAPK signaling pathways in human diseases.* Biochim Biophys Acta, 2010. **1802**(4): p. 396-405.
6. Tidyman, W.E. and K.A. Rauen, *The RASopathies: developmental syndromes of Ras/MAPK pathway dysregulation.* Curr Opin Genet Dev, 2009. **19**(3): p. 230-6.
7. Koseoglu, M.M., et al., *Aberrant Neuronal Cell Cycle Re-Entry: The Pathological Confluence of Alzheimer's Disease and Brain Insulin Resistance, and Its Relation to Cancer.* J Alzheimers Dis, 2019. **67**(1): p. 1-11.
8. Dagda, R.K. and C.T. Chu, *Mitochondrial quality control: insights on how Parkinson's disease related genes PINK1, parkin, and Omi/HtrA2 interact to maintain mitochondrial homeostasis.* J Bioenerg Biomembr, 2009. **41**(6): p. 473-9.
9. Bost, F., et al., *The extracellular signal-regulated kinase isoform ERK1 is specifically required for in vitro and in vivo adipogenesis.* Diabetes, 2005. **54**(2): p. 402-11.
10. Rodriguez, A., et al., *Mature-onset obesity and insulin resistance in mice deficient in the signaling adapter p62.* Cell Metab, 2006. **3**(3): p. 211-22.
11. Dhillon, A.S., et al., *MAP kinase signalling pathways in cancer.* Oncogene, 2007. **26**(22): p. 3279-90.
12. Norum, J.H., et al., *Epac- and Rap- independent ERK1/2 phosphorylation induced by Gs-coupled receptor stimulation in HEK293 cells.* FEBS Lett, 2007. **581**(1): p. 15-20.
13. Fernandez-Medarde, A. and E. Santos, *Ras in cancer and developmental diseases.* Genes Cancer, 2011. **2**(3): p. 344-58.
14. Bos, J.L., H. Rehmann, and A. Wittinghofer, *GEFs and GAPs: critical elements in the control of small G proteins.* Cell, 2007. **129**(5): p. 865-77.
15. Margolis, B. and E.Y. Skolnik, *Activation of Ras by receptor tyrosine kinases.* J Am Soc Nephrol, 1994. **5**(6): p. 1288-99.
16. Yang, L., et al., *Comprehensive Analysis of ERK1/2 Substrates for Potential Combination Immunotherapies.* Trends Pharmacol Sci, 2019. **40**(11): p. 897-910.
17. Mebratu, Y. and Y. Tesfaigzi, *How ERK1/2 activation controls cell proliferation and cell death: Is subcellular localization the answer?* Cell Cycle, 2009. **8**(8): p. 1168-75.
18. Kolch, W., *Coordinating ERK/MAPK signalling through scaffolds and inhibitors.* Nat Rev Mol Cell Biol, 2005. **6**(11): p. 827-37.
19. Grabbe, C., K. Husnjak, and I. Dikic, *The spatial and temporal organization of ubiquitin networks.* Nat Rev Mol Cell Biol, 2011. **12**(5): p. 295-307.

20. Lake, D., S.A. Correa, and J. Muller, *Negative feedback regulation of the ERK1/2 MAPK pathway.* Cell Mol Life Sci, 2016. **73**(23): p. 4397-4413.
21. Pouyssegur, J., V. Volmat, and P. Lenormand, *Fidelity and spatio-temporal control in MAP kinase (ERKs) signalling.* Biochem Pharmacol, 2002. **64**(5-6): p. 755-63.
22. Marshall, C.J., *Specificity of receptor tyrosine kinase signaling: transient versus sustained extracellular signal-regulated kinase activation.* Cell, 1995. **80**(2): p. 179-85.
23. Ebisuya, M., K. Kondoh, and E. Nishida, *The duration, magnitude and compartmentalization of ERK MAP kinase activity: mechanisms for providing signaling specificity.* J Cell Sci, 2005. **118**(Pt 14): p. 2997-3002.
24. Jang, E.R., et al., *HUWE1 is a molecular link controlling RAF-1 activity supported by the Shoc2 scaffold.* Mol Cell Biol, 2014. **34**(19): p. 3579-93.
25. Morrison, D.K. and R.J. Davis, *Regulation of MAP kinase signaling modules by scaffold proteins in mammals.* Annu Rev Cell Dev Biol, 2003. **19**: p. 91-118.
26. Chuderland, D. and R. Seger, *Protein-protein interactions in the regulation of the extracellular signal-regulated kinase.* Mol Biotechnol, 2005. **29**(1): p. 57-74.
27. Casar, B. and P. Crespo, *ERK Signals: Scaffolding Scaffolds?* Front Cell Dev Biol, 2016. **4**: p. 49.
28. Roy, M., Z. Li, and D.B. Sacks, *IQGAP1 is a scaffold for mitogen-activated protein kinase signaling.* Mol Cell Biol, 2005. **25**(18): p. 7940-52.
29. Kornfeld, K., D.B. Hom, and H.R. Horvitz, *The ksr-1 gene encodes a novel protein kinase involved in Ras-mediated signaling in C. elegans.* Cell, 1995. **83**(6): p. 903-13.
30. Therrien, M., et al., *KSR, a novel protein kinase required for RAS signal transduction.* Cell, 1995. **83**(6): p. 879-88.
31. Lunin, V.V., et al., *The structure of the MAPK scaffold, MP1, bound to its partner, p14. A complex with a critical role in endosomal map kinase signaling.* J Biol Chem, 2004. **279**(22): p. 23422-30.
32. Schaeffer, H.J., et al., *MP1: a MEK binding partner that enhances enzymatic activation of the MAP kinase cascade.* Science, 1998. **281**(5383): p. 1668-71.
33. Eishingdrelo, H., et al., *ERK and beta-arrestin interaction: a converging point of signaling pathways for multiple types of cell surface receptors.* J Biomol Screen, 2015. **20**(3): p. 341-9.
34. Ishibe, S., et al., *Paxillin serves as an ERK-regulated scaffold for coordinating FAK and Rac activation in epithelial morphogenesis.* Mol Cell, 2004. **16**(2): p. 257-67.
35. Murphy, L.O. and J. Blenis, *MAPK signal specificity: the right place at the right time.* Trends Biochem Sci, 2006. **31**(5): p. 268-75.
36. Sundaram, M. and M. Han, *The C. elegans ksr-1 gene encodes a novel Raf-related kinase involved in Ras-mediated signal transduction.* Cell, 1995. **83**(6): p. 889-901.
37. Roy, F. and M. Therrien, *MAP kinase module: the Ksr connection.* Curr Biol, 2002. **12**(9): p. R325-7.
38. Xing, H., K. Kornfeld, and A.J. Muslin, *The protein kinase KSR interacts with 14-3-3 protein and Raf.* Curr Biol, 1997. **7**(5): p. 294-300.
39. Selfors, L.M., et al., *soc-2 encodes a leucine-rich repeat protein implicated in fibroblast growth factor receptor signaling.* Proc Natl Acad Sci U S A, 1998. **95**(12): p. 6903-8.

40. Jeoung, M., et al., *Functional Integration of the Conserved Domains of Shoc2 Scaffold.* PLoS One, 2013. **8**(6): p. e66067.
41. Liau, N.P.D., et al., *Structural basis for SHOC2 modulation of RAS signalling.* Nature, 2022.
42. Li, W., M. Han, and K.L. Guan, *The leucine-rich repeat protein SUR-8 enhances MAP kinase activation and forms a complex with Ras and Raf.* Genes Dev, 2000. **14**(8): p. 895-900.
43. Rodriguez-Viciana, P., et al., *A phosphatase holoenzyme comprised of Shoc2/Sur8 and the catalytic subunit of PP1 functions as an M-Ras effector to modulate Raf activity.* Mol Cell, 2006. **22**(2): p. 217-30.
44. Young, L.C., et al., *An MRAS, SHOC2, and SCRIB complex coordinates ERK pathway activation with polarity and tumorigenic growth.* Mol Cell, 2013. **52**(5): p. 679-92.
45. Dai, P., W.C. Xiong, and L. Mei, *Erbin inhibits RAF activation by disrupting the sur-8-Ras-Raf complex.* J Biol Chem, 2006. **281**(2): p. 927-33.
46. Tao, Y., et al., *Erbin regulates NRG1 signaling and myelination.* Proc Natl Acad Sci U S A, 2009. **106**(23): p. 9477-82.
47. Shi, M., et al., *beta2-AR-induced Her2 transactivation mediated by Erbin confers protection from apoptosis in cardiomyocytes.* Int J Cardiol, 2013. **167**(4): p. 1570-7.
48. Harmon, R.M., et al., *Desmoglein-1/Erbin interaction suppresses ERK activation to support epidermal differentiation.* J Clin Invest, 2013. **123**(4): p. 1556-70.
49. Wilson, P., et al., *The role of USP7 in the Shoc2-ERK1/2 signaling axis and Noonan-like syndrome with loose anagen hair.* J Cell Sci, 2021. **134**(21).
50. Jang, H., et al., *VCP/p97 controls signals of the ERK1/2 pathway transmitted via the Shoc2 scaffolding complex: novel insights into IBMPFD pathology.* Mol Biol Cell, 2019. **30**(14): p. 1655-1663.
51. Jang, E.R., et al., *Spatial control of Shoc2-scaffold-mediated ERK1/2 signaling requires remodeling activity of the ATPase PSMC5.* J Cell Sci, 2015. **128**(23): p. 4428-41.
52. Fremin, C., et al., *Functional Redundancy of ERK1 and ERK2 MAP Kinases during Development.* Cell Rep, 2015. **12**(6): p. 913-21.
53. Yao, Y., et al., *Extracellular signal-regulated kinase 2 is necessary for mesoderm differentiation.* Proc Natl Acad Sci U S A, 2003. **100**(22): p. 12759-64.
54. Kunath, T., et al., *FGF stimulation of the Erk1/2 signalling cascade triggers transition of pluripotent embryonic stem cells from self-renewal to lineage commitment.* Development, 2007. **134**(16): p. 2895-902.
55. Chuang, J.H., L.C. Tung, and Y. Lin, *Neural differentiation from embryonic stem cells in vitro: An overview of the signaling pathways.* World J Stem Cells, 2015. **7**(2): p. 437-47.
56. Wong, K.L., et al., *ERK Activity Dynamics during Zebrafish Embryonic Development.* Int J Mol Sci, 2018. **20**(1).
57. Parada, C., et al., *Disruption of the ERK/MAPK pathway in neural crest cells as a potential cause of Pierre Robin sequence.* Development, 2015. **142**(21): p. 3734-45.

58. Newbern, J., et al., *Mouse and human phenotypes indicate a critical conserved role for ERK2 signaling in neural crest development.* Proc Natl Acad Sci U S A, 2008. **105**(44): p. 17115-20.
59. Tang, W. and M.E. Bronner, *Neural crest lineage analysis: from past to future trajectory.* Development, 2020. **147**(20).
60. Krens, S.F., et al., *Distinct functions for ERK1 and ERK2 in cell migration processes during zebrafish gastrulation.* Dev Biol, 2008. **319**(2): p. 370-83.
61. Vogiatzi, A. and G. Mavrothalassitis, *Craniofacial, orofacial and dental disorders: the role of the RAS/ERK pathway.* Expert Rev Mol Med, 2019. **21**: p. e2.
62. Dinsmore, C.J. and P. Soriano, *MAPK and PI3K signaling: At the crossroads of neural crest development.* Dev Biol, 2018. **444 Suppl 1**(Suppl 1): p. S79-s97.
63. Rauen, K.A., *Defining RASopathy.* Dis Model Mech, 2022. **15**(2).
64. Tajan, M., et al., *The RASopathy Family: Consequences of Germline Activation of the RAS/MAPK Pathway.* Endocr Rev, 2018. **39**(5): p. 676-700.
65. Hebron, K.E., E.R. Hernandez, and M.E. Yohe, *The RASopathies: from pathogenetics to therapeutics.* Dis Model Mech, 2022. **15**(2).
66. Mazzanti, L., et al., *Noonan-like syndrome with loose anagen hair: a new syndrome?* Am J Med Genet A, 2003. **118A**(3): p. 279-86.
67. Cordeddu, V., et al., *Mutation of SHOC2 promotes aberrant protein N-myristoylation and causes Noonan-like syndrome with loose anagen hair.* Nat Genet, 2009. **41**(9): p. 1022-6.
68. Avery, A., et al., *Cutaneous T-cell lymphoma in SHOC2 mutation-associated Noonan-like syndrome with loose anagen hair.* JAAD Case Rep, 2022. **24**: p. 52-55.
69. Bader-Meunier, B., et al., *Are RASopathies new monogenic predisposing conditions to the development of systemic lupus erythematosus? Case report and systematic review of the literature.* Semin Arthritis Rheum, 2013. **43**(2): p. 217-9.
70. Baldassarre, G., et al., *Phenotypic variability associated with the invariant SHOC2 c.4A>G (p.Ser2Gly) missense mutation.* Am J Med Genet A, 2014. **164A**(12): p. 3120-5.
71. Capalbo, D., et al., *Clinical Heterogeneity in two patients with Noonan-like Syndrome associated with the same SHOC2 mutation.* Ital J Pediatr, 2012. **38**: p. 48.
72. Chen, H., et al., *Clinical and mutation profile of pediatric patients with RASopathy-associated hypertrophic cardiomyopathy: results from a Chinese cohort.* Orphanet J Rare Dis, 2019. **14**(1): p. 29.
73. Cizmarova, M., et al., *New Mutations Associated with Rasopathies in a Central European Population and Genotype-Phenotype Correlations.* Ann Hum Genet, 2016. **80**(1): p. 50-62.
74. Couser, N.L., et al., *Cleft palate and hypopituitarism in a patient with Noonan-like syndrome with loose anagen hair-1.* Am J Med Genet A, 2018. **176**(9): p. 2024-2027.
75. Croonen, E.A., et al., *Noonan syndrome: comparing mutation-positive with mutation-negative dutch patients.* Mol Syndromol, 2013. **4**(5): p. 227-34.
76. Digilio, M.C., et al., *RASopathies: Clinical Diagnosis in the First Year of Life.* Mol Syndromol, 2011. **1**(6): p. 282-289.

77. Ekvall, S., et al., *Co-occurring SHOC2 and PTPN11 mutations in a patient with severe/complex Noonan syndrome-like phenotype.* Am J Med Genet A, 2011. **155A**(6): p. 1217-24.
78. Garavelli, L., et al., *Noonan syndrome-like disorder with loose anagen hair: a second case with neuroblastoma.* Am J Med Genet A, 2015. **167A**(8): p. 1902-7.
79. Gargano, G., et al., *Hydrops fetalis in a preterm newborn heterozygous for the c.4A>G SHOC2 mutation.* Am J Med Genet A, 2014. **164A**(4): p. 1015-20.
80. Gripp, K.W., et al., *Expanding the SHOC2 mutation associated phenotype of Noonan syndrome with loose anagen hair: structural brain anomalies and myelofibrosis.* Am J Med Genet A, 2013. **161A**(10): p. 2420-30.
81. Hoban, R., et al., *Noonan syndrome due to a SHOC2 mutation presenting with fetal distress and fatal hypertrophic cardiomyopathy in a premature infant.* Am J Med Genet A, 2012. **158a**(6): p. 1411-3.
82. Kane, J., et al., *Noonan syndrome with loose anagen hair associated with trichorrhexis nodosa and trichoptilosis.* Clin Case Rep, 2017. **5**(7): p. 1152-1154.
83. Komatsuzaki, S., et al., *Mutation analysis of the SHOC2 gene in Noonan-like syndrome and in hematologic malignancies.* J Hum Genet, 2010. **55**(12): p. 801-9.
84. Lee, B.H., et al., *Spectrum of mutations in Noonan syndrome and their correlation with phenotypes.* J Pediatr, 2011. **159**(6): p. 1029-35.
85. Li, X., et al., *Molecular and phenotypic spectrum of Noonan syndrome in Chinese patients.* Clin Genet, 2019. **96**(4): p. 290-299.
86. Lo, F.S., et al., *Moyamoya disease in two patients with Noonan-like syndrome with loose anagen hair.* Am J Med Genet A, 2015. **167**(6): p. 1285-8.
87. Mazzanti, L., et al., *GH Therapy and first final height data in Noonan-like syndrome with loose anagen hair (Mazzanti syndrome).* Am J Med Genet A, 2013. **161A**(11): p. 2756-61.
88. Okazaki, T., et al., *Recurrent Erythema Nodosum in a Child with a SHOC2 Gene Mutation.* Yonago Acta Med, 2019. **62**(1): p. 159-162.
89. Perrino, F., et al., *Psychopathological features in Noonan syndrome.* Eur J Paediatr Neurol, 2018. **22**(1): p. 170-177.
90. Simsek-Kiper, P.O., et al., *Clinical and molecular analysis of RASopathies in a group of Turkish patients.* Clin Genet, 2013. **83**(2): p. 181-6.
91. Takasawa, K., et al., *Improved growth velocity of a patient with Noonan-like syndrome with loose anagen hair (NS/LAH) without growth hormone deficiency by low-dose growth hormone therapy.* Am J Med Genet A, 2015. **167A**(10): p. 2425-9.
92. Takenouchi, T., et al., *Severe craniosynostosis with Noonan syndrome phenotype associated with SHOC2 mutation: clinical evidence of crosslink between FGFR and RAS signaling pathways.* Am J Med Genet A, 2014. **164A**(11): p. 2869-72.
93. Uehara, T., et al., *Systemic lupus erythematosus in a patient with Noonan syndrome-like disorder with loose anagen hair 1: More than a chance association.* Am J Med Genet A, 2018. **176**(7): p. 1662-1666.
94. van Trier, D.C., et al., *Ocular findings in Noonan syndrome: a retrospective cohort study of 105 patients.* Eur J Pediatr, 2018. **177**(8): p. 1293-1298.
95. van Trier, D.C., et al., *External ear anomalies and hearing impairment in Noonan Syndrome.* Int J Pediatr Otorhinolaryngol, 2015. **79**(6): p. 874-878.

96. Zmolikova, M., et al., *Coarctation of the aorta in Noonan-like syndrome with loose anagen hair.* Am J Med Genet A, 2014. **164A**(5): p. 1218-21.
97. Motta, M., et al., *Clinical and functional characterization of a novel RASopathy-causing SHOC2 mutation associated with prenatal-onset hypertrophic cardiomyopathy.* Hum Mutat, 2019. **40**(8): p. 1046-1056.
98. Motta, M., et al., *Expanding the molecular spectrum of pathogenic SHOC2 variants underlying Mazzanti syndrome.* Hum Mol Genet, 2022.
99. Martin, D.D., E. Beauchamp, and L.G. Berthiaume, *Post-translational myristoylation: Fat matters in cellular life and death.* Biochimie, 2011. **93**(1): p. 18-31.
100. Howe, K., et al., *The zebrafish reference genome sequence and its relationship to the human genome.* Nature, 2013. **496**(7446): p. 498-503.
101. Choi, T.Y., et al., *Zebrafish as an animal model for biomedical research.* Exp Mol Med, 2021. **53**(3): p. 310-317.
102. Keller, P.J., *In vivo imaging of zebrafish embryogenesis.* Methods, 2013. **62**(3): p. 268-78.
103. Jang, H., et al., *Hematopoietic and neural crest defects in zebrafish shoc2 mutants: a novel vertebrate model for Noonan-like syndrome.* Hum Mol Genet, 2019. **28**(3): p. 501-514.
104. Bronner, M.E. and M. Simões-Costa, *The Neural Crest Migrating into the Twenty-First Century.* Curr Top Dev Biol, 2016. **116**: p. 115-34.
105. Szabó, A. and R. Mayor, *Mechanisms of Neural Crest Migration.* Annu Rev Genet, 2018. **52**: p. 43-63.
106. Milet, C. and A.H. Monsoro-Burq, *Neural crest induction at the neural plate border in vertebrates.* Dev Biol, 2012. **366**(1): p. 22-33.
107. Simoes-Costa, M. and M.E. Bronner, *Establishing neural crest identity: a gene regulatory recipe.* Development, 2015. **142**(2): p. 242-57.
108. Martik, M.L. and M.E. Bronner, *Regulatory Logic Underlying Diversification of the Neural Crest.* Trends Genet, 2017. **33**(10): p. 715-727.
109. Rocha, M., et al., *Neural crest development: insights from the zebrafish.* Dev Dyn, 2020. **249**(1): p. 88-111.
110. Stuhlmiller, T.J. and M.I. Garcia-Castro, *Current perspectives of the signaling pathways directing neural crest induction.* Cell Mol Life Sci, 2012. **69**(22): p. 3715-37.
111. Steventon, B., et al., *Differential requirements of BMP and Wnt signalling during gastrulation and neurulation define two steps in neural crest induction.* Development, 2009. **136**(5): p. 771-9.
112. Schille, C. and A. Schambony, *Signaling pathways and tissue interactions in neural plate border formation.* Neurogenesis (Austin), 2017. **4**(1): p. e1292783.
113. Vadasz, S., et al., *Pax7 is regulated by cMyb during early neural crest development through a novel enhancer.* Development, 2013. **140**(17): p. 3691-702.
114. Montero-Balaguer, M., et al., *The mother superior mutation ablates foxd3 activity in neural crest progenitor cells and depletes neural crest derivatives in zebrafish.* Dev Dyn, 2006. **235**(12): p. 3199-212.
115. Stewart, R.A., et al., *Zebrafish foxd3 is selectively required for neural crest specification, migration and survival.* Dev Biol, 2006. **292**(1): p. 174-88.

116. Powell, D.R., et al., *Prdm1a directly activates foxd3 and tfap2a during zebrafish neural crest specification.* Development, 2013. **140**(16): p. 3445-55.
117. Hernandez-Lagunas, L., et al., *Zebrafish narrowminded disrupts the transcription factor prdm1 and is required for neural crest and sensory neuron specification.* Dev Biol, 2005. **278**(2): p. 347-57.
118. Dutton, J.R., et al., *An evolutionarily conserved intronic region controls the spatiotemporal expression of the transcription factor Sox10.* BMC Dev Biol, 2008. **8**: p. 105.
119. Olesnicky, E., L. Hernandez-Lagunas, and K.B. Artinger, *prdm1a Regulates sox10 and islet1 in the development of neural crest and Rohon-Beard sensory neurons.* Genesis, 2010. **48**(11): p. 656-66.
120. Carney, T.J., et al., *A direct role for Sox10 in specification of neural crest-derived sensory neurons.* Development, 2006. **133**(23): p. 4619-30.
121. Dutton, K.A., et al., *Zebrafish colourless encodes sox10 and specifies non-ectomesenchymal neural crest fates.* Development, 2001. **128**(21): p. 4113-25.
122. Yan, Y.L., et al., *A pair of Sox: distinct and overlapping functions of zebrafish sox9 co-orthologs in craniofacial and pectoral fin development.* Development, 2005. **132**(5): p. 1069-83.
123. Oh, C.D., et al., *SOX9 regulates multiple genes in chondrocytes, including genes encoding ECM proteins, ECM modification enzymes, receptors, and transporters.* PLoS One, 2014. **9**(9): p. e107577.
124. Sanchez-Martin, M., et al., *Deletion of the SLUG (SNAI2) gene results in human piebaldism.* Am J Med Genet A, 2003. **122A**(2): p. 125-32.
125. Sanchez-Martin, M., et al., *SLUG (SNAI2) deletions in patients with Waardenburg disease.* Hum Mol Genet, 2002. **11**(25): p. 3231-6.
126. Perez-Mancera, P.A., et al., *SLUG (SNAI2) overexpression in embryonic development.* Cytogenet Genome Res, 2006. **114**(1): p. 24-9.
127. Luo, R., et al., *Specific pan-neural crest expression of zebrafish Crestin throughout embryonic development.* Dev Dyn, 2001. **220**(2): p. 169-74.
128. Savagner, P., *Leaving the neighborhood: molecular mechanisms involved during epithelial-mesenchymal transition.* Bioessays, 2001. **23**(10): p. 912-23.
129. Savagner, P., *The epithelial-mesenchymal transition (EMT) phenomenon.* Ann Oncol, 2010. **21 Suppl 7**: p. vii89-92.
130. Thiery, J.P. and J.P. Sleeman, *Complex networks orchestrate epithelial-mesenchymal transitions.* Nat Rev Mol Cell Biol, 2006. **7**(2): p. 131-42.
131. Erickson, C.A. and R. Perris, *The role of cell-cell and cell-matrix interactions in the morphogenesis of the neural crest.* Dev Biol, 1993. **159**(1): p. 60-74.
132. Yang, J., et al., *Guidelines and definitions for research on epithelial-mesenchymal transition.* Nat Rev Mol Cell Biol, 2020. **21**(6): p. 341-352.
133. Scarpa, E., et al., *Cadherin Switch during EMT in Neural Crest Cells Leads to Contact Inhibition of Locomotion via Repolarization of Forces.* Dev Cell, 2015. **34**(4): p. 421-34.
134. Taneyhill, L.A. and A.T. Schiffmacher, *Should I stay or should I go? Cadherin function and regulation in the neural crest.* Genesis, 2017. **55**(6).

135. Serrano-Gomez, S.J., M. Maziveyi, and S.K. Alahari, *Regulation of epithelial-mesenchymal transition through epigenetic and post-translational modifications.* Mol Cancer, 2016. **15**: p. 18.
136. Bronner, M.E. and C. LaBonne, *Preface: the neural crest--from stem cell formation to migration and differentiation.* Dev Biol, 2012. **366**(1): p. 1.
137. Sperber, S.M., et al., *Zebrafish dlx2a contributes to hindbrain neural crest survival, is necessary for differentiation of sensory ganglia and functions with dlx1a in maturation of the arch cartilage elements.* Dev Biol, 2008. **314**(1): p. 59-70.
138. Cordero, D.R., et al., *Cranial neural crest cells on the move: their roles in craniofacial development.* Am J Med Genet A, 2011. **155A**(2): p. 270-9.
139. Li, I.M.H., et al., *Differential tissue specific, temporal and spatial expression patterns of the Aggrecan gene is modulated by independent enhancer elements.* Sci Rep, 2018. **8**(1): p. 950.
140. Yan, Y.L., et al., *A zebrafish sox9 gene required for cartilage morphogenesis.* Development, 2002. **129**(21): p. 5065-79.
141. Hou, L. and W.J. Pavan, *Transcriptional and signaling regulation in neural crest stem cell-derived melanocyte development: do all roads lead to Mitf?* Cell Res, 2008. **18**(12): p. 1163-76.
142. Mendez-Maldonado, K., et al., *Neurogenesis From Neural Crest Cells: Molecular Mechanisms in the Formation of Cranial Nerves and Ganglia.* Front Cell Dev Biol, 2020. **8**: p. 635.
143. McCallum, S., et al., *Enteric glia as a source of neural progenitors in adult zebrafish.* Elife, 2020. **9**.
144. Aspelund, A., et al., *Lymphatic System in Cardiovascular Medicine.* Circ Res, 2016. **118**(3): p. 515-30.
145. Oliver, G., et al., *The Lymphatic Vasculature in the 21(st) Century: Novel Functional Roles in Homeostasis and Disease.* Cell, 2020. **182**(2): p. 270-296.
146. Sevick-Muraca, E.M. and P.D. King, *Lymphatic vessel abnormalities arising from disorders of Ras signal transduction.* Trends Cardiovasc Med, 2014. **24**(3): p. 121-7.
147. Sleutjes, J., et al., *Lymphatic Abnormalities in Noonan Syndrome Spectrum Disorders: A Systematic Review.* Mol Syndromol, 2022. **13**(1): p. 1-11.
148. Isogai, S., et al., *Zebrafish as a new animal model to study lymphangiogenesis.* Anat Sci Int, 2009. **84**(3): p. 102-11.
149. Hannig, V., et al., *A Novel SHOC2 Variant in Rasopathy.* Hum Mutat, 2014. **35**(11): p. 1290-4.
150. Kaltschmidt, B., C. Kaltschmidt, and D. Widera, *Adult craniofacial stem cells: sources and relation to the neural crest.* Stem Cell Rev Rep, 2012. **8**(3): p. 658-71.
151. *Essentials of Anatomy and Physiology: Lymphatic System and Immunity. Anatomy of the Lymphatic System.*
152. Jung, H.M., et al., *Development of the larval lymphatic system in zebrafish.* Development, 2017. **144**(11): p. 2070-2081.
153. Kimmel, C.B., et al., *Stages of embryonic development of the zebrafish.* Dev Dyn, 1995. **203**(3): p. 253-310.
154. Kettleborough, R.N., et al., *A systematic genome-wide analysis of zebrafish protein-coding gene function.* Nature, 2013. **496**(7446): p. 494-7.

155. Cunningham, R.L. and K.R. Monk, *Whole Mount In Situ Hybridization and Immunohistochemistry for Zebrafish Larvae.* Methods Mol Biol, 2018. **1739**: p. 371-384.
156. Parada-Kusz, M., et al., *Generation of mouse-zebrafish hematopoietic tissue chimeric embryos for hematopoiesis and host-pathogen interaction studies.* Dis Model Mech, 2018. **11**(11).
157. *Gene Expression Omnibus*. 2022; NCBI]. Available from: https://www.ncbi.nlm.nih.gov/geo/query/acc.cgi?acc=GSE198231.
158. Thomas, P.D., et al., *PANTHER: a library of protein families and subfamilies indexed by function.* Genome Res, 2003. **13**(9): p. 2129-41.
159. Radu, M. and J. Chernoff, *An in vivo assay to test blood vessel permeability.* J Vis Exp, 2013(73): p. e50062.
160. Smith, S.J., et al., *Analysis of Zebrafish Larvae Skeletal Muscle Integrity with Evans Blue Dye.* J Vis Exp, 2015(105).
161. Jeoung, M. and E. Galperin, *Visualizing of signaling proteins on endosomes utilizing knockdown and reconstitution approach.* Methods Enzymol, 2014. **534**: p. 47-63.
162. Curran, K., et al., *Interplay between Foxd3 and Mitf regulates cell fate plasticity in the zebrafish neural crest.* Dev Biol, 2010. **344**(1): p. 107-18.
163. Rauen, K.A., *The RASopathies.* Annu Rev Genomics Hum Genet, 2013. **14**: p. 355-69.
164. Riller, Q. and F. Rieux-Laucat, *RASopathies: From germline mutations to somatic and multigenic diseases.* Biomed J, 2021. **44**(4): p. 422-432.
165. Jang, E.R. and E. Galperin, *The function of Shoc2: A scaffold and beyond.* Commun Integr Biol, 2016. **9**(4): p. e1188241.
166. Yi, J., et al., *Endothelial SUR-8 acts in an ERK-independent pathway during atrioventricular cushion development.* Developmental dynamics : an official publication of the American Association of Anatomists, 2010. **239**(7): p. 2005-13.
167. Roellig, D., et al., *Dynamic transcriptional signature and cell fate analysis reveals plasticity of individual neural plate border cells.* Elife, 2017. **6**.
168. Stuhlmiller, T.J. and M.I. Garcia-Castro, *FGF/MAPK signaling is required in the gastrula epiblast for avian neural crest induction.* Development, 2012. **139**(2): p. 289-300.
169. Li, W. and R.A. Cornell, *Redundant activities of Tfap2a and Tfap2c are required for neural crest induction and development of other non-neural ectoderm derivatives in zebrafish embryos.* Dev Biol, 2007. **304**(1): p. 338-54.
170. Rubinstein, A.L., et al., *Genes dependent on zebrafish cyclops function identified by AFLP differential gene expression screen.* Genesis, 2000. **26**(1): p. 86-97.
171. Barrallo-Gimeno, A. and M.A. Nieto, *The Snail genes as inducers of cell movement and survival: implications in development and cancer.* Development, 2005. **132**(14): p. 3151-61.
172. Theveneau, E. and R. Mayor, *Neural crest delamination and migration: from epithelium-to-mesenchyme transition to collective cell migration.* Dev Biol, 2012. **366**(1): p. 34-54.
173. Etchevers, H.C., E. Dupin, and N.M. Le Douarin, *The diverse neural crest: from embryology to human pathology.* Development, 2019. **146**(5).

174. Wang, W.D., et al., *Tfap2a and Foxd3 regulate early steps in the development of the neural crest progenitor population.* Dev Biol, 2011. **360**(1): p. 173-85.
175. Brosamle, C. and M.E. Halpern, *Characterization of myelination in the developing zebrafish.* Glia, 2002. **39**(1): p. 47-57.
176. Jessen, J.R., *Recent advances in the study of zebrafish extracellular matrix proteins.* Dev Biol, 2015. **401**(1): p. 110-21.
177. Mevel, R., et al., *RUNX transcription factors: orchestrators of development.* Development, 2019. **146**(17).
178. Komori, T., *Runx2, an inducer of osteoblast and chondrocyte differentiation.* Histochem Cell Biol, 2018. **149**(4): p. 313-323.
179. Dobin, A., et al., *STAR: ultrafast universal RNA-seq aligner*. Bioinformatics, 2013. **29**(1): p. 15-21.
180. Trapnell, C., et al., *Differential gene and transcript expression analysis of RNA-seq experiments with TopHat and Cufflinks.* Nat Protoc, 2012. **7**(3): p. 562-78.
181. Kanehisa, M., et al., *KEGG for representation and analysis of molecular networks involving diseases and drugs.* Nucleic Acids Res, 2010. **38**(Database issue): p. D355-60.
182. Carnovali, M., G. Banfi, and M. Mariotti, *Zebrafish Models of Human Skeletal Disorders: Embryo and Adult Swimming Together.* Biomed Res Int, 2019. **2019**: p. 1253710.
183. Perng, Y.C. and D.J. Lenschow, *ISG15 in antiviral immunity and beyond.* Nat Rev Microbiol, 2018. **16**(7): p. 423-439.
184. Wu, C.L., et al., *Single cell transcriptomic analysis of human pluripotent stem cell chondrogenesis.* Nat Commun, 2021. **12**(1): p. 362.
185. Vallet, S.D., et al., *Computational and experimental characterization of the novel ECM glycoprotein SNED1 and prediction of its interactome.* Biochem J, 2021. **478**(7): p. 1413-1434.
186. Barque, A., et al., *Knockout of the gene encoding the extracellular matrix protein SNED1 results in early neonatal lethality and craniofacial malformations.* Dev Dyn, 2021. **250**(2): p. 274-294.
187. Acevedo-Arozena, A., et al., *ENU mutagenesis, a way forward to understand gene function.* Annu Rev Genomics Hum Genet, 2008. **9**: p. 49-69.
188. *Zebrafish Mutation Project*. [cited 2022 7/27/2022]; Available from: https://www.sanger.ac.uk/resources/zebrafish/zmp/.
189. Breslin, J.W., et al., *Lymphatic Vessel Network Structure and Physiology.* Compr Physiol, 2018. **9**(1): p. 207-299.
190. Petrova, T.V. and G.Y. Koh, *Biological functions of lymphatic vessels.* Science, 2020. **369**(6500).
191. Deng, Y., X. Zhang, and M. Simons, *Molecular controls of lymphatic VEGFR3 signaling.* Arterioscler Thromb Vasc Biol, 2015. **35**(2): p. 421-9.
192. Shin, M., et al., *Vegfc acts through ERK to induce sprouting and differentiation of trunk lymphatic progenitors.* Development, 2016. **143**(20): p. 3785-3795.
193. Lawson, N.D. and B.M. Weinstein, *In vivo imaging of embryonic vascular development using transgenic zebrafish.* Dev Biol, 2002. **248**(2): p. 307-18.

194. Kanwal, Z., et al., *Deficiency in hematopoietic phosphatase ptpn6/Shp1 hyperactivates the innate immune system and impairs control of bacterial infections in zebrafish embryos.* J Immunol, 2013. **190**(4): p. 1631-45.
195. Solman, M., et al., *Inflammatory response in hematopoietic stem and progenitor cells triggered by activating SHP2 mutations evokes blood defects.* Elife, 2022. **11**.
196. Neve, A., et al., *Extracellular matrix modulates angiogenesis in physiological and pathological conditions.* Biomed Res Int, 2014. **2014**: p. 756078.
197. Frye, M., et al., *Matrix stiffness controls lymphatic vessel formation through regulation of a GATA2-dependent transcriptional program.* Nat Commun, 2018. **9**(1): p. 1511.
198. Lister, J.A., et al., *Zebrafish Foxd3 is required for development of a subset of neural crest derivatives.* Dev Biol, 2006. **290**(1): p. 92-104.
199. Thisse, C., B. Thisse, and J.H. Postlethwait, *Expression of snail2, a second member of the zebrafish snail family, in cephalic mesendoderm and presumptive neural crest of wild-type and spadetail mutant embryos.* Dev Biol, 1995. **172**(1): p. 86-99.
200. Haldin, C.E. and C. LaBonne, *SoxE factors as multifunctional neural crest regulatory factors.* Int J Biochem Cell Biol, 2010. **42**(3): p. 441-4.
201. Greenfeld, H., J. Lin, and M.C. Mullins, *The BMP signaling gradient is interpreted through concentration thresholds in dorsal-ventral axial patterning.* PLoS Biol, 2021. **19**(1): p. e3001059.
202. Alkobtawi, M., P. Pla, and A.H. Monsoro-Burq, *BMP signaling is enhanced intracellularly by FHL3 controlling WNT-dependent spatiotemporal emergence of the neural crest.* Cell Rep, 2021. **35**(12): p. 109289.
203. Jeoung, M., et al., *Shoc2-tranduced ERK1/2 motility signals--Novel insights from functional genomics.* Cell Signal, 2016. **28**(5): p. 448-459.
204. Kaduwal, S., et al., *Sur8/Shoc2 promotes cell motility and metastasis through activation of Ras-PI3K signaling.* Oncotarget, 2015.
205. Kota, P., et al., *M-Ras/Shoc2 signaling modulates E-cadherin turnover and cell-cell adhesion during collective cell migration.* Proc Natl Acad Sci U S A, 2019. **116**(9): p. 3536-3545.
206. Teng, L., et al., *Requirement for Foxd3 in the maintenance of neural crest progenitors.* Development, 2008. **135**(9): p. 1615-24.
207. Nelms, B.L. and P.A. Labosky, in *Transcriptional Control of Neural Crest Development*. 2010: San Rafael (CA).
208. Moon, B.S., et al., *Sur8/Shoc2 involves both inhibition of differentiation and maintenance of self-renewal of neural progenitor cells via modulation of extracellular signal-regulated kinase signaling.* Stem Cells, 2011. **29**(2): p. 320-31.
209. Buyuk, B., S. Jin, and K. Ye, *Epithelial-to-Mesenchymal Transition Signaling Pathways Responsible for Breast Cancer Metastasis.* Cell Mol Bioeng, 2022. **15**(1): p. 1-13.
210. Wu, W.S., et al., *Slug antagonizes p53-mediated apoptosis of hematopoietic progenitors by repressing puma.* Cell, 2005. **123**(4): p. 641-53.
211. Inoue, A., et al., *Slug, a highly conserved zinc finger transcriptional repressor, protects hematopoietic progenitor cells from radiation-induced apoptosis in vivo.* Cancer Cell, 2002. **2**(4): p. 279-88.

212. Wiig, H., D. Keskin, and R. Kalluri, *Interaction between the extracellular matrix and lymphatics: consequences for lymphangiogenesis and lymphatic function.* Matrix Biol, 2010. **29**(8): p. 645-56.
213. Chaudhury, S., et al., *Localised Collagen2a1 secretion supports lymphatic endothelial cell migration in the zebrafish embryo.* Development, 2020. **147**(18).
214. Hogan, B.M., et al., *Ccbe1 is required for embryonic lymphangiogenesis and venous sprouting.* Nat Genet, 2009. **41**(4): p. 396-8.
215. Choi, J.B., et al., *Dysregulated ECM remodeling proteins lead to aberrant osteogenesis of Costello syndrome iPSCs.* Stem Cell Reports, 2021. **16**(8): p. 1985-1998.
216. Jones, G.G., et al., *SHOC2 phosphatase-dependent RAF dimerization mediates resistance to MEK inhibition in RAS-mutant cancers.* Nat Commun, 2019. **10**(1): p. 2532.
217. Sulahian, R., et al., *Synthetic Lethal Interaction of SHOC2 Depletion with MEK Inhibition in RAS-Driven Cancers.* Cell Rep, 2019. **29**(1): p. 118-134 e8.
218. Henke, E., R. Nandigama, and S. Ergun, *Extracellular Matrix in the Tumor Microenvironment and Its Impact on Cancer Therapy.* Front Mol Biosci, 2019. **6**: p. 160.
219. Iwami, D., C.C. Brinkman, and J.S. Bromberg, *Vascular endothelial growth factor c/vascular endothelial growth factor receptor 3 signaling regulates chemokine gradients and lymphocyte migration from tissues to lymphatics.* Transplantation, 2015. **99**(4): p. 668-77.
220. Rauniyar, K., S.K. Jha, and M. Jeltsch, *Biology of Vascular Endothelial Growth Factor C in the Morphogenesis of Lymphatic Vessels.* Front Bioeng Biotechnol, 2018. **6**: p. 7.
221. Kerjaschki, D., *The crucial role of macrophages in lymphangiogenesis.* J Clin Invest, 2005. **115**(9): p. 2316-9.
222. Takahashi, K. and S. Yamanaka, *Induction of pluripotent stem cells from mouse embryonic and adult fibroblast cultures by defined factors.* Cell, 2006. **126**(4): p. 663-76.
223. Takahashi, K., et al., *Induction of pluripotent stem cells from adult human fibroblasts by defined factors.* Cell, 2007. **131**(5): p. 861-72.
224. Boland, M.J., et al., *Adult mice generated from induced pluripotent stem cells.* Nature, 2009. **461**(7260): p. 91-4.
225. Ju, Y., et al., *SHP2 mutations induce precocious gliogenesis of Noonan syndrome-derived iPSCs during neural development in vitro.* Stem Cell Res Ther, 2020. **11**(1): p. 209.
226. Choi, J.Y., et al., *Impaired Osteogenesis of Disease-Specific Induced Pluripotent Stem Cells Derived from a CFC Syndrome Patient.* Int J Mol Sci, 2017. **18**(12).
227. Gross, A.M., et al., *Advancing RAS/RASopathy therapies: An NCI-sponsored intramural and extramural collaboration for the study of RASopathies.* Am J Med Genet A, 2020. **182**(4): p. 866-876.
228. Ehrhardt, G.R., et al., *M-Ras, a widely expressed 29-kD homologue of p21 Ras: expression of a constitutively active mutant results in factor-independent growth of an interleukin-3-dependent cell line.* Blood, 1999. **94**(7): p. 2433-44.

229. Watanabe, H., M.P. de Caestecker, and Y. Yamada, *Transcriptional cross-talk between Smad, ERK1/2, and p38 mitogen-activated protein kinase pathways regulates transforming growth factor-beta-induced aggrecan gene expression in chondrogenic ATDC5 cells.* J Biol Chem, 2001. **276**(17): p. 14466-73.
230. Dolivo, D.M., S.A. Larson, and T. Dominko, *Crosstalk between mitogen-activated protein kinase inhibitors and transforming growth factor-β signaling results in variable activation of human dermal fibroblasts.* Int J Mol Med, 2019. **43**(1): p. 325-335.
231. Hayashida, T., M. Decaestecker, and H.W. Schnaper, *Cross-talk between ERK MAP kinase and Smad signaling pathways enhances TGF-beta-dependent responses in human mesangial cells.* Faseb j, 2003. **17**(11): p. 1576-8.
232. Banerjee, S., et al., *A novel role for Lh3 dependent ECM modifications during neural crest cell migration in zebrafish.* PLoS One, 2013. **8**(1): p. e54609.
233. Kulesa, P.M., et al., *Cranial neural crest migration: new rules for an old road.* Dev Biol, 2010. **344**(2): p. 543-54.
234. Jimenez, L., et al., *Phenotypic chemical screening using a zebrafish neural crest EMT reporter identifies retinoic acid as an inhibitor of epithelial morphogenesis.* Dis Model Mech, 2016. **9**(4): p. 389-400.

VITA

Rebecca G. Norcross

EDUCATION:

2015-Current	Graduate student, Ph.D., Molecular and Cellular Biochemistry Dept. University of Kentucky
2013-2015	Graduate student, MS, Dept. of Animal and Food Sciences University of Kentucky
2012	Undergraduate student, B.S. Dept. of Biology Indiana State University

EMPLOYMENT & RESEARCH EXPERIENCES:

2013	Quality Control Laboratory Tech., Roche Diagnostics, Diabetes Care, Inc., Indianapolis, IN.
2012	Tech. Services/Manufacturing Sciences Intern, Eli Lilly and Co., Elanco Clinton, IN.
2011-2012	Undergraduate researcher Indiana State University Mentor: Kathleen Dannelly, Ph.D.
2011	Undergraduate researcher Indiana State University Mentor: Richard Fitch, Ph.D.

ACADEMIC AWARDS AND HONORS:

2022	Oral Presentation Award, best graduate student presentation The Molecular and Cellular Biochemistry Departmental Spring Research Conference
2022 & 2017	Graduate Travel Award American Society for Biochemical and Molecular Biology meetings

2018	Max Steckler Award Molecular and Cellular Biochemistry Department University of Kentucky
2010-2012	Beta Beta Beta National Honor Society, Xi Kappa Chapter member Biology Department Indiana State University
2010 & 2011	Donald and Mary Jo Stanley Scholarship Biology Department Indiana State University
2010	Eli Lilly and Company Summer Undergraduate Fellowship Indiana State University's Summer Undergraduate Research Experience program Indiana State University

PUBLICATIONS:

1. **Rebecca Norcross**, Lina Abdelmoti, Eric C. Rouchka, Kalina Andreeva, Olivia Tussey, Daileen Landestroy, and Emilia Galperin. Shoc2 controls ERK1/2-driven neural crest development by balancing components of the extracellular matrix. ***Submitted***

2. Patricia Wilson, Lina Abdelmoti, **Rebecca Norcross**, Udeep Chawla, Eun Ryoung Jang, and Emilia Galperin. 2021. The role of USP7 in the Shoc2 - ERK1/2 signaling axis and Noonan-like syndrome with loose anagen hair (NSLAH). *Journal of Cell Science.*134 (21):jcs258922.

3. HyeIn Jang, Erin Oakley, Marie Forbes-Osborne, Melissa V Kesler, **Rebecca Norcross**, Ann C Morris, and Emilia Galperin. 2019. Hematopoietic and neural crest defects in zebrafish shoc2 mutants: A novel vertebrate model for Noonan-like syndrome. *Human Molecular Genetics*. 28.3:501-14.